CIRCULATING FLUIDIZED BED COMBUSTOR TOWARDS THIRD GENERATION OF OXY-FUEL COMBUSTION

A Thesis Submitted in Partial Fulfilment of the Requirements for the Degree of

DOCTOR OF PHILOSOPHY

By

AZD ZAYOUD

DEPARTMENT OF MECHANICAL ENGINEERING

INDIAN INSTITUTE OF TECHNOLOGY GUWAHATI

GUWAHATI -781039, INDIA

NOVEMBER 2016

Dedicated to My Parents

Sir Habib Zayoud

Lady Tamador (Assad) Zayoud

Whose endless faith and blessings always

Inspired me to move forward

Declaration

I hereby certify that the information presented in this dissertation '**CIRCULATING FLUIDIZED BED COMBUSTOR TOWARDS THIRD GENERATION OF OXY-FUEL COMBUSTION**' is entirely my own account of research performed under the guidance of **Professor Pinakeswar Mahanta** and **Professor Ujjwal K. Saha**. Any part of this work has not earlier been submitted for the award of any degree, diploma, associate-ship, fellowship or its equivalent to any University or Institution.

Azd Zayoud

Roll No. 126103038
Department of Mechanical Engineering
Indian Institute of Technology, Guwahati
Guwahati -781039, India
November 2016

Certificate

It is certified that the work presented in the thesis entitled '**CIRCULATING FLUIDIZED BED COMBUSTOR TOWARDS THIRD GENERATION OF OXY-FUEL COMBUSTION**' submitted by **Mr. Azd Zayoud**, a student in the Mechanical Engineering Department, Indian Institute of Technology Guwahati, India for the award of the degree of Doctor of Philosophy has been carried out under our supervision. This work has not been submitted previously elsewhere for the award of any other degree or diploma.

Dr. Pinakeswar Mahanta
Professor
Department of Mechanical Engineering
Indian Institute of Technology Guwahati
Guwahati -781039, India

Dr. Ujjwal K. Saha
Professor
Department of Mechanical Engineering
Indian Institute of Technology Guwahati
Guwahati -781039, India

Abstract

The carbon capture and sequestration (CCS) is gaining popularity to mitigate the CO_2 emission and Greenhouse gases. The oxy-fuel circulating fluidized bed (CFB) combustion is one of the most promised techniques of CCS, where CFB has advantages over the pulverized coal power combustors namely in situ SO_x and NO_x capturing and flexible utilized fuel. On the other hand, efficiency penalty of oxy-fuel CFB combustion is considered as a significant barrier of applying this technology. The R&Ds are running to overcome the high cost of implementing oxy-fuel CFB combustion technology. So far, there is no industrial application of this technology. Moreover, the hydrodynamic behaviour under oxy-fuel CFB combustion conditions needs more investigation. In the present work, two CFB units (cold and hot) of identical geometry are designed and fabricated to investigate the hydrodynamic and combustion under oxy-fuel combustion conditions. Also, the core of this work is the novel method of pure oxy-fuel CFB combustion technique, to enhance the efficiency of the oxy-fuel combustion and eliminate the recirculation of the flue gases. The proposed method suggests controlling the combustion temperature by the stoichiometric ratio for pure oxy-fuel combustion with multi-reaction stages rather than controlling the temperature by CO_2 recirculation. Secondly, the hydrodynamic behaviour is studied under different operating conditions viz. pressure, velocity, aeration flow rate, particle size, bed inventory and primary flow rate. The results obtained from the present investigation show a similar hydrodynamic behaviour of the oxy-fuel case with the conventional air case. Moreover, the proposed pure oxy-fuel combustion is subjected to experiments and shows promising results, where pure oxygen is used for combustion. And the temperature is controlled successfully by the stoichiometric ratio as the hypothesis suggests. Side by side, biomass fuel is used and leads to smooth operating condition. By combining, oxy-fuel CFB combustion and biomass utilisation, the CO_2 can be harvested from the atmosphere. Finally, a thermodynamic analysis (exergy and energy) is performed at the chemical reaction level. Applying pure oxygen reaction shows an improvement in efficiency due to minimizing the energy loss with flue gases where the pure oxygen is used rather than air or mixture of CO_2-O_2 as an oxidant. This novel proposed method could lead to the 3rd generation of the oxy-fuel CFB combustion, and adapting biomass as a fuel with CCS will drive to less than zero CO_2 capturing technology.

Acknowledgement

This part of my life journey in India is a great learning experience for me. Not only philosophy doctoral is achieved, but moreover, it brings a life spiritual knowledge and wisdom. It is full of support and encouragement from numerous individuals. It is a pleasure to express my thanks wholeheartedly to every, and each one contributed to make this Ph.D. achievable. It is an opportunity to gratefully acknowledge the Indian Council for Cultural Relations (ICCR), who gives this chance to pursue my Ph.D. at the Indian Institute of Technology Guwahati. I wish to express my heartfelt gratitude to Prof. Gautam Biswas (Director of the Institute), Prof. Anoop K. Dass (HOD, Mechanical Engineering Department) and the marvellous faculty and staff of the Indian Institute of Technology Guwahati for the familial environment the surrounded the scholars and student with. The constant help of academic affairs, Student Affairs and Alumina & External Relationship Affairs is highly appreciated.

I would like to express my gratitude to, Prof. P. Mahanta and Prof. U. K. Saha for their steady scientific guidance and support during my work. Their amazing skills of organization, planning and management tough me a lot, and their mesmerizing ability to bring me confidence and peaceful in any dilemma I have faced, and I indeed appreciate their parental supervision. Deep appreciation goes to my committee members: Prof. Subrata K. Majumder, Prof. P. S. Robi, and Prof. Niranjan Sahoo, for their constructive suggestions to my research. A warm thank goes to Prof. Aref Ali at Tishreen University for his steady support and encouragement through the years of work, since he supervised me in the M.Tech. A special appreciation goes to my close friend Captain Mohannad Al-Kaddar and his lovely family, for solid backing from the early degining. Appreciation goes to my Syrian friend who share the journey in Baharat (India), Mr. Sulieman Al-Ali. I would like to acknowledge the staff of Centre for Energy, Work Shop staff viz. Mr. Dillip Chetri, Mr. Mrinal Sharma, Mr. Jaikrishna Saikia, Mr. Nip Bora, Mr. Saiffuddin Ahmed, and Mr. Dhiren Huzuri. Also, many thanks to all graduate students and research assistants who supported me during my work.

Lastly, I am and always grateful to God for guiding me through this testing life.

November 2016 Azd Zayoud

Contents

Nomenclature

Notations		
Ar	Archimedes number	---
C_p	Specific heat value	kJ/kmol.K
$C_{p,eff.}$	Effective heat capacity of PCM	J/kg.K
C_{pf}	Specific heat of heat transfer fluid	kJ/kmol.K
C_v	Specific heating value	kJ/kg.K
E	Energy	kJ
Ex	Exergy	kJ/kmol
$Ex_{ch.}$	Chemical Exergy	kJ/kmol
$Ex_{ph.}$	Physical Exergy	kJ/kmol
$Ex_{kn.}$	Kinetic Exergy	kJ/kmol
$Ex_{pt.}$	Potential Exergy	kJ/kmol
g	Gibbs function	kJ/kmol
h	enthalpy	kJ/kmol
L_m	is the height of the taps	m
NL	Normal litre	litre
P	pressure	kPa
R	Reynolds Number	---
s	entropy	kJ/kmol.K
$T_{amb.}$	Ambient Temperature	K
$T_{ign.}$	Ignition temperature	°C, K
U_{tr}	Terminal velocity	m/sec
U_{mf}	Minimum fluidization velocity	m/sec

Greek Symbols		
ρ_{sus}	Suspension density	kg/m^3
ρ_{sus}	Solid density	kg/m^3
ρ_L	Density of measuring liquid	kg/m^3

Δh	difference of liquid levels in manometer	m

Abbreviation	
AFT	Adiabatic Flame Temperature
ASTM	American Society for Testing and Materials
ASU	Air Separation Unit
BSS	British Standard Sieve
CAS	Chinese Academy of Sciences
CFB	Circulating Fluidized Bed
CFBC	Circulating Fluidized Bed Combustion
CCS	Capturing and sequestration
CCUS	Carbon Capture Use and Storage
CLC	Chemical Looping Combustion
DPT	Dew Point Temperature
DTA	Differential Thermal Analysis
DTF	Drop Tube Furnace
DTG	Derivative Thermo-gravimetric
EGR	Exhaust Gas Recirculation
EIA	Energy Information Administration
EOR	Enhanced Oil Recovery
ETP	Energy Technology Perspectives
FD	Feeding Rate
GA	Gas Analyser
GC	Gas Chromatography
GHGs	Green House Gases
GPS	Gas Processing System
HHV	Higher Heating Value
ID	Inner Diameter

IEA	International Energy Agency
IGCC	Integrated Gasification Combined Cycle
IPCC	Intergovernmental Panel on Climate Change
LHV	Lower Heating Value
OC	Oxy-Combustion
OD	Outer Diameter
OEC	Oxygen Enhanced Combustion
OFR	Oxidant Fuel Ratio
O_2	Oxygen
PCFBC	Pressurised Circulating Fluidized Bed Combustion
R&D	Research and Development
RoHR	Rate of Heat Release
RPM	Revolution per Minute
SCR	Solid Circulation Rate
SRR	Solid Re-Circulating Rate
TGA	Thermos Gravimetric Analyser
VM	Volatile matter

List of Figures

List of Tables

1 Introduction:

Overview

The continuous movement of this world relies on the energy, and the consumption of energy harnessed from fossil and fissile such (nuclear) as well as from renewable energy as biomass is increasing with the increased needs of modernized life. Unfortunately, the utilization of conventional fuel like coal, oil, and gas has environmental negative effects, and on the other hand, these types of fuel are unreplaceable in the near future for two reasons. Firstly, there is no clean energy source can meet the huge global energy demand right now, secondly, the demand for energy is booming dramatically over the world. As a result, instant actions shall be of the most Green House Gases (GHGs) emissive. For these reasons, the oxy-fuel Circulating Fluidized Bed (CFB) combustion technology is commenced to mitigate the greenhouse gases (GHGs) emissions by capturing and storing mainly carbon dioxide CO_2. The first generation of oxy-fuel CFB combustors (CFBC) was a modification of existing power plants. Later on, the second generation of oxy-fuel combustion came to existing with higher oxygen (O_2) concentration; the main penalty of this generation is the lower overall efficiency due to auxiliary setup, and air separation unit (ASU) running cost. Subsequently, more matured generation is needed to meet both of the economic and environmental requirements. Present work focuses on the development of the third generation oxy-fuel CFBC, with improvement of efficiency to make the same profit to industrial power production scale.

Chapter outline:

1.1 Problem Motivation and Statement

Energy is the pulse of the life. Since human discovered the fire, the life style has been changed forever. After the commencement of the industrial revolution that relied on the coal as an energy source in 1760, the consumption of energy is being increased dramatically. Later on, oil and gas were discovered, and became an important energy source for the modern life. The world energy consumption will continue increasing (especially the fossil fuel consumption) due to continuous growth of world population and increased energy consumption of the modern life style. As reported, by 2050, the global population will rise from seven to over nine billion people (UN, 2013). The world energy demand is expected to increase by 50% over the next 20 years, and serious ecological impacts are being produced because of the GHGs especially the carbon dioxide (CO_2) emissions.

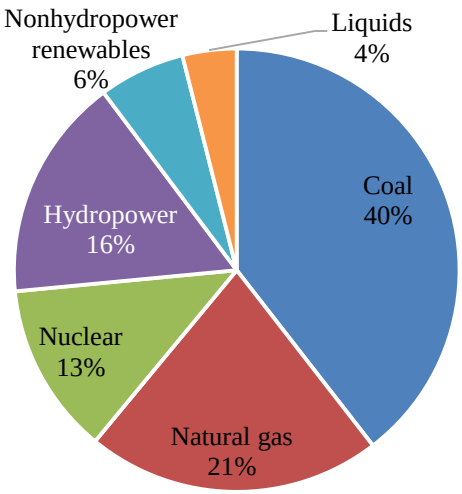

Figure 1.1 World electricity generation percentage by energy source, 2015 (trillion kilowatt-hours)

Further, the coal consumption is likely to increase by 50% in 2040 comparing with 2010 (Leahy et al., 2013). Interestingly, the coal contributes at least two times of any other energy source, and 40% of the overall electricity generation is generated using coal (Figure 1.1). Meanwhile, the rest of total energy sources liquid, non-hydropower, renewables, hydropower, nuclear and natural gas have 60% share of the electricity generation. Furthermore, the statistics of Greenhouse Gases (GHGs) by sectors show that high GHGs contribution comes from the power supply, it has more than ¼ of the total greenhouse gas emission impact (Metz et al., 2007). The fossil fuel utilization contributes 57% of carbon dioxide emissions (Metz et al., 2007; Quadrelli and Peterson 2007). In 2006, about 42% of the world energy-related to CO_2 emissions were attributable to coal use (Zheng, 2011).

On the other hand, Vostok station established in the Princess Elizabeth Land in Antractica shows that the CO_2 concentration in the atmosphere can be natural and/or anthropological (Petit et. al, 1999). The data of Vostok station displays an oscillated pattern of CO_2 concentration in the atmosphere. Presently, the unprecedented levels of GHGs emissions are the results of overlapping both natural and anthropological GHGs emissions.

Furthermore, since coal is one of the most stable, available, cheap, and huge energy sources (IEA, 2014), it will remain secure and demanded energy source. The coal is not affected by the international conflicts because it is distributed all over the world mainly in USA, India, Canada, Russia, South Africa, China, Brazil, Australia and New Zealand, and it is not concentrated only in a specific geographical regime like oil and gas in the middle East. These facts make the utilization of coal unavoidable. However, coal requires an improvements of the related technologies to mitigate the GHGs. Due to the importance of coal as an energy source and its companied ecological effects the international energy agency (IEA) predicts three scenarios of temperature increasing viz. 2°C, 4°C, and 6°C, as result of GHGs concentration in the atmosphere. These scenarios are presented in the following subsections (IEA, 2013a).

International Energy Agency (IEA) presents scenarios for controlling the GHGs, and the global increase in temperature.

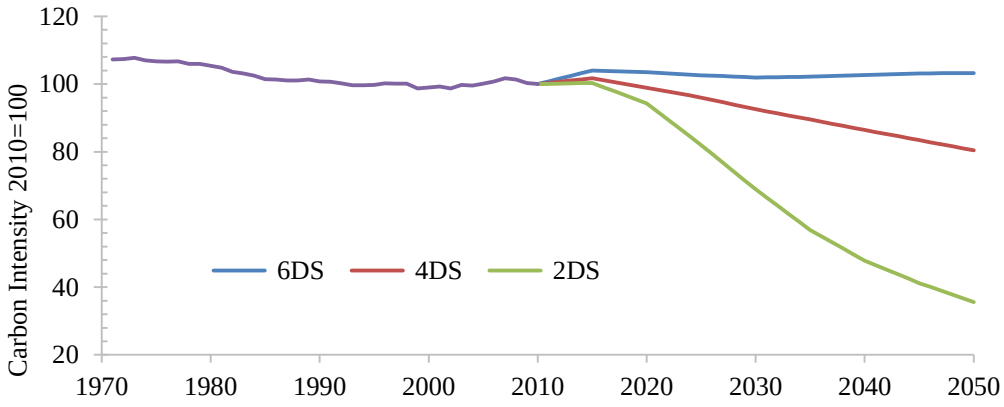

Figure 1.2 The variation of carbon intensity index and predicted scenarios

Figure 1.2 shows three Energy Technology Perspectives (ETP) of the energy carbon intensity index up to 2050 (IEA, 2013a). Applying either 2°C Scenario (2DS), or 4°C Scenario (4DS), or 6°C Scenario (6DS) aims to limit the global increase temperature by 2°C, 4°C, or 6°C respectively (depending on the applied scenario) in 2050 by limiting the concentration of CO_2 in the atmosphere to around 450, 550, or 1000 parts per million respectively (IEA, 2011a). To

achieve these pledges, an advanced technologies and techniques should be adapted such as improving the efficiency of the new power plants, retrofit the old plants, applying novel firing technologies such like Carbon Capturing and Storage (CCS), and increase the utilization of renewable and nuclear energy (IEA, 2010a; Hu, 2011). So far, CCS is one of the most promising technologies for immediate action to face GHGs problem, and it is highly recommended to improve the existing technology to mitigate CO_2 emissions from power plants that run using coal.

1.1.1 Methods for reducing greenhouse gases emissions

To mitigate consequences of GHGs' effects from 50 up to 80 % of GHGs must be reduced, according to Intergovernmental Panel on Climate Change (IPCC) (Stangeland, 2007). To meet IPCC aim to reduce 71% of GHGs (for less than 10 Gton/year road map) in 2050, Stangeland (2007) proposed a strategy of three key methods namely: (a) adapting CCS technology, (b) enhancing overall efficiency, and (c) rising renewable fuels' share. Intentionally, one or more of these key methods could be adapted by CFB technology.

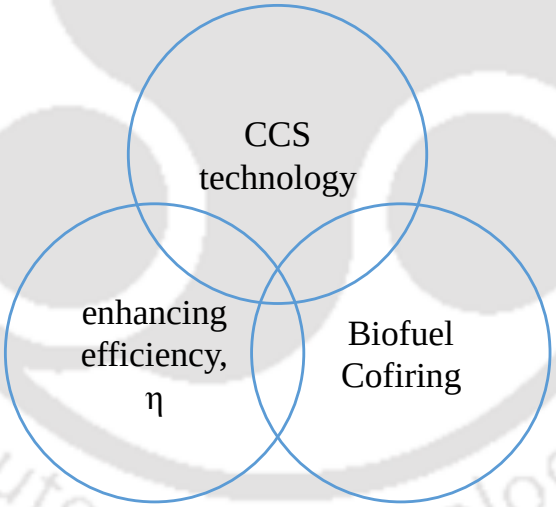

Figure 1.3 The key methods of reducing Greenhouse Gases emissions

Carbon Capture and Storage (CCS)

As illustrated in Figure 1.4, the CCS has three main categories viz. pre-combustion capture, oxy-fuel combustion capture, and post-combustion capture (Davison, 2007; Gibbins and Chalmers, 2008). On the other hand, creating a price for CO_2 by the Carbon Capture Use and Storage (CCUS) countries will accelerate the development of CCS (IEA, 2013a). Moreover,

utilising biofuel for CCS technology gives additional plus for CCS as a CO_2 harvesting technology from the atmosphere.

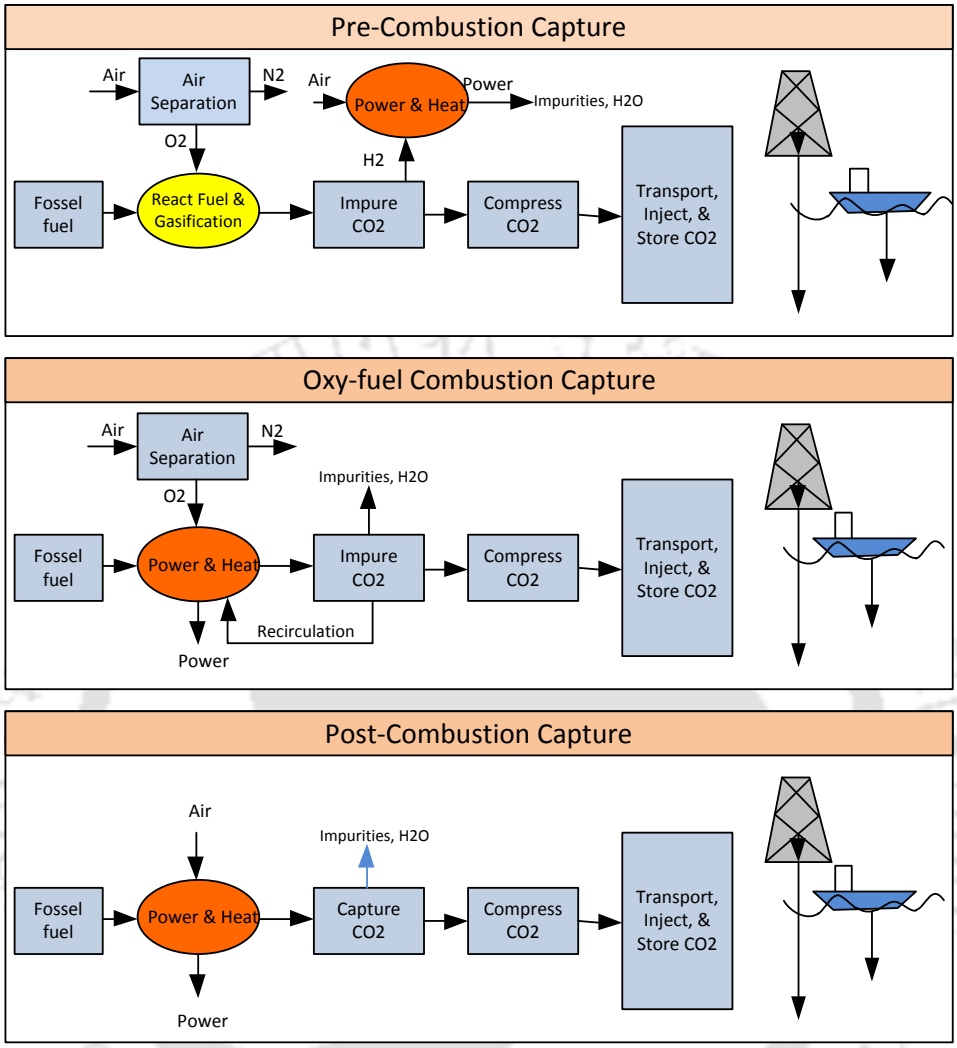

Figure 1.4 the three main categories of carbon capture technologies for power plants

Finally, enhancing the efficiency of CCS power plants leads to optimum CO_2 mitigating technology. The three categories of CCS are briefly explained below:

- *Pre-combustion Capture*: Coal gasification is the heart of this category. Pure O_2 is used to react with fuel under gasification condition. The main outputs are CO and H_2. After converting CO to CO_2, H_2 is oxidized directly by air to release energy; and N_2 and H_2O to the atmosphere directly. However, its application in the power sector is very limited due to the high cost. The integrated gasification combined cycle (IGCC) is one of the cleanest coal power generation technologies. However, IGCC's high cost of electricity generation, complexity of plant, and lower availability have limited the

technology's uptake in the power industry. Additionally, gasification of low rank coals, such as lignite, is still in the developmental stage (Liu et al., 2011).

- *Post-Combustion Capture*: In this category, the conventional combustion occurs using air, and subsequently the CO_2 is scrubbed out of the combustion flue gas using a chemical solvent such as amine or ammonia, to be compressed and stored later on (Liu et al., 2011). It is suitable and attractive for the existing plant, without modification of its structure. In October 2014, the first post-combustion power plant started by SaskPower in Canada (Stéphenne, 2014). Ammonia is used in an absorption tower to scrub CO_2 from the flue gas. The purity of CO_2 capturing in post-combustion capture technologies is higher than 90%. The post-combustion capture technology's minus is the intensive energy needed to regenerate solvent or to cool the flue gas when the chilled ammonia process is employed (Liu et al., 2011).
- *Oxy-fuel Combustion Capture*: Here, pure oxygen is used for fuel combustion directly; the main exhaust constituent will be CO_2 and moisture. CO_2 is separated to be compressed and stored later on. However, the disadvantages of oxy-combustion are the high cost of large quantity of high purity oxygen and lower overall efficiency of power plants. This pure oxygen typically requires high energy for cryogenic air separation. In the first generation of oxy-fuel combustion power plant (retrofitted power plant) large portion of the flue gas CO_2 is recycled back to the furnace to maintain operating temperature and to reconstitute the flue gas volume to ensure proper heat transfer and hydrodynamic behaviour (Liu et al., 2011).

Recently, Chemical Looping Combustion (CLC) is a dawning, and it could be applied for CCS: in this recent rising method, two stages (reactors) are used, one process is endothermic for abstracting oxidant from its carrier (O_2 from air), and the second process is exothermic process. The exhaust is rich of H_2O and CO_2. Finally, CCS is a promised technology and applying CCS could cut 14 Gton/year of CO_2 emission by 2050 (Stangeland, 2007).

Improving net efficiency effects over the GHGs emissions

The average of power plant efficiency is around 37%, which contributes CO_2 emission of 930 g/kWh. The efficiency of current CFBs is 47%, and this improvement cuts 21% of the CO_2 emission. Higher efficiency of 50% leads to more decreament of the CO_2 emission by 34%, and leads to lower fuel requirements (Hotta, 2010). Enhancing the net efficiency is considered

as key solution for mitigating GHGs, reducing fuel consumption. It would cut 27 Gton/year of CO_2 emission; and the reduction of emission by efficiency's contribution will be more than the contributions of both CCS and renewable energy (Stangeland, 2007).

Renewable energy effects over the GHGs emissions

Using biofuel (biomass, sawdust, wood, etc.) in power plant sector is considered as renewable energy. In this case, the released CO_2 is called neutral CO_2. According to (Stangeland, 2007; Hotta, 2010), Co-firing 10% of biomass fuel with coal decreases 10% of CO_2 emission and reduce 7.9 Gton/year of CO_2 emission by 2050.

1.2 Research Aims

Based on several earlier studies of techno-economic assessment, the oxy-fuel CFB combustion appears to be the most energy and cost efficient of the carbon capture technologies. Moreover, the biomass oxy-fuel CFB combustion is a neutral CO_2 emitter. On the other hand, oxy-fuel CFB combustion is only at the first mile, this march is too long, and enormous Research and Development (R&D) is required to outlook the path of oxy-fuel CFB combustion toward the 3rd generation of oxy-fuel CFBC.

The R&D of oxy-fuel CFB combustion is widely over the world. Numerous of CFBs are under design and construction in both industry and research centres. Figure 1.5 illustrates the distribution of some working CFBs under oxy-fuel combustion condition showing the international interest of this technology.

- 0.1 MWth CFBC, VTT, Finland (Pikkarainen et al., 2014; Hultgren et al. 2014).
- 0.8 MWth CFBC, CanMet, Ottawa, Canada (Stewart, 2009; Tan et al., 2012).
- 0.2 MWth CFBC, Cranfield, UK (UKCCSRD 2015).
- 50 kWth CFBC, South University, Nanjing (Duan et al., 2011).
- 1MWth, Chinese Academy of Sciences, Beijing, China (Li et al., 2014).
- 3.0 MWth CFBC, ALSTOM, U.S. Department of Energy, National Energy Technology Laboratory, USA; Oxy-Coal Combustion Test Facilities at University of Utah, USA (INC., 2003; Liljedahl et al., 2006; Eddings and Okerlund, 2009; Ahn et al., 2011).
- 0.1~4 MWth CFBC, Valmet, Chalmers University, Sweden (Seddighi et al., 2015a).
- 0.15 MWth CFBC, (IFK), University of Stuttgart, Germany (Hofbauer et al., 2014).

- 30 MWth CFBC, Foster Wheeler (Hack et al. 2012), CIRCE, Zaragoza, Spain (Lupion et al., 2013; Bolea et al., 2014; Gómez et al., 2014).

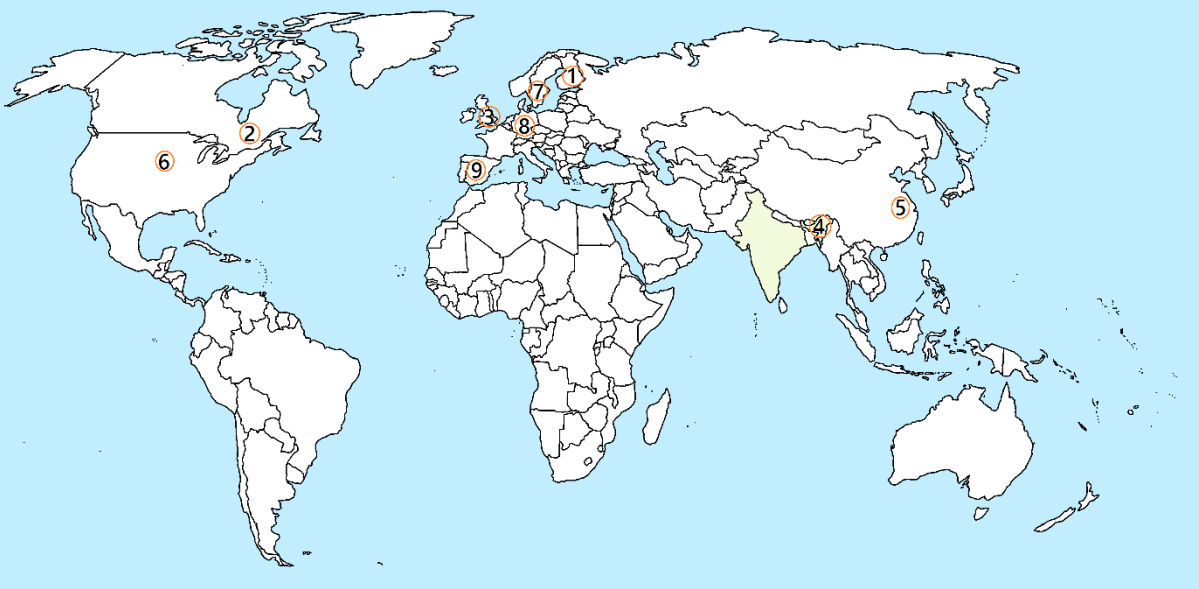

Figure 1.5 Major CFBs working under oxy-fuel combustion conditions at universities, R&D, power plants

Many techniques are being studied and used to mitigate GHGs, and still in progress. Applying CCS technology reduces the overall efficiency by 10-15%, which is caused by air separation unit (ASU) and exhaust gas recirculation (EGR). Therefore, it becomes necessary to improve the oxy-fuel CFB combustion efficiency. Figure 1.6 illustrates visually the main aims of this thesis to enhance the overall efficiency of oxy-fuel CFB combustion and stepping toward next generation of CFB oxy-fuel combustion by enhance efficiency η, minimizing cost of installation and operating, and harvesting CO_2 from atmosphere. In the same trend, Anthony (2014) emphasised on the need for more Research and Development (R&D) direction of oxy-fuel CFBC in the following topics:

- Biomass firing in FBC.
- Use of high O_2 concentrations in the inlet of oxy-fuel CFBC.
- SO_2 capture, NO_x and N_2O chemistry.
- Work on external heat exchangers to absorb the elevated heat release due to high O_2%.

For maturing high O_2 concentration oxy-fuel CFB combustion, experiments in bench and pilot scale facilities are required, and side-by-side, developing and validating the designed models (Anthony, 2014). Finally, the ultimate aims have been addressed in the present investigation:

- Enhance the overall efficiency of the power plant running under the oxy-fuel CFB combustion condition, by enhancing the oxygen concentration.
- Improve the overall efficiency of CCS power plant running under CFB oxy-combustion conditions, by simplifying the design of the power plant through eliminating the setup of recirculation of exhaust gases. In addition, waving the cost of its operation, by increase the concentration of oxygen at the inlet to reach pure oxy-combustion, with zero exhaust gas recirculation.
- Applying and studying biomass pure oxy-fuel combustion for less than zero CO_2 emission.

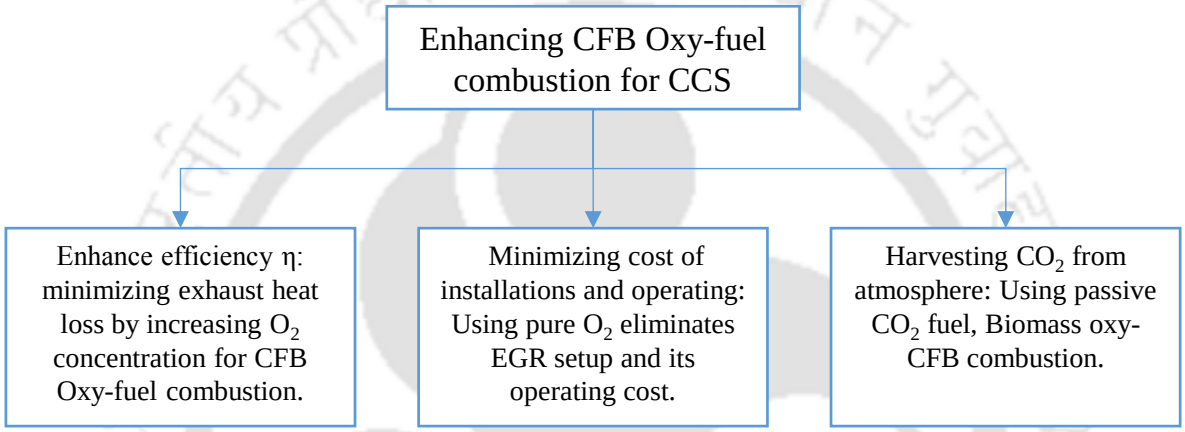

Figure 1.6 Diagram of main thesis's aims to enhance CFB oxy-fuel combustion for CCS, by Enhance efficiency η, Minimizing cost of installation and operating, and Harvesting CO_2 from atmosphere.

Figure 1.6 illustrate the aims of the present work viz. enhancing the efficiency, minimizing the overall cost of oxy-fuel combustion technology, and harvesting CO_2 from the atmosphere, these aims can be achieved by enhancing and applying oxy-fuel CFB combustion.

1.3 Organization of the Thesis

Chapter* 1** introduces the importance of fuel and combined anthropological problems along with promised dawning technologies to mitigate GHGs, and it offers the motivation of the oxy-fuel CFB combustion and followed by the objectives of the thesis. ***Chapter 2 reviews the hydrodynamic behaviour of CFB, fluidization regimes, and fluidization velocities, furthermore, it analyses the solid fuel (biomass and coal) and combustion characteristics, oxy-CFB combustion and its barriers are studied. And, at the end, the research gaps are specified and accordingly the objectives of the thesis are defined. ***Chapter* 3** explains the proposed novel hypothesis of this work for future pure oxy-CFB combustion. Also, it illustrates the new

feeding arrangements to control the combustion temperature; where the stoichiometric ratio is used to control the combustion. ***Chapter* 4** describes the designs of the cold and the hot CFBs, experimental procedures, measurement instaurations, and used materials. ***Chapter* 5** discusses the results for the cold CFB experiments and analysis of several parameters effects over the CFB hydrodynamic behaviour under air and oxy-fuel operating conditions, beside, discussion of the hot CFB units' results and clarifying the applicability of the proposed hypothesis in chapter 4. ***Chapter* 6** presents the thermodynamic study namely exergy and energy studies under air-combustion combustion and oxy-combustion conditions, with comparison at chemical reaction level. Finally, ***Chapter* 7** concludes the work of the cold CFB unit and hot CFB unit, with proposed future work. Figure 1.7 illustrates the road map of the thesis work.

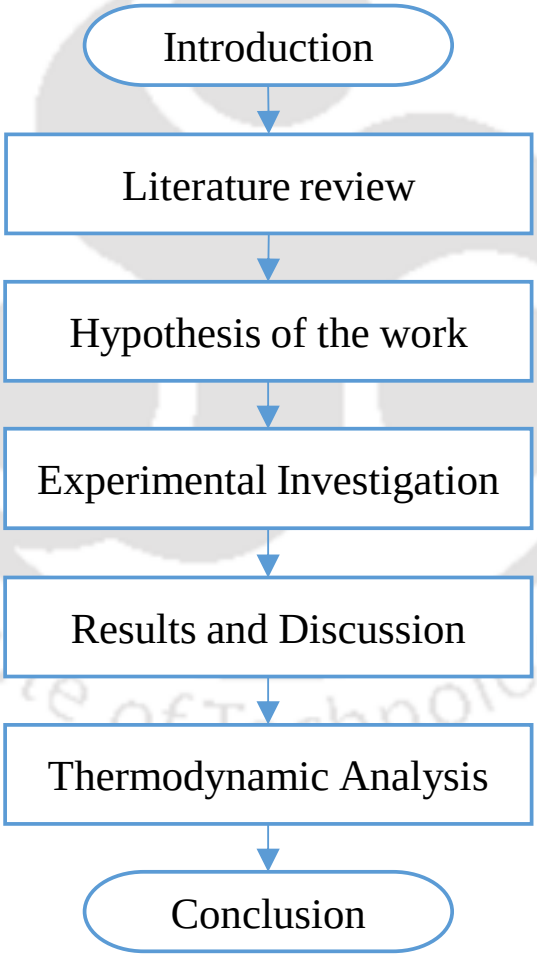

Figure 1.7 Schematic diagram of the Thesis outline

2 Literature Review

Overview

The industrial application of fluidized bed started long back. In 1923, Winkler's coal gasifier represented the first significant large-scale use of fluidized bed (Kunii and Levenspiel, 1991). Now days, the world's largest CFB unit is operating since 2009 at Lagisza, Poland, 460 MW supercritical CFB, Foster and Wheeler. Even though the cheap liquid and gaseous fuels have decelerated the coal and solid fuels R&D.; many sectors increasingly use CFB viz. electricity generation and industrial sectors, because of the CFB's advantages. The 1970th cries reactivated the interest to the solid fuel and coal again. Moreover, the increasing concern of GHGs, cheap cost of coal and its abundant sources motivate again the researches of CFB (IEA-CIAB, 2013). The CCS was considered as an important technology to mitigate GHGs. To apply CCS, novel techniques viz. pre-combustion, post-combustion, and oxy-combustion are raised. Subsequently the R&D are undertaken for understanding the effects of new operation conditions like using gaseous mixture comparing with conventional units. This chapter is dedicated toward the detailed review of literature in the fields of CFB's hydrodynamic behaviour, oxy-fuel combustion and generations of oxy-fuel combustion. It also discusses the literature on lower or zero carbon energy sources (biofuel). The special focus on the biofuel usage for CFB is to service lower or zero carbon energy technology. Finally, the key scopes of the work are identified conveniently with the aims drawn in the earlier chapter.

Chapter outline:

2.1 Hydrodynamics Behaviour in CFB

2.1.1 Fluidization regimes and classification:

Fluidization is the phenomenon by which solid particles are transported into a fluid like state through suspension in a gas or liquid. In fact, there is a simple and precise way to classify the various fluid-particle beds (Winaya et al., 2003; Souza-Santos, 2004; Basu, 2006). Most of the CFB operating and environmental characteristics are the direct results of the hydrodynamic behaviour. Numerous of searchers have studied the hydrodynamics of CFB (Yang, 1998; Basu, 2006; Rhodes, 2008; Scala, 2013). The fluidization is a function of several parameters such like the particles' shape, size and density, velocity of the gas, bed's geometries etc. Kunii and Levenspiel (1991), Oka and Dekker (2004), and Souza-Santos (2004) defined the regimes of fluidization as described below:

a) *Fixed Bed*: When the fluid is passed through the bottom of the bed at a low flow rate, the fluid merely percolates through the void spaces between stationary particles.
b) *Minimum fluidization*: When the gas velocity reaches (U_{mf}) minimum fluidization velocity, and all the particle are just suspended by the upward flowing fluid.
c) *Bubbling Fluid Bed*: When the flow rate increases beyond the minimum fluidization velocity, bed starts bubbling. The gas-solid system shows large instabilities with bubbling and gas channelling with rise in flow rate beyond minimum fluidization. Such a bed is called aggregative, heterogeneous, or bubbling fluidized.
d) *Turbulent Fluidized Bed*: When the gas flow rate sufficiently increases, the terminal velocity (U_{tr}) of solids is exceeded, the upper surface of the bed disappears, entrainment becomes appreciable instead of bubbling,
e) *Fast Fluidized Bed*: With further increasing in gas velocity, solids are carried out of the bed with the gas making a lean phase fluidized, this regime is used for operating CFB. In the present work, fast fluidized bed is used to operate the CFB where the pressure drop decreases dramatically in this regime.
f) *Pneumatic Transport*: Beyond the circulating fluidized bed operating regime, there is the pneumatic transport region, pressure drop increases in this regime.

An appreciated contribution by Geldart (1973) classified the particles based on size and density into four groups viz. C, A, B, and D. Group B (of particle size d_p between 40-500 μm and density of ρ_s<~1400 kg/m^3) is commonly used for CFB. Yang modified Geldart's classification

using Archimedes number *Ar*, under elevated pressure, temperature, and non-dimensional density (Yang, 2007).

2.1.2 Bed hydrodynamics and heat transfer

CFB belongs to the fluidized beds family, which use an inert material like sand to enhance the process in the bed through interacting between fuel and sand particles. The inventory plays a thermal roll. It is considered as a thermal wheel and it enhances the heat transfer where the sand particles contact the reactor wall and rises the hat transfer. The main hydrodynamic parameters of CFB are reviewed and discussed below.

Pressure and Pressure Drop

The flow in a CFB is multiphase. The unrecoverable pressure drop along the riser height is a basic value for design; and this results due to solid particles distribution, voidage, gas viscosity, gas velocity, gas density, and density of solid (Ergun and Orning, 1949). The pressure drop, a basic parameter, can be measured experimentally, calculated using empirical equation, and/or numerically. It is also used to calculate other parameters viz. voidage, and suspension density (Gupta and Nag, 2002). The pressure drop in CFB is the lowest one in the fluidized beds family (Oka and Dekker, 2004). Both of the interaction between particles and fluid, and pressure loss in Newtonian fluids cause the pressure drop (Gibilaro, 2001). The operating pressure affects the heat transfer, and the increased pressure increases the heat transfer (Gupta and Nag, 2002).

Suspension Density

The suspension density represents the density of multiphase fluid at each level of the CFB's riser. Suspension density is given by Eq. 2.1.

$$\rho_{sus} = \rho_s(1-\varepsilon) + \varepsilon\rho_g \tag{2.1}$$

where ρ_{sus} [kg/m^3] is suspension density. ρ_s [kg/m^3] is the solid particle density. ρ_g [kg/m^3] is the gas density. (ε) is voidage at the related level.

Gupta and Berruti (1999) compared and compiled database of suspension density using published experimental data of pilot, laboratory, and industrial scales. Two main zones were found in the riser compromises a dense zone at the bottom of the riser and the dilute zone at the top. The increasing solid flows increased the solids hold up mainly at the dense zone.

Meanwhile, riser's exit affected the upper part of solid hold up profile (Gupta and Berruti, 2000).

Gupta and Nag (2002) performed an experimental study using Circulating Fluidized Bed Combustor (CFBC), and air as an operating gas. They found that the suspension density increased with the decreasing velocity, due to decreased carrying up of particles and residence time of particle in the riser decreases at lower velocity, this results a higher sand inventory in the riser. On the other hand, suspension density increased with the increased pressure, hence, the density of gas increases and holding up buoyancy force rises (Gupta and Nag, 2002). Ersoy et al. (2004) focused on the secondary air injection effects over the CFB hydrodynamics behaviour. Above the secondary air level, they found dilute zone, and dense one below. Same suspension density profile was found viz. dense zone at the bottom, and dilute one at the upper zone of riser (Ersoy et al., 2004).

Subsequently, the suspension density affects heat transfer between bed and wall. Patil et al. (2011) studied CFB's heat transfer characteristics, suspension density, and pressure drop. Suspension density decreased with height of the riser, in the same trend of pressure drop. Likewise, heat transfer coefficient increased with height of riser. They developed an empirical correlation of Nusselt number of the bed as a function of Reynolds number, suspension to gas density, and riser height to hydraulic riser diameter. This study was carried out using air as operating gas.

Bed Voidage

Bed voidage represents the gas volumetric percentage of multiphase flow in the CFB. The voidage profile clarifies the solid distribution (inert material-sand, additives solid particles, and solid fuel particles), and the mobility of particles between the combustor wall and the bed. This mobility enhances the heat transfer characteristics of the CFB unit (Backhurst and Richardson, 2002). Bed inventory improves fuel particles reaction and the overall heat transfer in the CFB unit. Voidage can be experimentally determined by a several methods, for instance, through image analysis. Casleton et al., (2010) improved the image analysis by benefiting of particles' specular reflections. Mahmoudi et al. (2011) used single radioactive particle tracking technique. The bed voidage can be also calculated by measuring the pressure drop in U-tube manometer along the riser height, and then applying Eq. 2.2 (Kunii and Levenspiel, 1991).

$$\varepsilon = 1 - \frac{\rho_L \times \Delta h}{\rho_s \times L_m} \tag{2.2}$$

where, Δh $[m]$ is the difference of liquid levels in the manometer. ρ_s $[kg/m^3]$ is the density of the solid. ρ_L $[kg/m^3]$ is the density of the measuring liquid. L_m $[m]$ is the height difference of the sequenced taps. Voidage is represented by axial and lateral voidage, which finally gave a three dimensional (3-D) voidage visualization. Axial voidage of fast bed CFB is a flattened 'S' profile, at the bottom section, the solid fraction is higher compared to the upper section. Consequently, the voidage is low and varies at the bottom from 0.8 to 0.9, and it could touch 0.99 at the top of the riser (Basu, 2015).

Horizontal section area of the riser shows varied voidage, called as the lateral voidage. Friction near the wall decreases the velocity compared to the core of the riser and divides the section to *annular zone* (downward movement of the particles); and *core one* (upward movement of the particles). The thickness of wall layer increases from top to bottom and plays a crucial role in heat transfer (Basu, 2015).

Gupta and Nag (2002) studied the voidage and suspension using air in a PCFB with sand particles of 260μm diameter, and superficial velocity of air between 0.25 [m/s] and 1.25 [m/s]. Das et al. (2008) used sand, iron, and coal; and mixed particle system as an inventory, and found that axial bed voidage increased with an increased air velocity. In contrast, when solid circulation rate and particle size increased, the bed voidage decreased. In that investigation, less attention was paid for aeration (Das et al., 2008). A similar observation was found by Adfinez et al. (1994). Zhang et al. (2015) found that the overall voidage is a function of operating gas velocity (U), solid circulation rate (G_s), distance from distributing plate, and riser diameter. Zhang et al. (2015) used tomographic imaging technique for determining (ε); tomographic imaging gives real time results, non-obstructive measuring technique, even under high pressure and temperature.

Guedea et al. (2011) studied the fluid-dynamics under oxy-condition using O_2-CO_2 mixture of percentages from 3-97 % to 40-60 %, plus air as an operating gases. Pressure drop for oxy condition was higher compared to air case, due to the higher density of O_2-CO_2 mixture where CO_2-N_2 density ratio is 1.6. The minimum fluidization velocity, U_{mf} of 21-97% O_2-CO_2 case is lesser than U_{mf} of air case. This study is carried out for bubbling fluidized bed (BFB) (Guedea

et al., 2011). Li et al. (2014) performed an experimental study of CFB using air, loop-seal as a non-mechanical valve, and Geldart group *A* of silica gel particle. Rate of solid circulation is increased by increasing the velocity and aeration flow rate. Elevated rate of solid circulation from 25 to 60 kg/h raised the velocity in the standpipe from 0.00125 to 0.0045 m/s.

2.1.3 Fluidization velocities

The gas velocity and interaction with particles play a crucial rule in characterizing the fluidization behaviour of the CFB. To calculate the fluidization velocities some basic dimensionless numbers such like Reynolds number (*Re*), Archimedes' number (*Ar*), and particle dimensionless size (d_p^* .) are required. These are represented below by Eqs. 2.3, and 2.4, respectively.

$$\mathrm{Re} = \frac{d_p u_g \rho_g}{\mu} \tag{2.3}$$

$$Ar = \frac{d_p^3 \rho_g (\rho_s - \rho_g) g}{\mu^2} \tag{2.4}$$

Minimum Fluidization Velocity, U_{mf}

The minimum fluidization velocity is a basic required value for designing and developing a fluidized bed. Many researcher studied the relation between unrecoverable pressure loss ΔP and gas velocity U_g (Gibilaro, 2001; Ergun and Orning, 1949). The results of their experiments show a clear decrease in minimum fluidization velocity with increased pressure for particle larger than 100μm (Geldart B and D groups) compering with particle of size less than 100 μm. The convenient relation Ergun and Orning (1949) gives the pressure drop as expressed in Eq. 2.5.

$$\Delta P = 150 \cdot \frac{\mu_f L U}{d_p^2} \cdot \frac{(1-\varepsilon^2)}{\varepsilon^3} + 1.75 \cdot \frac{\rho_f L U^2}{d_p} \cdot \frac{(1-\varepsilon)}{\varepsilon^3} \tag{2.5}$$

Eq.2.6 can also be expressed in terms of Reynolds number

$$\Delta P = 1.75 \cdot \frac{\mu_f L U}{d_p^2} \cdot \frac{(1-\varepsilon)}{\varepsilon^3} \cdot [85.7(1-\varepsilon) + \mathrm{Re}_p] \tag{2.6}$$

To calculate the minimum fluidization velocity (U_{mf}) for minimum voidage (ε_{min}), Ergun equation is rearranged as following, in Eq. 2.7 as a function of $U_{mf}, \rho_g, and\ \mu$ or Eq. 2.8 as a function of *Re*.

$$\frac{1.75}{\varepsilon_{mf}^3 \varphi_s}\left(\frac{d_p U_{mf} \rho_g}{\mu}\right)^2 + \frac{150\left(1-\varepsilon_{mf}\right)}{\varepsilon_{mf}^{\ 3} \varphi_s^{\ 2}}\left(\frac{d_p U_{mf} \rho_g}{\mu}\right) = \frac{d_p^3 \rho_g (\rho_s - \rho_g) g}{\mu^2} \tag{2.7}$$

$$\frac{1.75}{\varepsilon_{mf}^3 \varphi_s}\mathrm{Re}_{mf}^2 + \frac{150\left(1-\varepsilon_{mf}\right)}{\varepsilon_{mf}^{\ 3} \varphi_s^{\ 2}}\mathrm{Re}_{mf} = Ar \tag{2.8}$$

The voidage at minimum fluidization condition for group of species and different particle sizes (Leva, 1959). Whereas, many researchers developed correlations to calculate Reynolds number at minimum fluidization (U_{mf}), at onset of fluidization, Re_{mf} is given by Eq. 2.9.

$$\mathrm{Re}_{mf} = \frac{U_{mf} d_p \rho_g}{\mu} = \sqrt{C_1^2 + C_2 Ar} - C_1 \tag{2.9}$$

As reported, Ergun equations (Eq. 2.7 and Eq. 2.8) gave a closer fit for spherical particles, on the other hand, the correlation of Wen and Yu (1966) was in better agreement for irregular solids. Table 2.1 provides the comparison of correction constant C_1 and C_2 developed by various researchers for prediction of the minimum fluidization velocity at elevated pressures. As observed, the minimum fluidization velocity, the bubbling velocity, and the terminal velocity were found to decrease with an increased operating pressure, due to increase in gas density with pressure.

Table 2.1 Comparison of correlation constants

Reference	Pressure range	Bed Material	Constant C_1	Constant C_2	$\frac{1-\varepsilon_{mf}}{\varepsilon_{mf}^{\ 3}\varphi_s^{\ 2}}$	$\frac{1}{\varepsilon_{mf}^3 \varphi_s}$
Wen and Yu (1966)	Atmospheric	Fine powder	33.70	0.0408	11	14
Wen and Yu (1977)	179-834 kPa	Core dolomite	25.28	0.0571	---	---
Chitester et al. (1984)	2169, 4238 and 6306 kPa	Ballotini particles	28.70	0.0494	7.94	11.57
Nakamura et al. (1985)	4900 kPa	Geldart B and D Glass beads	33.95	0.0465	---	---
Basu (2006)	High	---	25.25	0.0651	5.19	8.81

Terminal velocity

Reynolds number which matches terminal velocity is given by Eq. 2.10 for all flow fluidization regimes (Gibilaro, 2001) and the terminal velocity of spherical particles is calculated by Eq. 2.11.

$$\mathrm{Re}_t = \left[-3.809 + (3.809^2 + 1.832 \times Ar^{0.5})^{0.5}\right]^2 \tag{2.10}$$

$$u_t = \mathrm{Re}_t \, \mu / (d_p \rho_g) \tag{2.11}$$

Haider and Levenspiel (1989) proposed Eq.2.12 to calculate the drag coefficient $C_D = F_D / \left(\frac{1}{2}\rho U^2\right)$ for non-spherical particles with root mean square deviation (RMS) errors of 3.1% (Haider and Levenspiel, 1989).

$$C_D = \frac{24}{\mathrm{Re}}\left[1 + \left[8.1716\exp\left(-4.0655\phi\right)\right]\right]\mathrm{Re}^{(0.0964+0.5565\phi)} + \frac{73.69\,\mathrm{Re}\exp\left(-5.0748\phi\right)}{\mathrm{Re} + 5.378\exp(6.2122\phi)} \tag{2.12}$$

Meanwhile, Eq. (2.13) is more accurate but is more complex as compared to Eq.2.12.

$$C_D = \frac{24}{\mathrm{Re}}\left[1 + \exp\left(2.3288 - 6.4581\phi + 2.4486\phi^2\right)\mathrm{Re}^{(0.0964+0.5565\phi)}\right] + \frac{\mathrm{Re}\times\exp\left(4.905 - 13.8944\phi + 18.4222\phi^2 - 10.2599\phi^3\right)}{\mathrm{Re} + \exp\left(1.4681 + 12.2584\phi - 20.7322\phi^2 + 15.8855\phi^3\right)} \tag{2.13}$$

The terminal free-fall velocity is estimated by Eq. 2.14.

$$u_t = \left[\frac{4 d_P \left(\rho_s - \rho_g\right)}{3\rho_g C_D}\right]^{1/2} \tag{2.14}$$

Transport Velocity of spherical particles is calculated by Eq. (2.15) (Basu, 2006).

$$u_{tr} = 1.45 \times \frac{\mu}{(\rho_g d_p)} Ar^{0.484}, \text{where } 20 < \mathrm{Ar} < 50,000. \tag{2.15}$$

Moreover, fluidization regime is important to predict the fluidization behaviour; whether the inventory is bubbling, circulating, etc. Grace (1986) mapped the fluidization regimes viz. bubbling fluidized bed, spouted bed, fast fluidized bed, pneumatic transport, minimum

fluidization, and onset of turbulent fluidization bed as shown in Figure 2.1 (Grace, 1986). Dimensionless particle size and dimensionless gas velocity are defined by Eqs. 2.16 and 2.17.

$$d_p^* = d_p\left[\frac{\rho_g\left(\rho_s-\rho_g\right)g}{\mu^2}\right]^{1/3} = Ar^{1/3} = \left(\frac{3}{4}C_D\,\mathrm{Re}_p^2\right)^{1/3} \tag{2.16}$$

$$u^* = u\left[\frac{\rho_g^2}{\mu\left(\rho_s-\rho_g\right)g}\right]^{1/3} = \frac{\mathrm{Re}_p}{Ar^{1/3}} = \left(\frac{4}{3}\frac{\mathrm{Re}_p}{C_D}\right)^{1/3} \tag{2.17}$$

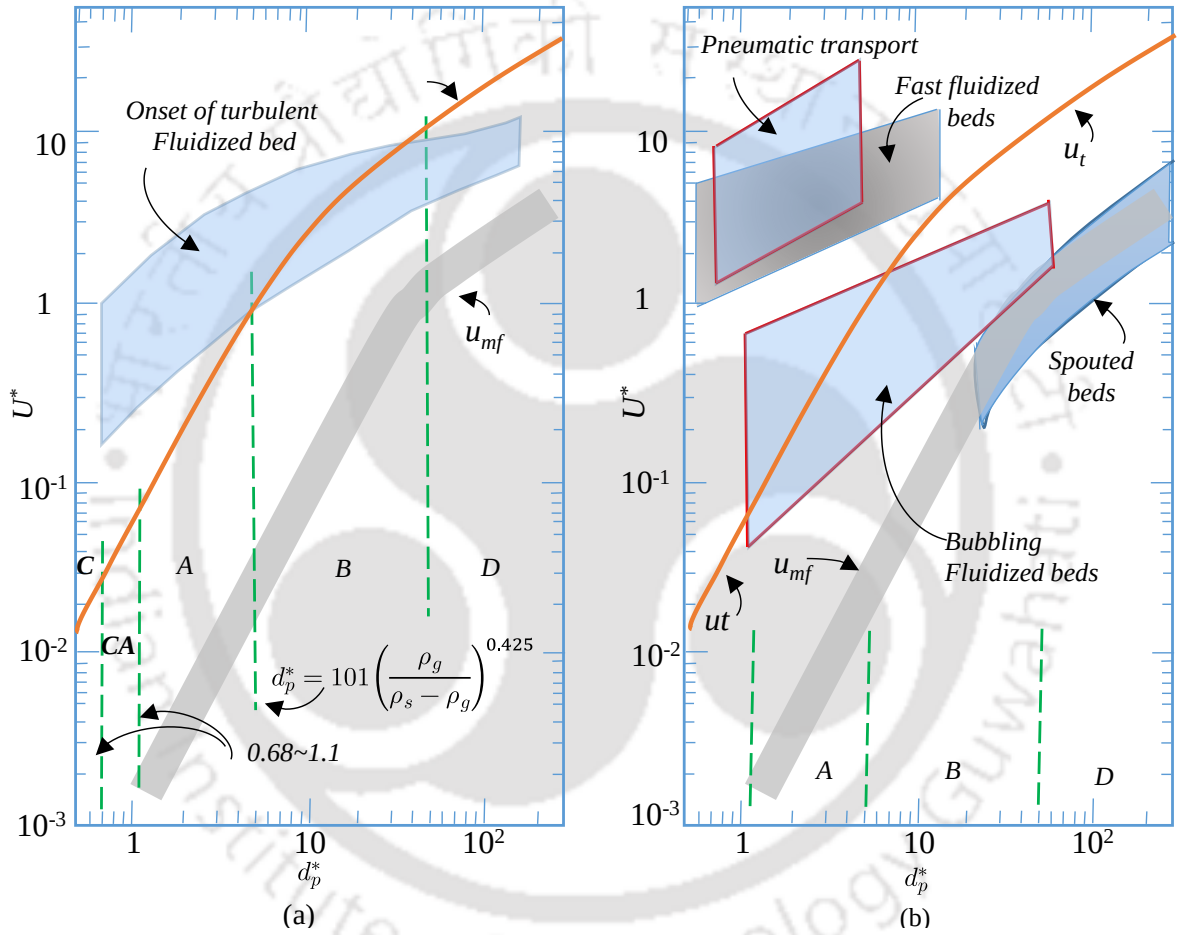

Figure 2.1 General flow regime diagram over a wide range of dimensionless velocity, dimensionless particle size, and solid particle Geldart classification (Grace, 1986).

This diagram can be used for the design procedure by choosing fluidization regime, then calculating dimensionless velocity and dimensionless particle size based on characteristics of operating gas and solid using Eqs.2.16, and 2.17, and subsequently operating velocity and particle size, which match with the required fluidization regime.

2.2 Combustion and Hot CFB Unit Review

This section of literature review is dedicated for discussing coal and biomass fuels characteristics and combustion, oxy-combustion characteristics, evaluation and generations of oxy-fuel CFB combustion along with a review of recent studies on oxy-fuel CFB combustion.

2.2.1 Coal characteristics and classification

Coal is ranked based on proximate analysis, which detects moister, volatile matter, fixed carbon, and ash. Figure 2.2 shows the main coal ranks with calorific values, which are mainly Lignite, Bituminous, and Anthracite. *Lignite coal*: the youngest coal, and has the highest moisture and lowest fixed carbon contents. Lignite's calorific value is very low as compared to the rest sorts of coal. Lignite tends to fragment during firing.

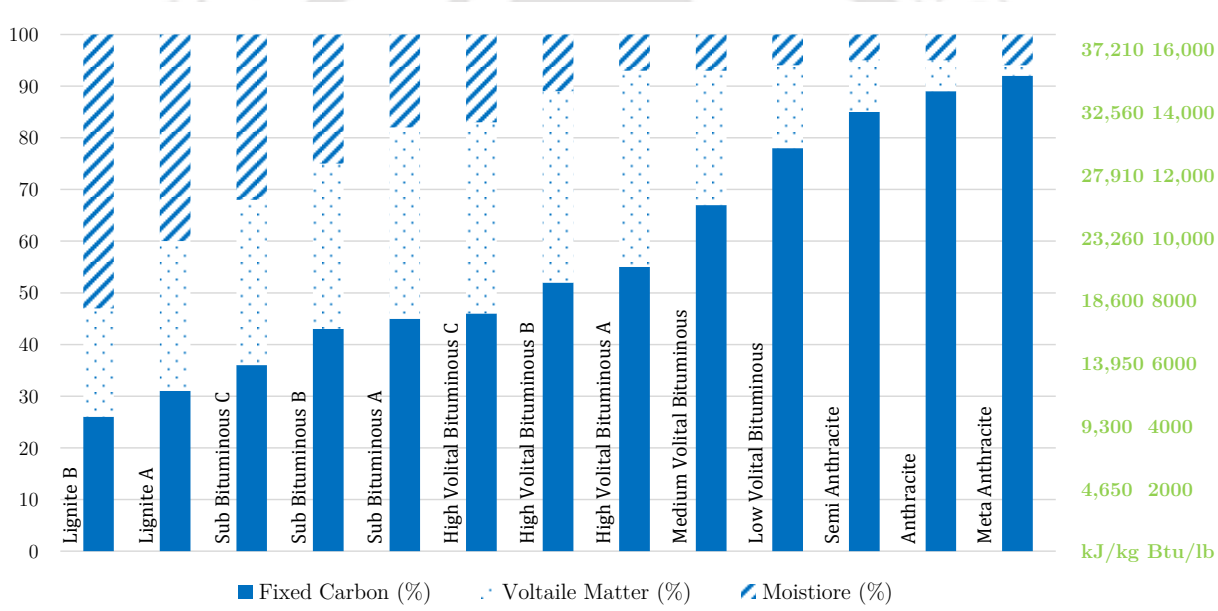

Figure 2.2 Coal rank with calorific value and proximate analysis (Nag, 2008).

Sub-bituminous coal: its colour becomes black, fixed carbon and calorific value increase, and moisture decreases slightly comparing with lignite coal.

Bituminous coal: the most utilised coal. It has the highest calorific value, black colour, and has three sub-ranks; high volatile matter, medium volatile matter, and low volatile matter.

Anthracite coal: the higher rank and has high calorific value, but less than bituminous. It contains small amount of moisture, volatile matter, and high fixed carbon percentage. Its

structure is like graphite. Anthracite has three sub-ranks; Semi anthracite, anthracite, and meta-anthracite (Nag, 2008).

2.2.2 Biomass characteristic and classification

Biomass is considered as a renewable energy source, and biomass fuel generally contains low percentage of nitrogen and sulphur as compared to with coal and it has a superiority over the conventional fuels, since biomass fuel is a carbon neutral. Biomass is a part of the carbon cycle, and its combustion is a quick way to release its energy compared to natural decomposition. As a result, biomass fuel has a promised potential to mitigate GHGs, NO_x, and SO_x (Khan et al., 2009; Agbor et al., 2014).

In 1961, Van Krevelen mapped solid fuel (coal and biomass) as a function of O/C ratio and H/C ratio, where the biomass has the heist ratios of H/C and O/C, and gradually these ratios decrease for peat, lignite, bituminous and anthracite (Figure 2.3). Additionally, the biomass is the raw material of coal, where organic materials are subjected to geological pressure and heat over a millions of year. Gradually, the structure of the biomass is changing over the time, both of H/C and O/C ratios decreas from 1.2 to 0.4, and from 0.5 to 0.05 respectively, with increased calorific value (Maffei and Milano, 2013).

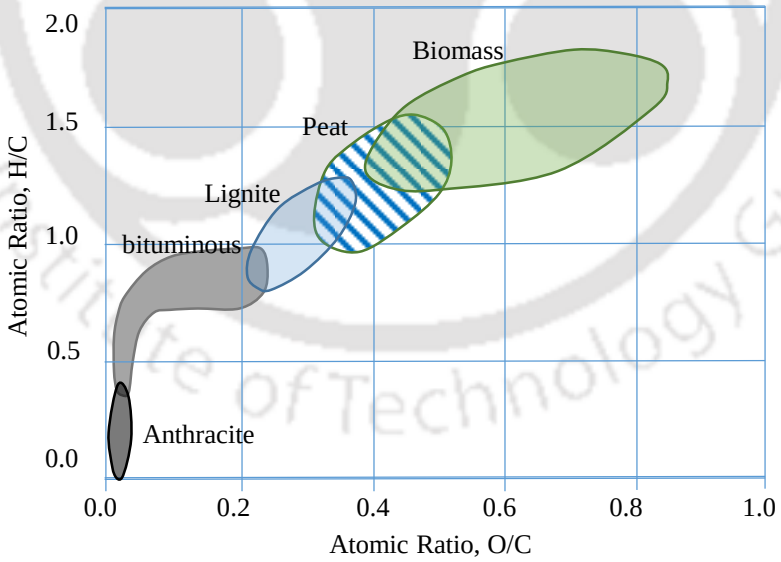

Figure 2.3 Van Krevelen diagram of O/C and H/C atomic ratio (Maffei and Milano, 2013)

Cremers (2009) sorted the biomass into four categories namely agriculture products, forestry products, domestics and municipal wastes, and energy crops. Interestingly, the biomass usage is older than fossil fuel viz. oil, gas, and coal. And, it is considered to be the first used fuel

(hydrocarbon) by human. Now days, a special energy crops are planted to produce carbon neutral energy. Moreover, the biomass could be categorized based on its properties viz. aquatic biomass, woody biomass, energy crops, wastes, and derivate fuel from paper waste and food industries (Scarlat et al., 2011). Beside the environmental advantages, biomass fuel has a reasonable price comparing with other renewable energy (Spliethoff and Hein, 1998). Generally, the carbon (C), hydrogen (H_2), and oxygen (O_2) compositions of biomass are in ranges of 45±15%, 5±1%, and 40±10% respectively (Khan et al., 2009).

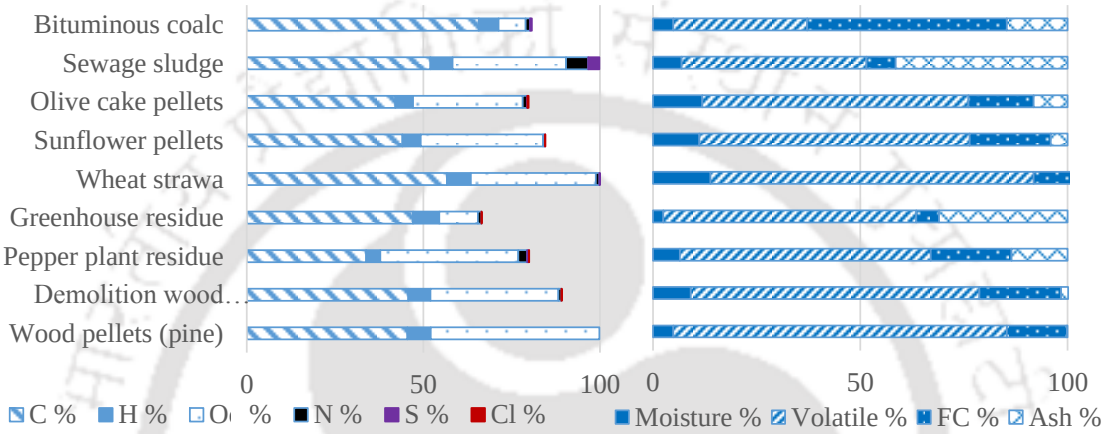

Figure 2.4 Proximate and ultimate analyses of bituminous and some biomass (adapted from Khan et al. (2009)).

On the other hand, there are some technical issues related to biomass fuel utilization viz. ash, agglomeration, NO_2, NO_x, dust emission and corrosion (Nussbaumer, 2003), and meeting the high future demand of biomass can be achieved by energy farming, where the cost vary based on the land and labour (Broek, 2000).

Both of coal and biomass belong to the same family of natural solid fuel. Where coal is the result of natural breaking down of the biomass. Figure 2.4 shows the proximate analysis and ultimate analysis of bituminous, wood pellets, demolition wood pellets, pepper plant residue, greenhouse residue, wheat straw, sunflower pellets, olive cake pellets, and sewage sludge (Khan et al., 2009). The ultimate analysis of biomass shows a high carbon concentration in a range of 45±15%; meanwhile, the oxygen concentration of biomass (except greenhouse residue) is as high as 40±10 compared to 7.7% of bituminous; the hydrogen content counts 4±1%; and small percentages of nitrogen (N), sulphur (S), and calcium (Ca). On other hand, the proximate analysis shows a moisture, and a volatile matter fall in ranges of 8±4%, 55±25% respectively; in contrast, fixed carbon of bituminous is the highest for 48% compared to 17±4% of biomass. It may be inferred that there is similarity between the coal and the biomass in terms

of the chemical components. Still the physical properties viz. density, porosity, internal surface area, and friability differ, which required different pre-processing techniques and feeding systems for fluidized beds. Khan et al. (2009) stated that neither of the technical, economical, nor environmental could be an insurmountable barriers of the sustainable biomass sources. As a result, it is a promised area to be studied in details with new combustion aspects like oxy-combustion.

2.2.3 Combustion characteristics

Combustion is a rapid chemical reaction (oxidization), where the stored energy is released mainly in thermal form (high temperature gases). Minor portion of released energy is electromagnetic (light), mechanical (noise), electric (free ions and electrons). Almost the process steps of combustion are the same for coal and biomass (Figure 2.5).

Figure 2.5 illustrate the steps of single coal particle combustion. Coal involves several species (moisture, volatile matter, char, and ash), coal and biomass combustion is complex multi-phase process involves drying, devolatilization, homogeneous reactions, heterogeneous reactions, pyrolysis releases light gaseous species and heavy species (TAR).

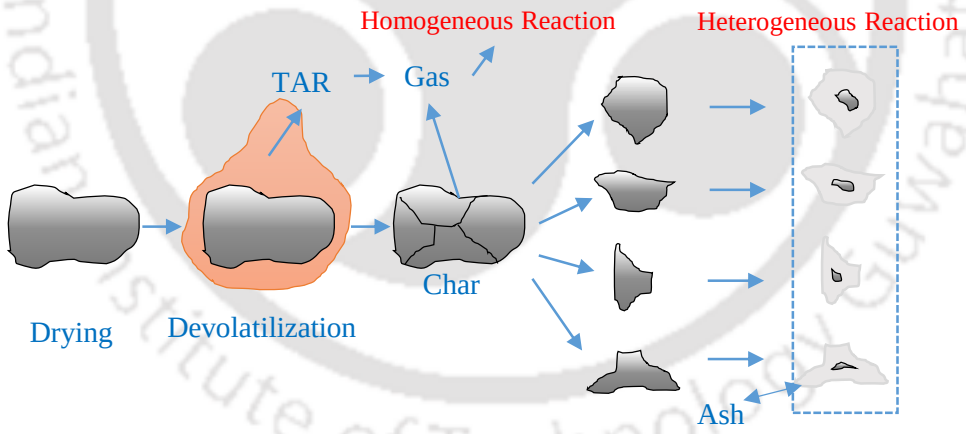

Figure 2.5 Single particle combustion process

The combustion phenomena is affected by several factors namely the physical and chemical fuel characteristics, fuel structure, the combustion atmosphere surrounding the fuel like O_2 percentages, temperature, heat transfer and physical properties of the gases. The oxy-fuel combustion condition changes the combustion characteristics such like ignition temperature, drying, devolatilization, homogeneous and heterogeneous reaction, since, the physical and chemical properties of O_2-CO_2 differs from of air.

In the following, several fundamental and applied studies have been reviewed.

A. Combustion Fundamental studies

Molina and Shaddix (2007) carried out experiments in optical entrained flow reactor, they used bituminous coal particles of 106-125 μm, temperature of 977°C and oxygen concentration of 20-30%, and they found that ignition delay time increase with decreasing of O_2 and presence of CO_2. Complete time of volatile matter combustion remained almost constant. Interestingly, oxygen combustion of 32% oxygen concentration of O_2-CO_2 mixture gave compared flame temperature to air combustion.

In 2012, Khatami et al. worked on single particles bituminous coal combustion and char combustion. The experiments were conducted with size of 75-90 µm in both O_2-CO_2 and O_2-N_2 atmospheres of 20-100% oxygen concentration and furnace wall temperature of 1127 °C. Drop Tube Furnace (DTF) is used. They found that increased oxygen concentration in flow O_2-CO_2 mixture from 21 up to 70% decreased the ignition delay. This agrees with the results of Molina and Shaddix (2007). Meanwhile, the ignition delay remained constant for O_2-N_2 mixture. The ignition delay time for O_2-CO_2 mixture case is longer compared to ignition delay time for O_2-N_2. This is due to, the higher specific heating value C_v of CO_2 compared to N_2 ($C_{v\text{-}CO2}/C_{v\text{-}N2}$=1.66); the O_2 diffusivity in CO_2 is lower comparing with O_2 diffusivity in N_2. Also, higher specific heating value C_v of CO_2 compared to C_v of N_2 leads to lower temperature of the flow at constant furnace wall temperature for O_2-CO_2 mixture case (Khatami et al., 2012).

Bejarano and Levendis (2008) investigated single coal (bituminous and lignite) particle of size 45-180 μm, using DTF at temperature of 1127 °C and 1327 °C, and 21-30-35% oxygen concentration. Expectedly, the particle temperature in O_2-N_2 was higher comparing with O_2-CO_2, this finding matched those of Molina and Shaddix (2007) and Khatami et al. (2008). Increased oxygen concentration and similarly decreased particle sizes raised the particles temperature and lowered the burning time. For lignite coal, the equivalent temperature of air combustion was attained to 25% O_2 content in O_2-CO_2 (Bejarano and Levendis, 2008). Rathnam et al. (2009) conducted experiments to measure pulverised Australian coal using a thermosgravimetric analyser (TGA) at 1200 °C and drop tube furnace (DTF) at 1490 °C. Used oxygen concentrations were 3-21 vol. % in O_2-N_2 mixture, and 5-30 vol. % in O_2-CO_2mixture. Additional mass loss of coal in O_2-CO_2 thermo-gravimetric analysis (TGA) experiment was

recognized, and this could be pertained to CO_2 gasification reaction with coal. Char reactivity increased significantly by increasing O_2 concentration.

Shaddix and Molina (2009) reported ignition and devolatilization of coal at 1427 °C, and O_2 concentration range of 12–36 vol. % in O_2-N_2 mixture and O_2-CO_2 mixture. They found that increased O_2 concentration led to shrinking soot cloud size; and led to increased devolatilization and combustion temperature; and led to decreased ignition delay because of enhanced local mixture reactivity. Brix et al. (2009) examined devolatilization and char conversation at 900-1400 °C and 5-28 vol. % of oxygen concentration in O_2-N_2 mixture and O_2-CO_2 mixture. Char morphology behaved similarly in both atmospheres O_2-N_2 mixture and O_2-CO_2. And, Char conversion rates was not influenced by char CO_2 reaction.

Maffei et al. (2013) paid attention to combustion time and temperature of particles surface. Additionally, coal combustion model was proposed. The increased O_2 concentration raised up the particle surface temperature for both lignite and bituminous coal over the O_2 concentration range of 20-100%; and decreased significantly the lifetime of particle over the O_2 concentration range of 20-60%. The measured particle temperature of Lignite was 100-200 K higher comparing with bituminous particle. And, the 80μm bituminous particle life time is 25ms, 55ms, and 160ms at 100%, 40%, and 21% O_2 in O_2-N_2 mixture respectively. The 80μm particle life time is almost the same for bituminous and lignite for 60% O_2 concentration 60% and above (Maffei et al., 2013). Table 2.2 summarizes operating temperature and oxygen percentages of the reviewed researches.

Table 2.2 Temperature and oxygen concentration ranges for oxy-fuel combustion experiments

Researchers	T [°C]	O_2 [%]	Year
Molina and Shaddix	977	21-30	2007
Bejarano and Levendis	1727-2927	20-100	2008
Rathnam et al.	1200-1490	3-30	2009
Shaddix and Molina	1427	12-36	2009
Brix et al.	900-1400	5-28	2011
Khatami et al.	1127	20-100	2012
Maffei et al.	1450-3200	20-100	2013

Through time, higher concentration of O_2 is being used for oxy-fuel combustion observation by researchers, to clarify the effects of high O_2 over the combustion behaviour.

B. Ignition Characteristics

The ignition temperature, T_{ign}, is an important parameter for designing the starting up method of the CFB (Yang et al., 2005). Many factors affect the ignition temperature viz. fuel type and components, oxygen concentration, steam, and the temperature of the furnace. Yang et al. (2005) studied the ignition temperature of seven types of coal and found that the ignition index increased with decreased particle size, increased furnace temperature, increased volatile matter. The moisture contents increase the ignition index at higher temperature since evaporated moisture increases the porosity, which increases the specific surface area. However, the moisture decreases the ignition index at lower temperature. The ignition temperature increased from 450°C to 800°C for decreased volatile matter from almost 50% to 7% for foreign CFBs; and from 600°C to 750°C for Chines CFBs. We have derived two equations from fitting the experimental data to get relationship between $T_{ign.}$ and VM. This derivation Eq. (2.18) for foreign CFBs is based on Yang et al. data (2005).

$$T_{ign.} = 854.48 \times VM^{-0.097} \qquad : R^2 = 0.9932 \tag{2.18}$$

And the derivation for Chines CFBs (Eq. (2.19) is based on Yang et al. (2005).

$$T_{ign.} = 1367.8 \times VM^{-0.285} \qquad : R^2 = 0.9962 \tag{2.19}$$

Riaza et al. (2011) studied the coal ignition under oxy-fuel combustion atmosphere viz. 21%-79%, 30%-70%, 35%-65% (O_2-CO_2). The ignition temperature decreased with increased O_2 concentration. Where the added steam increased the ignition temperature and worsened the coal burning. For semi-anthracite coal of 9.2% of volatile matter (VM), the ignition temperatures of 732°C, 669°C, and 642°C for oxygen concentrations of 21%, 30%, and 35% subsequently; meanwhile for high-volatile bituminous of 33.9% VM, the ignition temperatures were 554°C, 498°C, and 490°C for the same O_2 concentration correspondingly. In all cases, the ignition temperature for air case were less comparing with oxy-fuel case at the same O_2 concentration 21%.

A study by Wu et al. (2015), showed the effects of air and oxy-fuel conditions over the self-ignition of coal dust. The coal dust was tested in hot-oven and over a hot plate, which covered with a layer of coal dust. The ignition temperature varied between 120°C and 145°C, where, increased O_2 concentration led to lower ignition temperature and shorter ignition delay time. On the other hand, recently, Moroń and Rybak (2015) studied the ignition temperature of a

single coal particles of size between 215 and 815 μm. This study shows a higher ignition temperature of 375°C to 475°C compared to this results of Wu et al. (2015). This is pertained to higher particle size.

Jones et al. (2015) studied the risk of biomass ignition for olive cake, mesquite, sunflower husk, miscanthus, plane, pine, and red berry juniper. Based on Derivative Thermo-gravimetric Analysis (DTG) analysis, the maximum weight loss temperature T_{MWL} full in range of 286°C up to 330°C. The pyrolysis active energy increased with the increased T_{MWL}, and in contrast, the risk of ignition decreased increased active energy and T_{MWL}.

Cahyadi et al. (2013) studied the coal ignition for three species under air namely 21%-79% O_2-N_2 and different oxy-fuel combustion conditions viz. 21%-79%O_2-CO_2, 30%-70%O_2-CO_2, and 40%-60%O_2-CO_2 using (TGA) and differential thermal analysis (DTA). They burn out of sub-bituminous coal decreased from 948°C to 663°C and then to 639°C, for 21%-79% O_2-CO_2, 30%-70% O_2-CO_2, and 40%-60% O_2-CO_2 concentration. Meanwhile, burn out temperature under air condition was only 754°C compared to 948°C of 21%-79% O_2-CO_2. This could be pertained to lower diffusion rate of O_2 in O_2-CO_2 mixture comparing with mixture O_2-N_2. Moreover, a lower ignition temperature was indicated for higher particle size. The ignition temperatures of bituminous and sub-bituminous coal were higher compared to lignite, since the ignition mechanism of lignite is homogeneous, while it is heterogeneous for bituminous and sub-bituminous.

An interesting study of single coal particle ignition was carried out by Ponzio et al. (2008) under O_2 concentration from 5% up to 100%, and oxidizer temperature of 600 °C, 800 °C, and 1000 °C. Under O_2 concentration from 5% to 50%, the particle temperature at the moment of ignition decreases for all oxidant temperature till reaching 50% O_2 concentration of the oxidant. Furthermore, for 50~100% O_2 concentration of the oxidant, the particle temperature at the moment of ignition becomes uniformed for all oxidant temperatures. Qiao et al. (2010) discovered similar findings.

2.2.4 Oxy-fuel CFB combustion

For long time, the oxygen of air was the main source of oxidant with fixed volumetric percentage of 21%. Almost 50 years ago, the Oxygen Enhanced Combustion (OEC) was proposed to enhancing the efficiency of combustion. But, the expensive oxygen separation was

one of this technique's barriers. When the cost is being mitigated, the door was opened widely for OEC (Baukal, 1998). Main purposes of applying OEC are enhancing thermal efficiency, reducing volume of exhaust gases, reducing pollutant emission, and increasing processing rate. Abraham et al. (1982) suggested *Oxy-Fuel Combustion* to generate CO_2 exhaust gas for *Enhanced Oil Recovery* (EOR). Wang et al. (1988) applied this idea in. Technically, the modern generation of oxy-Combustion for CCS could be considered as a development and combination of enhanced oxy-combustion and oxy-combustion for enhanced oil recovery (Figure 2.6).

The similarity between Oxy-Combustion for CCS and Enhanced Oxy-Combustion is the increased concentration of oxygen in the oxidant compared to conventional combustion with 21% O_2 in air, and the difference is in the oxidant components, which is O_2-N_2 for EOC compared with O_2-CO_2 mixture for oxy-combustion. On the other hand, the similarity between Oxy-Combustion for CCS and Oxy-combustion for Enhanced Oil Recovery (EOR) is the eliminating of Nitrogen from oxidant by Exhaust Gas Recirculation (EGR); and ability to inject the exhaust in the oil reservoir.

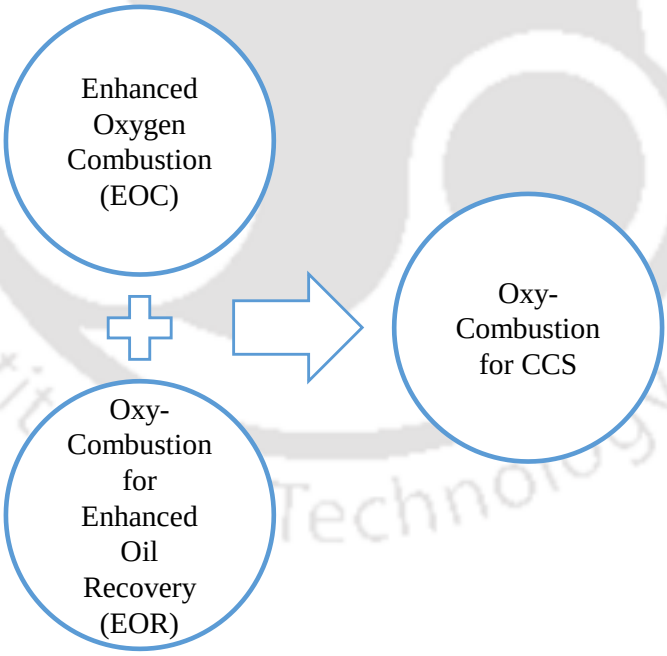

Figure 2.6 Oxy-Combustion for Carbon capture and sequestration (CCS) as a Technical combination of Enhanced Oxygen Combustion (EOC) and Oxy-Combustion for Enhanced Oil Recovery (EOR)

In the following, a fundamental works and experiments of oxy-fuel CFB combustion are reviewed, to conclude the previous studies and find out the main gaps.

Oxy-fuel CFB Combustion Penalties

CCS can reduce up to 29% of the CO_2 emission by 2050 comparing with 2010 to reach global CO_2 emission as less as 10 Gton/year by 2050 (Stangeland, 2007). So far, oxy-fuel CFB combustion is considered as the most promised CCS technology, and still the oxy-combustion has challenges viz. decreased efficiency as a result of air separation unit (ASU) consumption and Gas Processing System (GPS). This efficiency penalty could reach 15-20% of the overall power plant efficiency (Nsakala et al., 2004). Other technical challenges, the need of controlling the temperature of the elevated oxy-fuel combustion by circulating exhaust gases, this necessity increases the installation and operating cost. In CFBs, both of fluidization conditions and thermal conditions must be maintained. The recirculation of exhaust gases leads to maintaining the fluidization conditions by supplying sufficient flow rate, since, supplying pure oxygen for the same thermal load will not be sufficient to achieve the fluidization condition. Supplying sufficient pure oxygen (which leads to higher efficiency) to reach fluidization condition will overload the power plant and lead to higher operating temperature, unless new methods are applied to absorb the elevated released energy.

Toward enhancing the overall efficiency

Many research groups and industrial companies adopted enriched oxy-combustion (OC) (Anthony, 2013; Shiyuan et al., 2013; Bolea et al., 2014; Seddighi et al., 2015b). This technique has many advantages viz. compactness, utilizing low rank of fuel, improved temperature stability and heat transfer, increased efficiency due to minimizing exhaust gas flue, and lower emissions. Therefore, oxygen concentration in CFBC is being increased gradually (Gibbins and Chalmers, 2008). Moreover, oxy-fuel CFB combustion has pluses over pulverized fuel combustion viz. uniform temperature, in situ desulfurization, high combustion efficiency, low nitric oxide (NO_x) emissions, and fuel flexibility. Moreover, there is no need of new combustors for oxy-fuel CFBCs in contrast with oxy-fuel pulverized combustors (Tan et al., 2014). Table 2.3 shows selected oxy-fuel CFB research groups with the O_2 concentration and power of the setup.

A study by Stangeland (2007) shows the importance of enhancing the efficiency over cutting CO_2 emission. This improved efficiency can reduce 55% of the CO_2 by 2050 comparing with 2010, to reach global CO_2 emission less than 10 Gton/year by 2050.

Table 2.3 Oxy-fuel CFB research groups with their setups' operating oxygen concentration

Group	Power	O_2 %	Reference
ALSTOM	3.0 MW_{th}	30-50	(Liljedahl et al. 2006)
University of Utah	0.3 MW_{th}	21-33	(Eddings and Okerlund 2009)
CANMET	0.1 MW_{th}	60-70	(Jia et al. 2010)
Czestochowa Univ.	0.1 MW_{th}	35	(Czakiert et al. 2010)
Metso Power Oy	5 MW_{th}	16-36	(Seddighi et al. 2011)
TU-Wien	0.1 MW_{th}	30	(Tondl et al. 2011)
CIUDEN	30 MW_{th}	30	(Hack et al. 2012; Lupion et al. 2013)
VTT	4 MW_{th}	21-25	(Seddighi K et al. 2013)
CAS	0.1 MW_{th}	50	(Tan et al. 2014)
Chalmers	0.1-4 MW_{th}	70	(Seddighi et al. 2015)

Interestingly, the same general trend of research (in terms of increasing the O_2 concentration) is found at the level of fundamental studies Table 2.2, and at the level of pilot scales of oxy-fuel CFBC Table 2.3.

Oxy-fuel CFB Combustion Generation

Oxy-fuel CFB Combustion is subjected to development since it was commenced, it may classified based of generations into three categories as described below:

1st Generation

The first generation of oxy-fuel CFB plants are mainly a retrofitted conventional power plants and operating under air or oxy conditions (Tourunen et al., 2014; Pikkarainen et al., 2014). Here the thermal load is limited for the oxy-fuel CFB plant, since it must simulated the air combustion parameters viz. thermal load, maximum temperature, and fluidization conditions of the air combustion mode. This generation is suitable for low O_2 concentration 21% up to 30%, which are initially designed based on the air combustion conditions.

2nd Generation

The second generation CFB plants are designed and manufactured to operate under the high oxygen mode 45%, 60-70%, 70% O_2 concentration (Jia et al., 2010; Abdulally, 2012; Seddighi et al., 2015b). Interestingly, applying oxy-fuel techniques is more expensive with 10~30% efficiency penalty compared to conventional CFB plants (Nsakala et al., 2004). This extra cost is pertained to installing auxiliary units viz. air separation unit (ASU) and re-circulation system, and the operation cost. This accelerates the research on oxy-fuel CFB to reduce the overall penalty of CCS, for instance, O2GEN European project aims to reduce 50% of the efficiency penalty (Tourunen et al., 2014). To absorb the released heat, an external fluidized bed heat

exchanger (FBHX) is installed, and the heat duty of FBHX is 25% up to 50% with enhanced solid circulation. Additionally, this generation is more compact comparing with the first one, and Alstom 45-O_2 CFB power plant is cheaper by 12% compared to air based CFB power plant (Abdulally, 2012). The O_2 concentration is being increased within an aim to enhance the overall efficiency (Anthony, 2013; Shiyuan et al., 2013; Bolea et al., 2014; Seddighi et al., 2015). This technique has many advantages viz. compactness, utilizing low rank of fuel, improved temperature stability and heat transfer, increase efficiency due to minimizing exhaust gas flue, and lower emissions. Therefore, the oxygen concentration in CFBC is being increased gradually (Gibbins and Chalmers, 2008). Moreover, oxy-fuel CFB combustion has pluses over pulverized fuel combustion viz. uniform temperature, in situ desulfurization, high combustion efficiency, low nitric oxide (NO_x) emissions, and fuel flexibility. There is no need of new combustors for oxy-fuel CFBCs in contrast with oxy-fuel pulverized combustors (Tan et al., 2014).

3rd Generation

The number of third generation CFB plants (Pure oxygen fuel CFB combustion) is than 1000 industrial and pulverized coal furnaces, these plants were converted from air-combustion mode to oxy-combustion without EGR (Kobayashi and Bool, 2011). As reported, using pure oxygen combustion could save fuel between 10-70% within flue gas temperature 260-1650 (U.S. DOE, 2005). In CANMET, Canada, they have suggested pure O_2 slagging combustion technology, and Hydroxy-Fuel Burner Prototypes with zero EGR (Zanganeh et al., 2008). To the best of authors' knowledge, there is no single CFB power plant operating under pure oxygen condition. In this work, the pure oxy-fuel CFB combustion method is proposed, with series of experiments to verify the possibility of applying this method.

Barriers of Oxy-fuel CFB combustion

In terms of economic difficulties, the efficiency penalty is very high for oxy-fuel combustion, which could exceed 15% of the overall power plant efficiency. As a result, enhancing the efficiency of oxy-fuel CFB combustion is required (Nsakala et al., 2004). The enhanced O_2% of the oxidant improves the efficiency of oxy-fuel combustion drastically (U.S. Department of Energy, 2007). Continuously, many research groups aim to increase the O_2 percentage of CFBC, where temperature is controlled by re-circulating CO_2 and aim to enhance the solid circulation for absorbing the elevated generated heat (Seddighi et al., 2015a). The main barrier

of utilizing higher or pure O_2 is the operating temperature limit of the plant, where the temperature must meet the material design limits. So far, the maximum oxygen concentration has been achieved is 70%, and still they are using EGR to regulate temperature of the CFB unit. The technical problem (controlling the temperature) shall be studied intensively to reach the desired economic pure oxy-fuel CFB combustion.

2.2.5 Biomass combustion and co-combustion with coal

Biomass combustion plays a crucial role in reducing the CO_2 emission, since, it takes a place in the carbon natural loop, where the carbon is called a neutral carbon. The renewable energy utilization reduce 16% of the CO_2 by 2050 comparing with 2010, to reach global CO_2 emission less than 10 Gton/year by 2050 (Stangeland, 2007). Figure 2.7 shows the decrement in CO_2 emission with enhanced efficiency and the effect of using biomass co-firing comparing with pure coal combustion as base line. As illustrated, using 20% of biomass as a fuel with enhanced efficiency up to 45% can cut 34% of the CO_2 emission based on Foster and Wheeler solution for Lagisza CFB boiler.

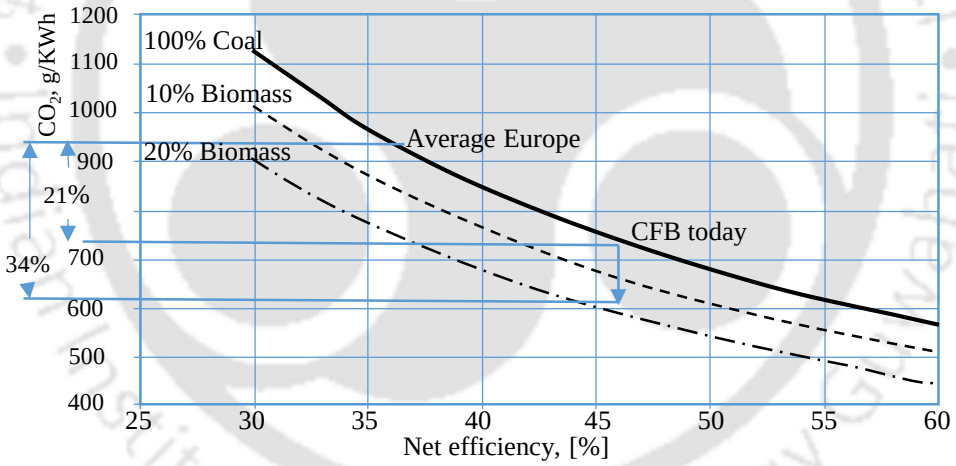

Figure 2.7 Foster wheeler's solutions for large scale CFB boiler technology: Features and operational performance of Lagisza 460 MW CFB boiler (Hotta, 2009)

Now a days, the biomass co-firing is common in Nordic countries and North America, where an abundant amount of sustained forests are being used. Never the less, it has a promising future. The biomass co-firing has three main category based on the percentage of co-fired biomass and boiler system design as following: direct, indirect, and parallel co-firing (Agbor et al., 2014). In our own opinion, using co-firing technique complicates the design of the power plant, and increases the cost of setting up and operating, and designing a pure biomass power plants can simplify the design and minimize both of building up and operating costs.

2.3 Exergy Analysis of Fuel and Chemical Reaction

Energy consumption increases according to population increment, and modernized lifestyle. Nowadays, 80% of the world energy consumption is supplied from fossil fuel. The first law of thermodynamics can assess only the quantity of energy, meanwhile, exergy analysis is based on the second law of thermodynamics and justify the real useful energy, and exergy assesses both of quality and quantity of energy (Kaushik et al. 2011). Moreover, the thermodynamic analysis gives better understanding of the process and way which energy flows through. On the other hand, new tactics and technologies are proposed to maximize the efficiency of power plants such like (Enhanced oxygen combustion, oxy-fuel CFB combustion, Gas Turbine Companied Cycle (GTCC) etc.). Therefore, thermodynamic analysis is highly required for clarifying the changes over the thermal system performance, clarifying the effects of different parameters (pressures, temperatures, flow rates etc.), and maximizing the overall efficiency. Moreover, the fuel analysis is desirable to be extended to use second law of thermodynamics (exergy) side by side with the first law of thermodynamics, and quality of the fuel is presented as a ratio of exergy to energy (Ghamarian and Cambel, 1982). In general, solid fuel (biomass, coal) can be categorized based on O/C and H/C atomic ratio (Krevelen, 1961). In literature, several papers concerns the exergy analysis of coal combustion power plant and assessing the performance of the different parts of power plant as reported in reference (Yazdanfar et al., 2015); these studies analyse air combustion mode of the power plant only, therefor, an exergy study is required to assess the oxy-fuel CFB combustion. This is a fundamental study to compare air combustion case with several scenarios of oxy-fuel combustion.

2.4 Research Gaps

The literature review shows a considerable research on CFB hydrodynamic behaviour over wide range operating conditions viz. bed inventory, particle size, operating pressure, superficial velocity, different types of non-mechanical valves, and different geometries. It is clear that the majority of studies considered air-operating case. Still, there are areas that need to be explored for deeper understanding of CFB behaviour. The following gaps are found out from literature review, for both of Cold and Hot CFB units:

- The hydrodynamics study of CFB under wide range of gaseous O_2-CO_2 mixture (oxy condition) is required. This is important to clarify the operating differences under oxy condition, since the hydrodynamics and combustion behaviour are coupled in the

CFB. Moreover, CO_2 properties (viz. density, diffusivity etc.) differ from N_2 ones, which leads to change in the hydrodynamic behaviour of the CFB unit. Furthermore, it is an elementary design step toward hot CFB unit design.

- The studies on aeration effects over the voidage and suspension density profile in CFB are limited. Many researchers have studied the voidage, pressure drop, and suspension density variation in a CFB riser. Hussain et al. (2013) studied the hydrodynamic behaviour of CFB with primary airflow rate only. Kunii and Levenspiel (1991) studied the aeration's effect over the solid flux in a CFB. Adfinez et al. (1994) used aeration for their experiments, and proposed two equations to estimate the axial voidage as a modified model of Kunii and Levenspiel model. Arena et al. (1998) investigated the effect of aeration over the solid flow rate through L-valve. It is observed that aeration rate is required to be increased for a smooth non-obstructed flow if particle size and density of inventory increase. Thus, there is a need for detailed investigation to see the effect of aeration for non-obstructed flow in a CFB.
- Several fundamental studies focused on single coal particle combustion under oxy-fuel combustion condition (O_2-CO_2) and enriched oxy-combustion (O_2-N_2). Used Oxygen concentration was between 3-100% O_2. So far, oxy-fuel CFB combustion with high concentration of O_2 is hardly reported. In conclusion, increased oxygen in the mixture increases the flam temperature; decreases combustion time, ignition delay and soot formation cloud. Reactivity in O_2-N_2 is higher comparing with O_2-CO_2. In contrast, maximum oxygen concentration in oxy-fuel CFB combustion barely touched 70%. More work is required to achieve higher oxygen concentration toward 100% O_2.
- Biomass co-firing is common, and has its own difficulties in terms. Whereas pure biomass combustion under oxy-fuel CFB condition is rare and more developments are required.

2.5 Objectives

Based on the research gaps, two units (cold and hot) CFBs of identical geometries are developed to carry out the hydrodynamic and reaction studies. This is to improve and clarify the oxy-fuel technology and its applications in the CFB toward 3rd generation of oxy-fuel CFB combustion. Several objectives are specified to achieve the aims of the present work. The studies pertaining to cold CFB and hot CFB are mentioned below:

A. The Cold CFB is used to achieve the first package of objectives; simulate the hydrodynamic behaviour in Hot CFB; and answering the following questions:
   - ✓ Does this designed CFB work properly, and inventory circulate well?
   - ✓ How this CFB behaves using different inventories weight?
   - ✓ What are the hydrodynamics behaviour changes under CO_2-O_2 mixture operating condition comparing with air operating condition?

B. The hot CFB is used to achieve the second package of objectives:
   - ✓ Defining and investigating the 3rd generation of oxy-fuel CFB combustion process in CFB, for CCS.
   - ✓ Proposing novel feeding strategy for 100% Oxy-firing in CFB (Controlling the combustion by fuel feeding rate control).
   - ✓ Investigating pure Oxy-coal combustion with zero recirculation EGR – 3rd Generation of oxy-fuel CFBC.
   - ✓ How does the temperature profile change with oxy-fuel combustion comparing with air-fuel combustion?
   - ✓ Investigating pure biomass oxy-fuel CFB combustion.
   - ✓ Conducting a thermodynamic analysis (energy and exergy analysis) under oxy-combustion conditions. And comparing air combustion case with oxy-combustion case.

2.6 Summary

To sum up, the review of the earlier work have clearly suggested that oxy-fuel CFB combustion is a promising technology for CCS. And, the primary barrier of applying oxy-fuel CFB combustion is the high cost. The oxy-fuel CFBC is investigated under low concentration of O_2. More effort is needed to clarify the CFB combustion under higher O_2 concentration. Only at the level of particle reaction, the oxy-fuel combustion is explored under high or pure O_2 concentration. The TGA and DTF are used for fundamental studies of particle oxy-combustion. The future generation of CFBs are required to be more efficient and likely to operate under higher O_2 concentration. Present work is a contribution towards pure oxy-fuel CFB combustion. And it proposes a novel method for pure oxy-fuel CFB combustion, with techniques to control the combustion and its temperature. Finally, the need of improving oxy-fuel CFB combustion and its efficiency are highly essential, and accordingly the objectives of the present study are defined.

3 Novel Method for Pure Oxy-fuel CFB Combustion

Overview

As it has been mentioned in chapter 1, oxy-fuel CFB combustion is a promised technology for CCS, but practically, the efficiency penalty is very high for oxy-fuel combustion, which could exceed 15% of the overall power plant efficiency. As a result, the efficiency enhancing of oxy-fuel CFB combustion is required (Nsakala et al., 2004). The enhanced oxy-combustion improves the efficiency drastically (U.S. Department of Energy, 2007). Continuously, many research groups aim to increase the O_2 percentage of oxy-fuel CFB combustion, where temperature is controlled by re-circulating CO_2 and enhanced solid circulation in aim to absorb the elevated generated heat (Seddighi et al., 2015a). The main barrier of utilizing higher concentration or pure O_2 is the operating temperature limit of the plant, where the temperature must meet the material design limits. So far, the maximum oxygen concentration has been achieved is 70%, and still EGR is being used to regulate temperature of the CFB unit. The technical problem (controlling the temperature) shall be studied intensively to reach the desired economic oxy-fuel CFB combustion.

In this chapter, a novel method of pure oxy-fuel CFB combustion is proposed. And, two techniques are illustrated to control the temperature by controlling the stoichiometric ratio.

Chapter outline:

Chapter 3

3.1 Preface

Combustion is a rapid chemical reaction, liberating energies viz. thermal (high-temperature gases), electromagnetic (light), electric (ions), and mechanical (noise). Controlling rate of heat release (RoHR) in combustion engines – both internal and external – is essential to control parameters namely temperature, emissions and performance. Multiple injection system was used in internal combustion engines with pre-injection, post-injection, and split-injection, aiming to control *RoHR*, temperature, NO_x, and So_x (Hiwase et al., 2013; Finesso and Spessa, 2014; Cung et al., 2015). In general, we may categories the combustion methods into four main types (Kiriishi et al., 2009; Yuzbasi and Selçuk, 2011; Lin et al., 2013; Duan and Zhao, 2014) as indicated below:

- Conventional Air-fuel Combustion: the oxidant is a pure air
- Enriched Oxygen Combustion: the oxidant is a mixture of air with added O_2
- Oxy-fuel Combustion: the oxidant is a mixture of O_2 and recirculated CO_2
- Pure Oxy-fuel Combustion: the oxidant is a pure oxygen

The pulverized power plants have adapted and run under the four types. In contrast, CFB power plant has not yet operated under pure oxy-fuel combustion condition. Moreover, increasing the oxygen concentration enhances the overall efficiency, and pure oxy-coal pulverized burners are already installed to stabilize flame, to capture high concentration of CO_2, and to recover latent and sensible heat from exhaust. The number of oxy-coal pulverized burners are being increased (Schoenfield, 2009; Ochs et al., 2009).

The pure oxy-coal pulverized plants are achieved by employing special arrangements of the burners in such a way that the fuel is injected through several points, and hence, the temperature is controlled. So far, there is no pure oxy-fuel CFB combustion plant where the fuel is injected once to the unit, usually through the lower part of the unit. Additionally, the flow staging technique is used to enhance the CFB combustion by supplying primary oxidant through the lower part of the unit and secondary oxidant at a higher level of the riser. Furthermore, oxygen staging technique is being recently used by controlling the oxygen percentage in the primary and secondary flows (Tan et al., 2014). In our opinion, both techniques are affecting the hydrodynamic behaviour of the CFB unit (Ersoy et al., 2004). In this chapter, a novel method for pure oxy-fuel CFB combustion is presented.

3.2 Problem and Motivation

As it has been mentioned in chapter 1, oxy-fuel CFB combustion is a promised technology for CCS, but practically, the efficiency penalty is very high for oxy-fuel combustion, which could exceed 15% of the overall power plant efficiency. As a result, the efficiency enhancing of oxy-fuel CFB combustion is required (Nsakala et al., 2004). The enhanced oxy-combustion improves the efficiency drastically (U.S. Department of Energy, 2007). Continuously, many research groups aim to increase the O_2 percentage of CFBC, where temperature is controlled by re-circulating CO_2 and enhanced solid circulation in aim to absorb the elevated generated heat (Seddighi et al., 2015a). The main barrier of utilizing higher or pure O_2 is the operating temperature limit of the plant, where the temperature must meet the material design limits. So far, the maximum oxygen concentration has been achieved is 70%, and still they are using *EGR* to regulate temperature of the CFB unit. The technical problem (controlling the temperature) shall be studied intensively to reach the desired economic oxy-fuel CFB combustion.

3.3 Objectives

In this work, we are aiming to achieve pure oxy-fuel CFB combustion without affecting the hydrodynamic behaviour of the unit, by proposing a novel technique and experimentally validating the hypothesis. Achieving pure oxy-fuel CFB combustion will lead to eliminate the re-circulation flue gases and the cost of installing and operating. Additionally, the loss of energy and exergy with exhaust could be minimized.

3.4 Hypotheses

In the conventional CFB power plant, solid fuel is being fed into the (reactor) riser, where the combustion takes place. In case of oxy-fuel CFB combustion, EGR is used to control the temperature. Additionally, Bolea et al., (2015) and Seddighi et al. (2015b) used external heat exchanger with enhanced solid circulation rate for controlling the bed temperature. In this work, the control of temperature is attempted using stoichiometric ratio (λ). Where the Oxidant Fuel Ratio (OFR) represents the mass of oxidant to the mass of the fuel (2.9).

$$OFR = \frac{m_{oxidant}}{m_{fuel}} \tag{3.1}$$

where, $m_{oxidant}$ and m_{fuel} represents the mass of the oxidant and fuel, respectively. The combustion is a stoichiometric one, when the fuel is fired entirely without excess oxidant; and

the OFR becomes OFR_{stoich}. For instance, Eq. (3.3) shows a stoichiometric *OFR* where 12 kg of carbon react perfectly with 32 kg of O_2 to form 44 kg of CO_2. In the light of OFR definition, we may define the stoichiometric ratio λ as a ratio of OFR to $OFR_{stochio}$ as shown in Eq. (3.2).

$$\lambda = \frac{\mathrm{OFR}}{\mathrm{OFR}_{\mathrm{stochio}}} \tag{3.2}$$

Figure 3.2 illustrates the effects of oxygen percentage in oxidant (mixture of O_2-N_2) with range of 21% to 100% O_2 and λ ratio of 1 to 5 over the adiabatic flame temperature (AFT) of carbon combustion. These *AFTs* are calculated for non-equilibrium single reaction of carbon reaction with oxygen as illustrated in Eq. (3.3). It is a simple theoretical reaction, which is used for calculating theoretical *AFT*. Dissociation effect at high temperature is neglected here for the sake of simplification.

$$\mathrm{C} + \mathrm{O}_2 \rightarrow \mathrm{CO}_2 \tag{3.3}$$

In all the cases, increased stoichiometric ratio decreases the adiabatic flame temperature (*AFT*), since the excess oxygen absorbs the heat energy, and is not like the reacted oxygen, which takes a part in exothermic reaction. Our hypothesis suggests controlling *AFT* by stoichiometric ratio rather than applying *EGR*. Figure 3.1 shows the theoretical process of ideal pure oxy-fuel combustion. The process starts in first reactor with pure oxygen as an oxidant and fuel that react under conditions of λ=3. Then, the products of the first stage are mixture of CO_2-O_2 and this mixture is used as an oxidant for the second stage, where the combustion takes place with stoichiometric ratio of λ=2. In the same manner, the fuel and oxidant react to release CO_2. This thermodynamic principle is the basis of controlling temperature, which allows to control the temperature, and minimizing the exhaust flow rate. As a result, the overall efficiency is enhanced. Stoichiometric ratio (λ) itself is controlled by feeding of fuel as explained below.

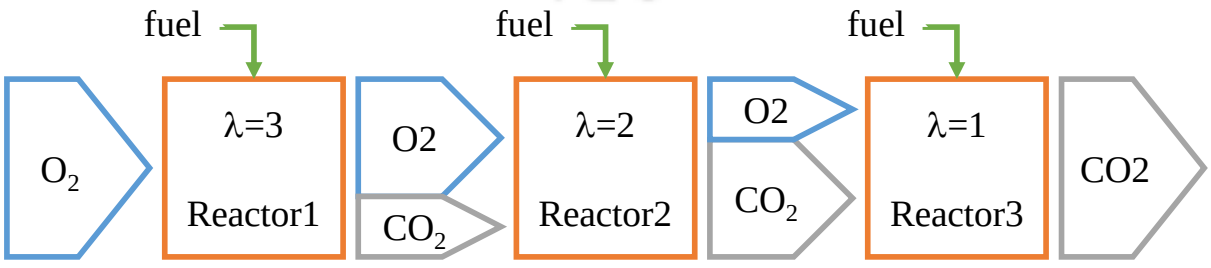

Figure 3.1 Schematic diagram of proposed process for pure oxy-fuel CFB combustion

The number of stages (sub-process) are not fixed; the number of stages could be (n) stages viz. two, three, or four. As shown in Figure 3.2, theoretically, *AFT* of 100% oxygen concentration in the oxidant at λ=5 gives almost the same AFT of 21% oxygen concentration case in the oxidant at stoichiometric ratio of λ=1.

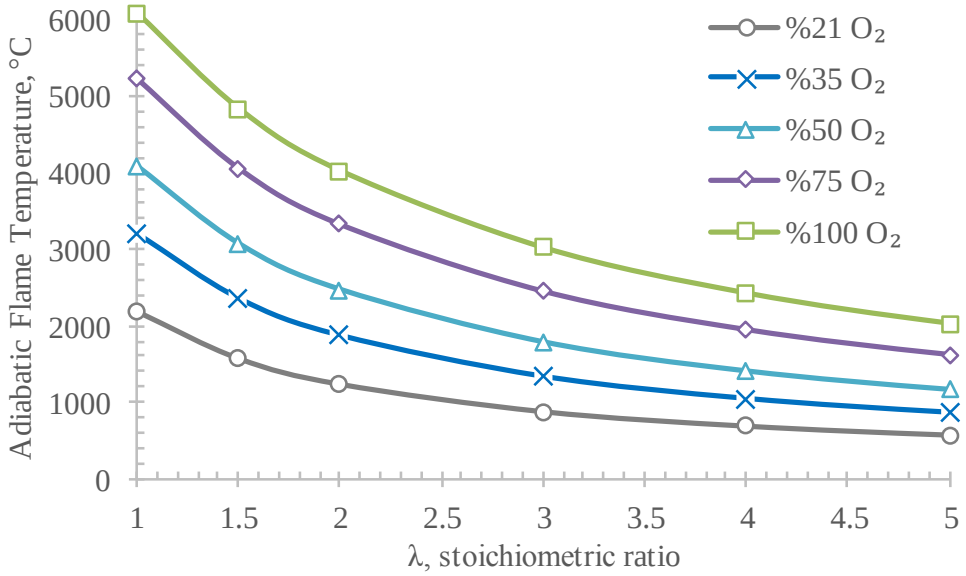

Figure 3.2 Estimated flame temperature in a conventional boiler for air and oxy-combustion with different oxygen concentrations and Stoichiometric ratios.

The proposed method of controlling combustion by stoichiometric ration can be reached by applying tow arrangements of feeding systems. In the following two feeding arrangements are explained.

3.4.1 One CFB with multi-feeders along the riser

In the first arrangement, the main fuel feeding is split into multiple fuel feeding along the riser by using n-feeders (Figure 3.3). Rather than feeding the required fuel once at the lower part of the riser-1 and releasing the heat rapidly under high oxygen concentration, we can feed X_n % fractions of the whole fuel feeding rate where the fuel combustion starts and increase the temperature. In this case, λ (oxygen/fuel ratio) becomes higher than 1. Controlling λ leads to control flame temperature in the riser-2. Two or more feeders could be fixed along the height of the riser; the reactants of the first reaction contain excess oxygen, which will react with fresh fuel at higher level of the riser under conditions of lower λ and oxygen concentration. Finally, the ratio of oxygen to accumulative fuel becomes nearly one. Figure 3.3 also shows the general

predicted profile of oxygen concentration and λ along the riser height, where both of oxygen concentration and λ decrease gradually.

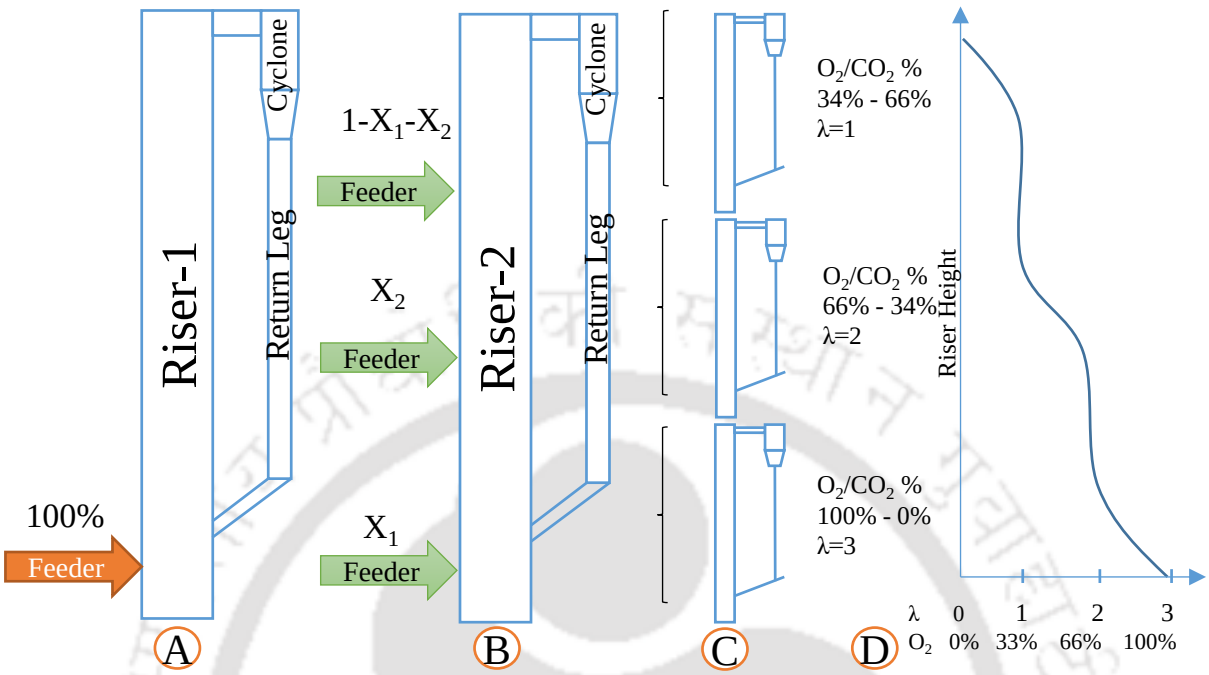

Figure 3.3 Proposed fuel injection strategy for oxy-fuel CFBC

3.4.2 Series of mini-CFBs

The available mini-CFB of 2 m height (Figure 3.4) shows an alternative arrangements to simulate combustion in CFB of 6 m riser height, with three stages. On the other hand, the absorbed heat by water jacket, radiation and convection sections decreases the temperature. This technique can be used side by side with a high solid recirculation rate of inventory (sand) to control the temperature in the CFB.

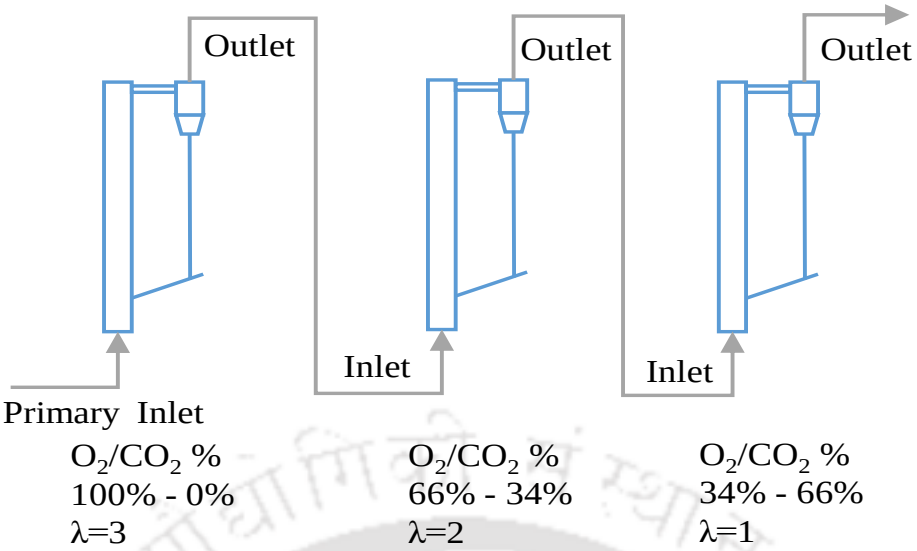

Figure 3.4 Alternative arrangement of multiple fuel feeding technique.

In the second arrangement, the primary flow is the pure oxygen that enters the first mini-CFB, where the combustion of fuel take a place under stoichiometric ration of 3. The exhaust of the first mini-CFB is enriched of oxygen and forwarded to the second mini-CFB to react with amount of fuel (under stoichiometric ratio of 2) to result flue gases enriched of oxygen at percentage of 33%.

The exhaust flows to the final mini-CFB to react with sufficient amount of fuel to perfect the combustion with minimal wasted excess oxygen. In the following two chapters, the design of experiments is followed by results and discussion to experience the suggested hypothesis.

3.5 Summary

Both of these techniques (multi-stage feeder and multi-mini-CFBs) lead to pure oxy-fuel CFB combustion, with eliminated re-circulation setup. The proposed method needs to be validated experimentally. The success of pure oxy-fuel CFB combustion will minimize the cost of oxy-combustion. Then, the overall efficiency will be increased. Furthermore, the complexity of the oxy-fuel CFB power plant will decrease due to eliminating the re-circulation setup.

Up to the best of our knowledge, there is no single CFB is working under pure oxy-fuel combustion conditions, even in R&D. In the following chapters, the setup and experiments procedures are illustrated. Then, the result and discussion are been followed. Lastly, the thermodynamic analysis is conducted to find the effects of pure oxy-fuel combustion over the energy and exergy efficiency.

4 Experimental Setup and Procedure

Overview

This chapter describes the CFB experimental setups of the hot and cold units. Both units are designed and manufactured in-house (at the workshop and mechanical engineering department laboratories of Indian Institute of Technology Guwahati). The cold CFB unit and hot CFB unit have an identical geometry in the aim of simulating and investigating the hydrodynamic behaviour of hot CFB using the cold CFB. Also, this chapter details the operation procedures of the cold and hot units. The operating parameters are varied for analysing the effects over beds' behaviours. Along with the two CFBs, there are auxiliary setups viz. electric heaters, feeding system, exhaust heat exchanger, filtering and sampling exhaust equipment, gas mixing, gas supplying, gas flow rate controlling, temperature measuring and measuring, and data acquisition. Then, the utilised materials are described in details, which are coal, biomass, and silica sand and collected from Assam state, India. Plus, the chapter explains the designed experiments and the steps for both of cold and hot units in details. The gas supplying system is same for cold and hot rigs, and used for preparing the required mixture (CO_2-O_2 and/or air) and preheating for hot CFB unit. The Cold unit is used to study bed voidage, suspension density, and solid re-circulation rate under two solid inventories, aeration, and primary flow rates, with different operating gases (air, mixture of CO_2-O_2). The hot unit is run with two fuel types namely coal, and biomass (sawdust), and the oxidant used gases are air, mixture of CO_2-O_2, different stoichiometric ratios are used between 1 up to 3.

Chapter outline:

4.1 Description of Cold Circulating Fluidized Bed Unit

4.1.1 Body of the cold circulating fluidized bed unit

The CFB is designed and fabricated at IITG. The cold CFB unit operates in two modes, viz. atmospheric, and pressurized conditions (Figure 4.1).

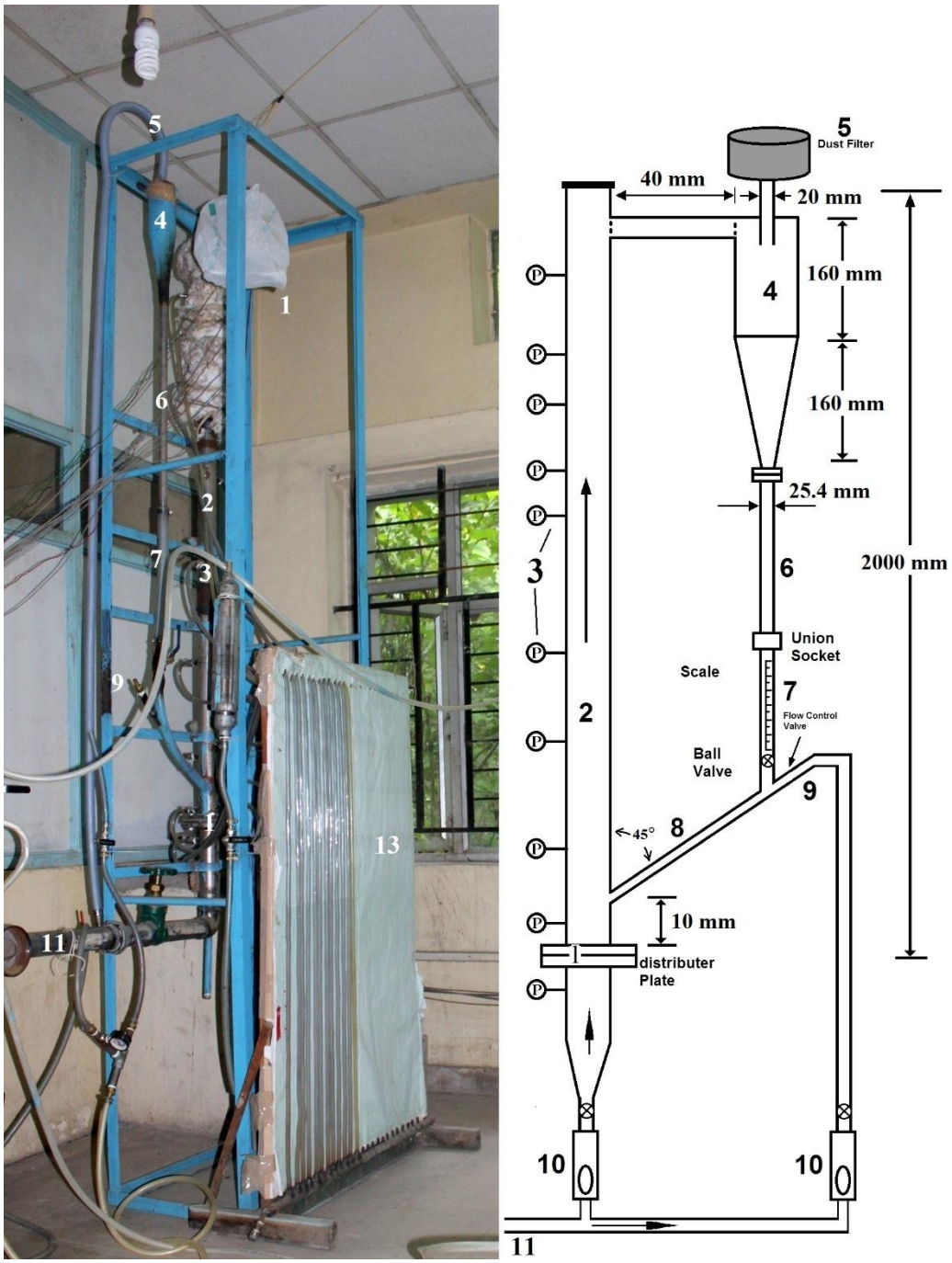

1- Distributor plate, 2-Riser, 3-Pressure Gauge, 4-Aero-Cyclone Separator, 5-Dust Filter, 6-Transparent Stand Pipe, 7-Scale, 8-Return Leg, 9-Aeration Tube, 10-Rotameter, 11-Gas Mixer, 12-U-Manometer.

Figure 4.1 Photograph and sketch of the Cold CFB unit with CFB's parts

The recycling system includes a standpipe of 25.4 mm ID, with a transparent scaled part to observe the solid flux, the standpipe is connected at the upper side to aero-cyclone separator (4) with rectangular entrance which is designed and manufactured based on state-of-the-art studies (Wang, 2004; Faulkner et al., 2008; Elsayed, 2011). The standpipe is connected to the riser by a return-leg of 25.4 mm ID with a 45° slope. A dust filter is used at the outlet of aero-cyclone. The aeration flow nozzle (9) is aligned with the axis of return-leg. The riser (2) has a 2000 mm height, 54 mm ID and 3 mm thickness with pressure nozzles along the riser (3) at levels of (13.5, 22, 36, 50, 64, 80, 110, 140, 170 mm). U-manometer is connected to the nozzles for pressure drop measurements. The exit is at a right angle with the internal baffle as this design reduces the solids volume fraction (Hussain et al., 2013). The distributor plate with 46.7% opening area is fixed at the bottom of the riser.

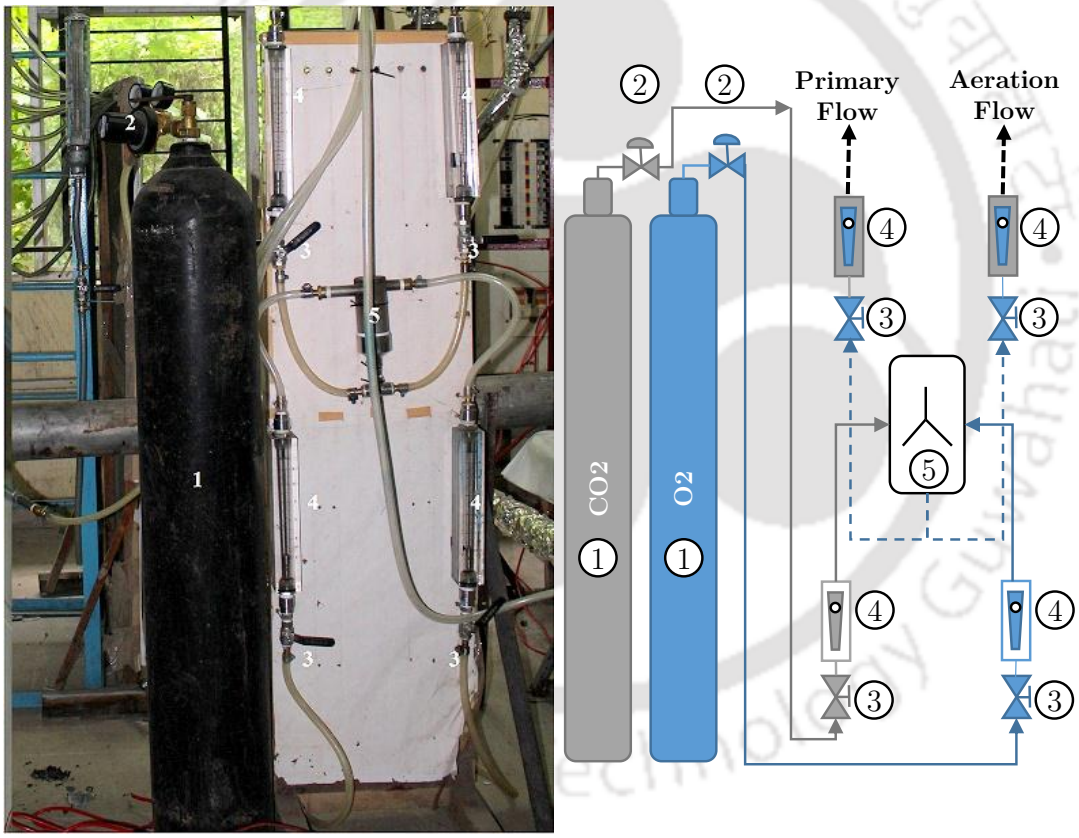

1- Gas cylinders, 2- Pressure Regulator, 3- Control Valve, 4- Rotameter, and 5- Static Mixer.

Figure 4.2 Gas cylinders with mixer and flow rate controlling system

A compressor (Make Ingersoll Rand, Model No. S-01480) is used to supply primary and aeration air to the CFB unit through the bottom of the riser and return-leg. Rotameters for measuring flows of different gas species (CO_2, O_2, mixture O_2-CO_2, and air) are used to measure the flow rates. The air flow rates are regulated by air control valves. Cylinders of O_2

and CO_2 are used to supply O_2 and CO_2 for oxy-condition case. Static cyclone mixer is used to mix O_2 and CO_2 (Figure 4.2). The same gas mixer is used to supply gaseous mixtures for both of cold CFB and hot CFB. A pre-heater is used to avoid cryogenic temperature, which occur as a result of drastic gas pressure dropping (A) (Figure 4.3). The pre-heater is supplied with 240 V alternative current, and it heats up the released CO_2 from the cylinder (B) (Figure 4.3).

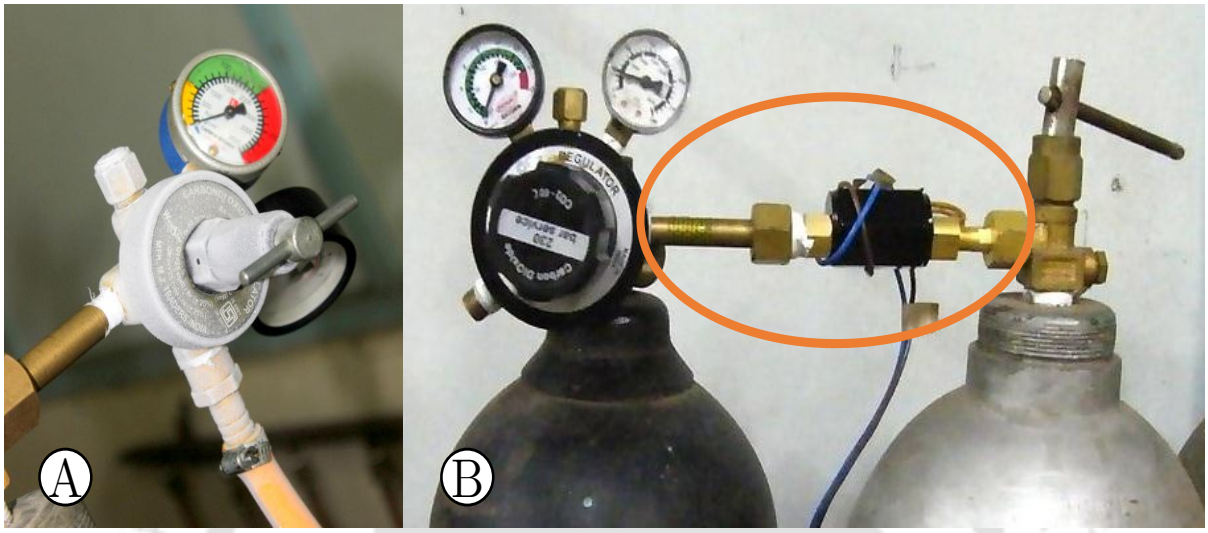

Figure 4.3 (a) Ice forming without pre-heater (b) pre-heater for regulator of CO_2 cylinder

4.2 Experimental Procedure of Cold CFB

A local sand having density of 2600 kg/m3 is sieved and used as an inventory. Three groups of particle sizes viz. 160, 302, and 427 µm (belonging to Geldart-B group (Geldart, 1973) and have a sphericity of Φs=0.70 (Kunii and Levenspiel, 1991)) are used. Table 4.1 shows the terminal velocity U_{tr} and minimum fluidization velocity U_{mf} (Haider and Levenspiel, 1989; Kunii and Levenspiel, 1991) of each particle size. The inventory weights are 500 and 750 g.

Table 4.1 Particle sizes, minimum and terminal velocity of used inventory

d_p [µm]	160	302	427
U_{mf} [m/s]	0.021	0.075	0.145
U_{tr} [m/s]	0.61	1.11	1.50

Sandy inventory is fed into the riser through a removable transparent tube at the bottom of the stand-pipe. In each experiment, flow rate (Q) [m^3], particle size (dp) [μm], and operating pressure (P) [kPa] are varied. In all cases, the air is supplied at three pressure levels of 100, 200, and 250 kPa. The primary and aeration flows are fed from the compressor and are controlled to maintain the required pressure and flow rates for air case experiments. Meanwhile, O_2 and CO_2 are fed from cylinders in oxy-cases. The superficial velocity (U_{sup}) is

expressed in Eq. (4.1), where (A_{riser}) [m^2] is the section area of the riser, (Q) [m^3/s] is the flow rate of air.

$$U_{\sup} = \frac{Q}{A_{riser}} \tag{4.1}$$

Once the steady state is reached, the experimental data are recorded. The static pressure along the riser height is measured, and hence bed voidage and suspension density are calculates along the riser height. The voidage (ε) is calculated using the Eq. (4.2), where (Δh) [m] is the difference between liquid levels in manometer, (ρ_s) [kg/m^3] is the density of the solid, (ρ_L) [kg/m^3] is the density of the measuring liquid and L_m [m] is the height of the taps. The suspension density (ρ_{sus}) is calculated from Eq. (4.3) (Kunii and Levenspiel, 1991).

$$\varepsilon = 1 - \frac{\rho_L \times \Delta h}{\rho_s \times L_m} \tag{4.2}$$

$$\rho_{sus} = \rho_s(1-\varepsilon) + \varepsilon\rho_g \tag{4.3}$$

In the investigation, the time is measured using stop watch during accumulating a specific amount of sand in the stand-pipe. The sand is stopped by closing ball valve at the lower part of stand-pipe. A graduated scale is used to measure the height of sand column in aim to calculate the solid re-circulating rate (G_s) [$kg.m^{-2}.s^{-1}$] using Eq. (4.4).

$$G_s = \frac{\rho_s \times L_a \times A_D \times (1-\varepsilon_{mf})}{A_B t} \tag{4.4}$$

where ε_{mf} =0.5 is the bed voidage at minimum fluidization condition. L_a [m] is the solid accumulation height, A_D [m^2] is the cross section area of the standpipe, A_B [m^2] is the cross section area of the bed, t [s] is the time of sand particles accumulating after closing ball valve and G_s [$kg.m^{-2}.s^{-1}$] is the solid circulation rate.

The same procedure is followed with each experiment, for different levels of pressure and primary flow rate. In the oxy-condition case, four blending percentages of O_2-CO_2 are used namely 21%-79%, 25%-75%, 35%-65%, and pure oxygen, to study the effects of mixture species over the hydrodynamic behaviour of the bed. Several types of non-mechanical valves could be used in CFBs like L-valve used by Arena et al. (1998) and Das et al. (2008); Loop-seal used by Ersoy et al. (2004); Basu and Butler (2009); and Hu et al. (2009); and Return-leg used by Adfinez et al. (1994) and in this present study. A series of experiments are conducted to study the influence of aeration on the hydrodynamic behaviour and to optimize the aeration

flow rate. Three aeration rates of 0.25×10^{-3} m^3/s, 0.75×10^{-3} m^3/s, and 1.25×10^{-3} m^3/s (match with three superficial velocities, U_{sup}= 0.65 m/s, 1.94 m/s, and 3.23 m/s respectively) are used. For each experiment, the pressure drop is measured along the riser, and this is used to calculate the axial voidage, suspension profiles, and rate of solid circulation G_s by using Eqs. (4.2), (4.3) and (4.4) respectively.

4.3 Description of Hot Circulating Fluidized Bed Unit

4.3.1 Body of the hot circulating fluidized bed unit

Hot CFB unit as shown in Figure 4.4 is designed and fabricated at IITG, with identical geometries (Riser, cyclone, return leg) of cold CFB unit, and is used for hydrodynamic studies. It is made up of 415 stainless steel. As illustrated in (Figure 4.4). The Riser (2) has an ID of 54 mm, 2000 mm of height and 3 mm of thickness, with fitted distributor plate (1) at its bottom. The distributor plate is covered with fine stainless steel mesh of 80 µm size. The detailed design of the distributor plate is presented in appendix A. Along the riser 8 thermocouples are fitted at the heights of 50 mm, 250 mm, 350 mm, 500 mm, 750 mm,1000 mm, 1500 mm, and 2000 mm above the distributor plate level, consecutively. The topper exit of the riser is connected to an aero-cyclone (4) with a rectangular channel. The detailed design of the aero-cyclone is presented in appendix B.

The cyclone has two exits viz. the upper one (5) for exhaust which leads to the heat exchanger (water cooler) for gas sampling, and the lower one leads to a stand pipe (6). The particles are captured by the cyclone and entrained into the bottom of the riser through a return-leg of 22 mm ID and 29 mm OD. Two thermocouples are fitted at the top and bottom of the standpipe, which is connected at the lower side to the return leg (8).

The sections of the bed viz. riser, heater, and aero-cyclone are connected with help of flanges and metallic gaskets between the flanges to airtight the connections. The aeration gas mixer is fed to the return-leg through nozzle (9). Preheater (10) is fixed before the distributor plate with electric Kanthal heating elements of 2×5 kW power. Additionally, one electric heater is fitted along the riser (11) with power of 5 kW for accomplishment of the required starting up temperature. Thermal insulation is maintained using three layers of ceramic wool of 50 mm thickness (12). The standpipe is left without thermal insulation with an aim to simulate heat exchanger (heat sink).

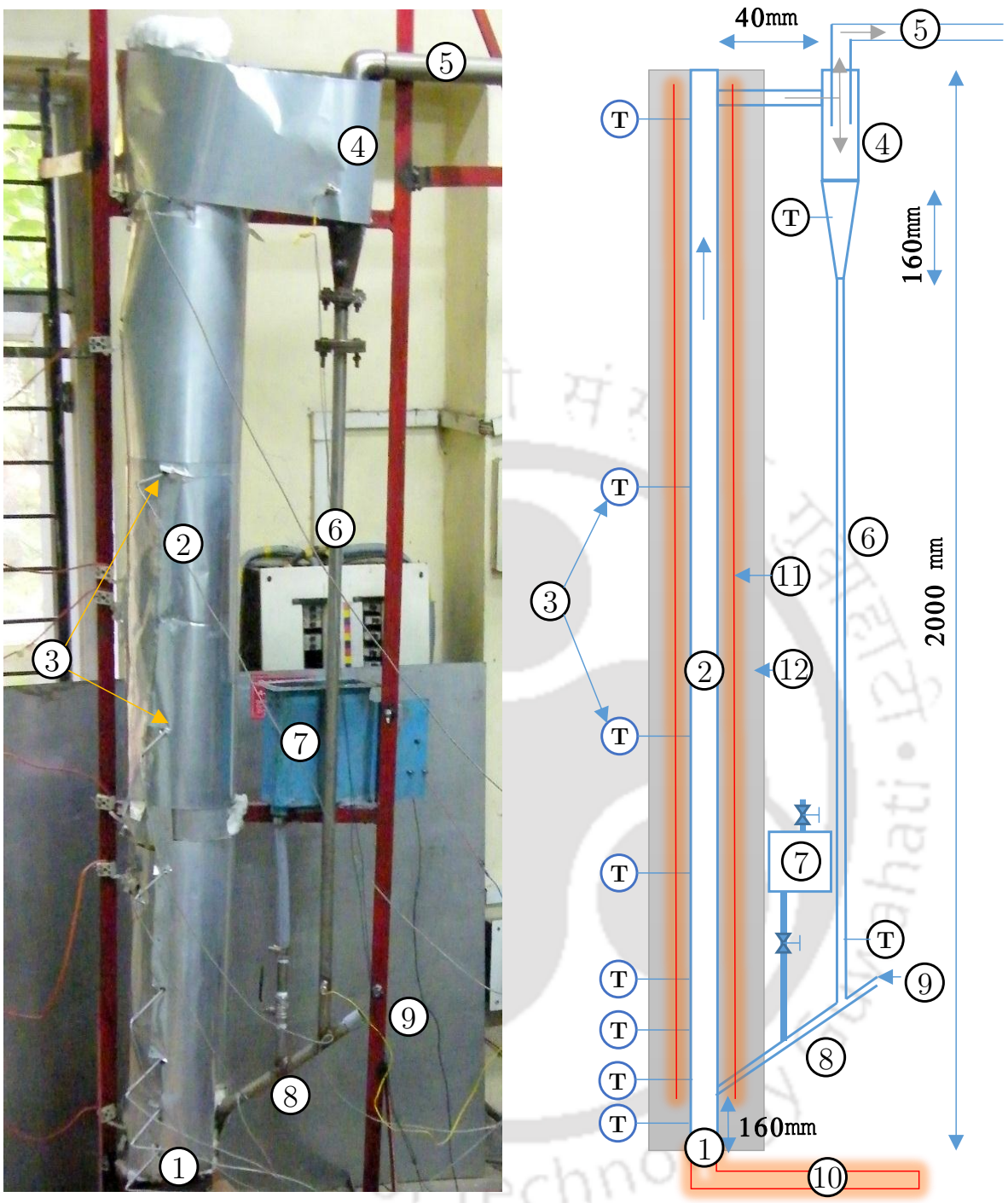

1- Distributor plate, 2-Riser, 3-thermocouples, 4-Aero-Cyclone Separator, 5-Exhaust outlet, 6-Stand pipe, 7-Feeder, 8-Return Leg, 9-Aeration inlet, 10-Primary inlet through Pre-heater, 11-Riser heater, 12-Thermal insulation.
Figure 4.4 Photograph and sketch of the Hot CFB unit

A brief video shows the whole setups viz. (hot CFB unit, data acquisition system, distributor plate, riser, thermocouples, aero-cyclone separator, exhaust outlet, stand pipe, feeder, return leg, aeration inlet, primary inlet through pre-heater, thermal insulation, CO_2 and O_2 cylinders, gas mixer).

4.3.2 Measurement instruments

A. Temperature measurement

Figure 4.5 shows a sketch of the used thermocouple with dimensions. A screw feeder is used for feeding the solid fuel and sand inventory. The screw feeder is driven by a direct current (DC) electric motor (Make PARVALUX, 25W), which is controlled by a dual regulated power supply (Make BETECH, Model: DC-3005, II) with an output of 0~30 V /0~5A (Figure 4.6). Temperature is measured using "K" type thermocouples (Fabricated by: M/S Aparajit Instruments, Chennai 600116). Figure 4.5 shows the thermocouples' parts viz. a shield (B) of ID 4.5 mm, OD 6.35 mm, and 200 mm length, a prop (A) of OD 4.5 mm and 40 mm length INCONEL 600×4.5 mm, a SS Spring (D), braided (C) 1/24 FG/FG/SS Braided and Cable (E) 2 m long.

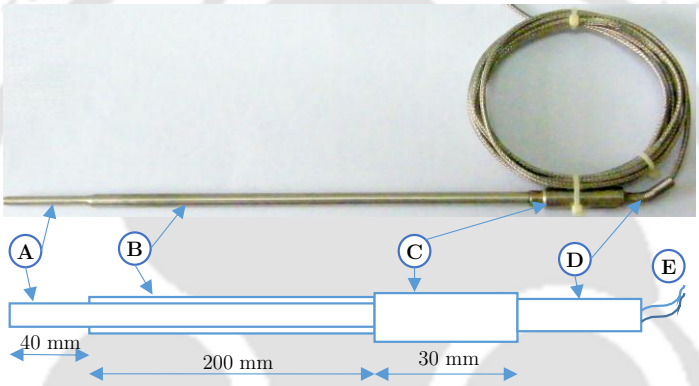

Figure 4.5 Sketch and picture of "K" type thermocouple

B Data Acquisition System and Fuel Feeding Control

All thermocouples are connected to data acquisition system (*Make Agilent LXI, Model: 34972A*) which is connected to a desktop computer for auto-data recording using a software, as illustrated in Figure 4.6.

Figure 4.6 a: Direct current regulated power supply b: Data acquisition system and c: desktop computer.

An Alternative Current-Direct Current converter (AC/DC) is used to control a DC motor of 60 W power, 7.2 A current, and up to 4000 RPM (Figure 4.6, d).

C Emissions Measurement

Two main instruments are used for measuring the exhaust components viz. gas chromatography (GS) (*Make: Thermo Scientific, Model No.: RACE™ 1110*) and a gas analyser (GA) (*Make: Testo, Model No.:350*) (Figure 4.7).

Figure 4.7 (a) Gas Chromatography and (b) Gas Analyser

GA is used mainly for testing NO_x, SO_x, and CO while GC is used for measuring the concentrations of CO_2, O_2. Additionally, GA could be used as a controlling devise of the stoichiometric ratio of combustion, by measuring the O_2 concentration at the outlet of the CFB unit to control the fuel feeding rate accordingly.

4.3.3 Materials

All the fuels used in the experiments were obtained locally from Assam, India. Indian bituminous coal of higher heating value (HHV) 29959 kJ/kg, Assam (Indian) coal of HHV 13359 kJ/kg, and sawdust of HHV 17757 kJ/kg were used (Coal India Limited, 2015).

Table 4.2 Coal ultimate and proximate analysis with heating value used for hot CFB unit

Analysis	Unit	Bituminous	Sawdust	Assam
Moisture	weight%, wet	2.2	13.3	2.18
Ash	weight%, dry	10.6	4.6	35.916
Volatiles	weight%, dry	30.15	62.9	22.96
Fixed Carbon	weight%, dry	57.05	19.2	38.9
Carbon	weight%, dry	77.97	44.87	38.944
Hydrogen	weight%, dry	5.591	5.323	3.608
Nitrogen	weight%, dry	1.348	0.57	0.994
Sulphur	weight%, dry	2.171	-	1.71
HHV	kJ/kg	29959	17757	13359

.

Table 4.2 shows fuel compositions, for ultimate analysis *EuroEa Elemental Analyser* was used to determine CHNS components. For proximate analysis (Moisture, Ash, Carbon, Volatiles matter), *ASTM D1762-84* standard was used (ASTM, 2007). We have used local sand of 2600 kg/m^3 and mean particle sizes viz. 160, 302, and 427 μm. The detailed procedure of determining the particle size distribution and mean particle size is presented in Appendix 0.

4.4 Experimental Procedure of Hot CFB

At the beginning of the experiments, the compressor is turned on to supply air to the CFB loop and the CFB is heated up using an electric heater during start up. The power of each electric heater is controlled by using a variac. After maintaining the required temperature, a temperature of 600 °C is found to be sufficient for starting up the unit. The air flow is then replaced by a mixture of bottled O_2 and CO_2 (primary mixture), where the concentration is controlled using valves. The flow rate is monitored using rotameter (rotameters are manufactured and calibrated by *Flow Star Engineering Pvt. ltd., 121005, Haryana, India*); and atmospheric pressure is maintained using regulators. A static mixer is used for mixing O_2 and CO_2. The primary flow is controlled to maintain the required superficial velocity for each different sand inventory based on the particle size. Meanwhile, pure CO_2 is supplied as an aeration for safety purpose and to avoid oxidant leakage to the fuel feeder. The feeding rate is organised by controlling the revolution per minute (RPM) of the screw feeder. The electric motor is controlled using direct current regulated power supply, the details of feeder calibration is presented in Appendix F. The screw feeder can supply multiple fuel kinds, inventory, and sorbents, with solid supply rate of up to 10 kg/h. Generally, the bed temperature lies between 750 °C – 950 °C. The superficial gas velocity U_{sup} is up to 6 m/sec. The analysis of the fuel is given by .

Table 4.2, where the coal has two particle sizes of 0.85 mm and 1.7-3.35 mm, and biofuel has a particle size of 0.5-0.9 mm. The used bed inventory is sand of 160-302-427 μm is used in all cases. The CFB is designed to operate under air or oxy conditions, with fittings for connecting and mixing the utilized gases. The unit is started up under air-combustion mode, and when the bed temperature is reached the required level, the air flow is replaced with CO_2-O_2 mixture. Both of fuel and inventory are fed using screw feeder connected to the return leg. The fuel is entrained to the riser using aeration flow through a port of 10 cm height above the distributor plate. Once the stable combustion is achieved, the temperature profile along the riser is

measured using series of 'K' type thermocouples fitted along the riser. The thermocouples are connected to a data acquisition system for continuous temperature measurements. The product gas is cooled down by tubular water heat exchanger, and filtered. The gas is then sampled and analysed. All experiments are repeated thrice to achieve the repeatability.

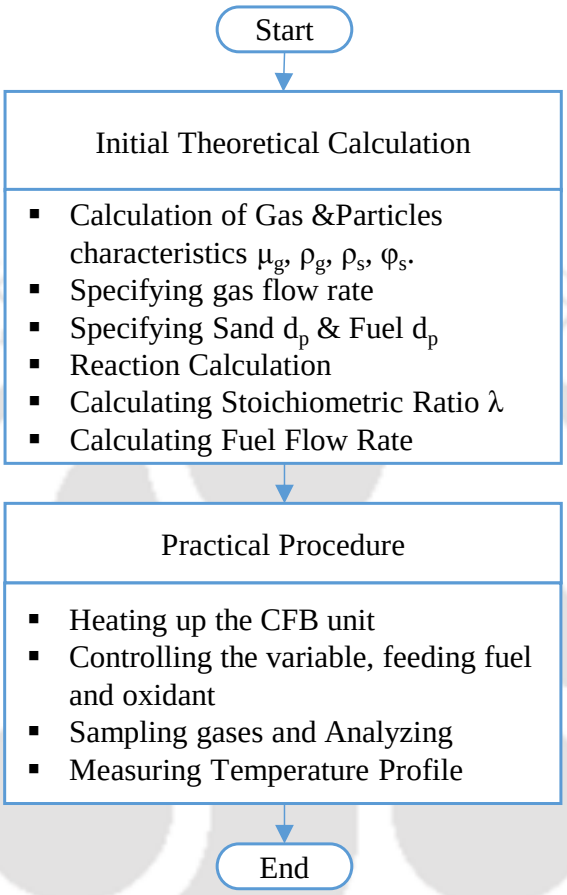

Figure 4.8 Flow chart of the experiments' calculation and procedures

Figure 4.8 shows the steps of preparing the calculation and the procedure of conducting each experiment.

4.4.1 Precautions for Running the Oxy-fuel experiments

- It is highly recommended to use CO_2 for aeration for safety purpose, neither air nor O_2-CO_2 mixture is accepted for this design where the feeder (Figure 4.4) is connected to the return-leg where the aeration flow takes a place. If the aeration flows back to the feeder, it may cause a fire.
- Start up the setup with air primarily, then switch over to oxy-fuel combustion condition. Lastly, it is necessary to switch down the unit using air to wash the remained O_2-CO_2

mixture. This action leads a safer to the next start up since the accumulated O_2-CO_2 mixture may lead to an unexpected sudden reaction, especially, when the O_2 concentration is high, the same procedure is followed for CIUDEN Oxy-CFB boiler (Lupion et al., 2013).

- The feeding of fuel shall be started after reaching the ignition temperature. This to avoid the accumulation of fuel in the reactor and getting an explosion.

We have categorised the experiments into the following groups as following, and the same procedure is repeated for each experiment with different fuel feeding rate, fuel blending percentages, and O_2-CO_2 mixture percentages.

4.4.2 Pure oxy-fuel CFB combustion (100% O_2)

The same general procedure of the hot bed is followed. A mixture of bottled O_2 and CO_2 (primary mixture) is supplied to the riser, after heating up the unit using preheater during and air flow. Meanwhile, pure CO_2 is supplied as an aeration for safety purpose and to avoid oxidant leakage to the fuel feeder. A temperature of 650 °C is sufficient to start up the unit with biomass fuel (sawdust) of particle size from 0.5 to 1.0 mm; and Assam bituminous coal of particle size from 0.8 to 1.7 mm (.

Table 4.2). The mixture concentrations of O_2-CO_2 are controlled by rotameters, and atmospheric pressure is maintained using regulators. Both of fuel and inventory (sand of 160 µm particle size) are fed using a screw feeder connected to the return leg. the inventory of 750 grams is used. Air is used for heating up the unit during starting up, then a mixture of O_2-CO_2 is used directly. The temperature profile along the riser is measured continuously using data acquisition and series of 'K' type thermocouples fitted along the riser. In all cases, a CO_2 aeration of 0.25 litter/s is used to entrain fuel and sand particles into the riser, without risk of oxidant leakage to the feeder. The primary flow rate is fixed at 3.0 normal l/s for 1.5 m/s superficial velocity at grid level. Since the setup is a mini-CFB, a barrier of minimizing and fitting three feeders appeared. As a result, it is decided to simulate a CFB of 6 m height as per the following:

a) Simulating the lower part by using the mini-CFB of 2 m height setup with pure oxygen primary inlet. This stage is sensitive since pure oxygen is used. Therefore, we have varied the stoichiometric ratio taking λ=3.0, 2.0, and 1.5. This is to optimize the fuel

feeding rate to reach the desired working temperature of the CFB, which is 800 °C up to 950 °C in general. In other words, the excess oxidant is taken 2.0, 1.0, and 0.5 for mitigating the temperature. Two groups of experiments are conducted, first using biomass (sawdust), and then, using coal (Assam bituminous). The stoichiometric ratio is varied for each group as following λ=3.0, 2.0, and 1.5.

b) Simulating the middle part by using the mini-CFB of 2 m height setup with 2/3 O_2 concentration and 1/3 CO_2 as a primary inlet and fuel feeding to meet the stoichiometric ratio of λ=2. Two types of fuel are used biomass (sawdust), and coal (Assam bituminous). Also, the same procedure of the previous section is used in terms of heating up, feeding fuel and inventory.

c) The last stage simulates the combustion at the upper part of 6 m CFB by using the mini-CFB of 2 m height setup with 1/3 O_2 concentration and 2/3 CO_2 as a primary inlet and fuel feeding to meet the stoichiometric ratio of λ=1.

In all cases, a static mixer is used to mix O_2 and CO_2, and pure CO_2 aeration flow is used. Table 4.3 shows the cases of experiments with percentages of the mixture and the stoichiometric ratios for mini-CFB to simulate the combustion along the riser of CFB of 6 m height. The rate of solid recirculation was in the range of 15-20 $kg.m^{-2}.sec^{-1}$.The exhaust gases have been cooled down by water tubular heat exchanger, filter, and samples are collected by Tedlar bags. The gas chromatography is used to analyse the gaseous samples. The main aim of this part of the experiments is to verify the feasibility of using pure oxygen for oxy-fuel CFB combustion.

Table 4.3 Experiments' parameters for Pure Oxy-fuel CFB Combustion (100% O_2)

Case	O_2/CO_2 %	Stoichiometric ratio, λ	U [m/s]	Fuel feeding rate [kg/h]	Fuel
1	100%-0%	1.25	1.0	4.212	Biomass
2	100%-0%	2.0	1.0	2.700	Bit.
3	100%-0%	1.5	1.0	3.578	Bit.
4	66%-34%	1.0	1.0	3.578	Bit.
5	34%-66%	1.0	1.0	1.789	Bit.

4.4.3 Oxy-fuel combustion

Oxy-Coal CFB Combustion

The procedure of the pure oxy-fuel CFB combustion (subsection 4.4.2) is followed for coal oxy-fuel combustion experiments also, with different fuel feeding rates and CO_2-O_2 mixture percentages. The matrix of experiments is presented in Table 4.4. The same procedure of

heating and starting up the rig is followed for coal oxy-coal CFB combustion as well as pure oxy-fuel CFB combustion, and the mixing system is used for supplying the gaseous mixture of CO_2-$O_2$of calculated percentages.

Table 4.4 Experiments' parameters for Coal Oxy-fuel CFB combustion

Case	O_2-CO_2 %	Stoichiometric ratio, λ	U [m/s]	Fuel feeding rate [kg/h]	Fuel
6	17%-83%	1.05	1.0	1.005925	Bit.
7	22%-78%	1.05	1.0	1.301785	Bit.
8	28%-72%	1.05	1.0	1.656817	Bit.
9	33%-67%	1.05	1.0	1.952677	Bit.

The O_2 and CO_2 concentrations are varied with fixed stoichiometric ratio of 1.05. The feeding rate for each case is calculated based on stoichiometric balance and accordingly the supplying voltage of the DC motor.

Oxy-biomass CFB Combustion (Sawdust)

The calculation of stoichiometric balance is repeated for biomass fuel, which has different ultimate analysis. Subsequently, the mass flow rate is calculated and the supplying voltage of the DC motor is adjusted accordingly. Table 4.5 shows the parameter of the oxy-biomass CFB combustion experiments, with different oxygen concentration and fuel mass flow rate.

Table 4.5 Experiments' parameters for Biomass Oxy-fuel CFB combustion

Case	O_2-CO_2 %	Stoichiometric ratio	U [m/s]	Fuel feeding rate	Fuel
10	33%-67%	1.05	1.0	1.539216 [kg/h]	Biomass
11	67%-33%	1.05	1.0	1.991926 [kg/h]	Biomass

4.5 Summary

In this chapter, the design and two circulating fluidized bed units are discussed, first CFB is a cold unit for studying the hydrodynamic behaviour, and the second unit is a hot one for conducting the experiments of reaction. The specifications of the auxiliary equipment and measurement equipment are explained. The design of distribution plate, aero-cyclone, calculation of the mean particle size, design calculation of the CFB, and feeder calibration are presented in details in the appendices. Additionally, the procedures of operating the cold and hot units are detailed. The experiments are specified for both units. Lastly, the pure oxy-fuel CFB experiments are proposed to validate the possibility or impossibility of applying the proposed method. In the next chapter, the results and discussion of the experiments have been presented.

5 Results and Discussion

Overview

The prime objectives of this investigation are to studying the oxy-fuel CFB combustion for CCS, and enhancing the efficiency of the oxy-fuel CFB combustion by proposing a novel method for pure oxy-fuel combustion. However, to reach these, it is necessary to explore the hydrodynamic behaviour of cold CFB for a better understanding of the oxy-condition effects and ensure that the designed unit does fluidize well with good solid circulation rate (SCR). In the following subsections, the results of cold unit experiments are presented and discussed. The effects of several operating parameters viz. primary and aeration flow rates, operating pressure, particle sizes, bed inventory, and CO_2-O_2 are explored over the hydrodynamic behaviour.

The oxy-fuel CFB combustion condition experiments are conducted, after achieving fluidization condition with good solid circulation conditions. To enhance the overall efficiency of the oxy-fuel CFB combustion, a pure oxy-fuel CFB combustion is proposed in chapter 4, this hypothesis is subjected to series of experiments which show a practical suitability of applying stoichiometric ratio for controlling the temperature of pure oxy-fuel CFB combustion. The biomass fuel is used also to outlook the possibility of utilizing biomass for oxy-fuel CFB combustion, to harvest CO_2 from the atmosphere, the experiments results promise of CCS and renewable energy integration by using biomass for oxy-fuel CFB combustion. Finally, the effect of the stoichiometric ratio is explored over the exhaust gases' contents of CO_2 and O_2.

Chapter outline:

5.1 Experimental Results of Cold CFB unit

In this chapter, the bed hydrodynamic behaviour (pressure drop, axial voidage, suspension density, rate of solid recirculation) has been explored under air and oxy-combustion condition. Side-by-side, the unit hydrodynamic behaviour is studied under several operating parameters viz. operating pressure, particle size, bed inventory weight, aeration flow rate, and superficial velocity. Three groups of particle size namely 160, 302, 427 μm are used. The experiments are conducted under three aeration rates of 0.25×10^{-3}, 0.75×10^{-3}, and 1.25×10^{-3} m^3/s (to match with three superficial velocities, U_{sup}= 0.65, 1.94, and 3.23 m/s, respectively), and three velocities of primary flows viz., 0.65, 1.94, and 3.23 $m.s^{-1}$. In each experiment, the air is supplied at three pressure levels of 100, 200, and 250 kPa.

5.1.1 Effects of the primary flow rate

The primary flow rate and the resulted superficial velocity affect the CFB hydrodynamic behaviour in several aspects viz. bed voidage, suspension density, and solid recirculation rate (SRR). In this presented work, the axial voidage is found to be very high along the riser height in all the cases, and it is more than 0.98. In this dilute bed, we may assume that particle velocity matches the terminal velocity $U_p=U_{tr}$ according to Kunii and Levenspiel (1991). Figure 5.1 shows the variation of the axial bed voidage along the riser height at three different primary superficial velocities viz. 2.72, 3.4, and 4.08 m/s; at a bed inventory of 500 g; a particle size of 427 μm, an operating pressure of 150 kPa, and an aeration flow of 1.94 m/s. The increased superficial velocity (from 2.72 to 4.08 m/s) leads to higher axial voidage, since the drag force increases with the increased velocity. As a result, the CFB operating condition moves toward the pneumatic regime and the carryover of the solid particles increases. This agrees with the findings of Kalita et al. (2013) and Das et at. (2008). In all cases, a peak of axial voidage is located above the level of return-leg inlet. This pertains to dense bed at the bottom of the riser. And, between riser dimensionless height 0.2 and 0.5 [h/H], voidage decreases, then at 0.55 [h/H], the voidage increases again. This shape occurs as a result of particle diffusion in the axial riser as explained by Kwauk et al. (1985).

The comparison of suspension density sand is shown in Figure 5.3 at the following operating conditions of 200 kPa operating pressure; three primary velocities of 2.72, 3.4 and 4.08 m/s; particle size of 427 μm; and 500 g bed inventory weight. When the primary flow rate (and hence primary velocity) increases, the suspension density decreases along the riser height. This

is because, the higher primary velocity increases the voidage. Moreover, the Eq. (4.3) which has two terms [$\rho_{sus} = \rho_s(1-\varepsilon)+\varepsilon\rho_g$] are affected by the voidage change. It is clear that the density of the solid particles is higher than the density of air, the change in voidage changes the magnitude of first term more than the magnitude of the second term. For instance, when the primary velocity increases, voidage will also increase, and the increment in the second term is less than the decrement of the first term. Thus, the overall suspension density decreases. Gupta and Nag (2002) reported also similar behaviour. A dense suspension density zone is observed at the lower half of the riser, whereas, a diluted zone is found at the upper half of the riser, as a direct result of voidage profile and particles diffusion.

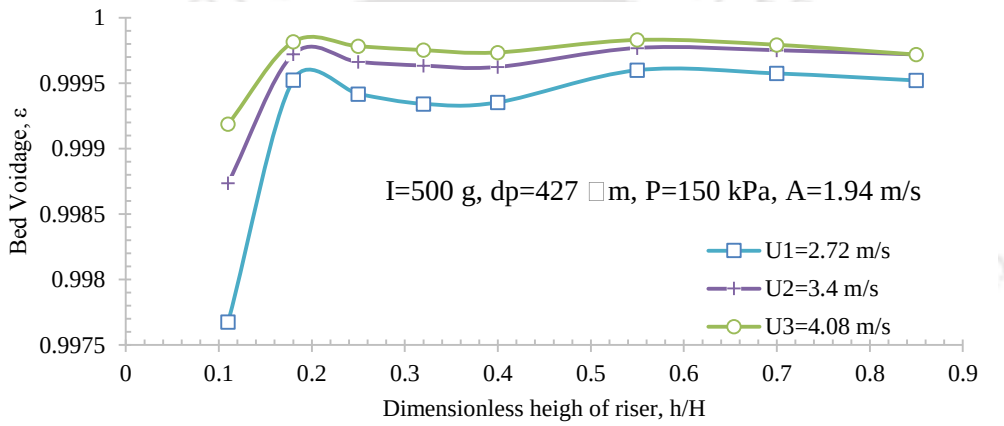

Figure 5.1 Variation of axial bed voidage along the riser height with primary superficial velocity.

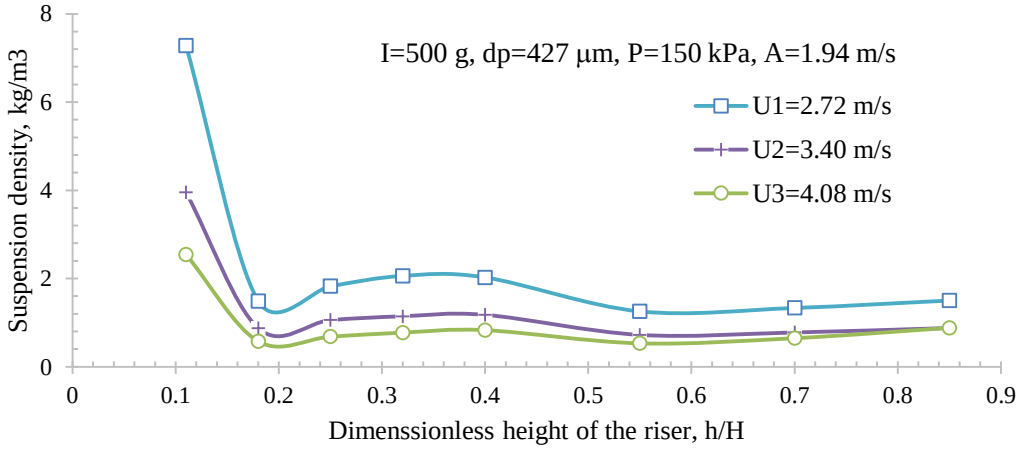

Figure 5.2 Variation of suspension density along the riser height with three primary flow rates.

Figure 5.3 illustrates the variation of solid re-circulating rate with three primary velocities viz. 2.72, 3.4, and 4.08 m/s; three aeration velocities namely 0.65, 1.94, and 3.23 m/s (which counts 4.4, 13.4, and 22.3 times of minimum fluidization velocity (U_{mf}) respectively); particle size of 427 μm; and operating pressure of 100 kPa.

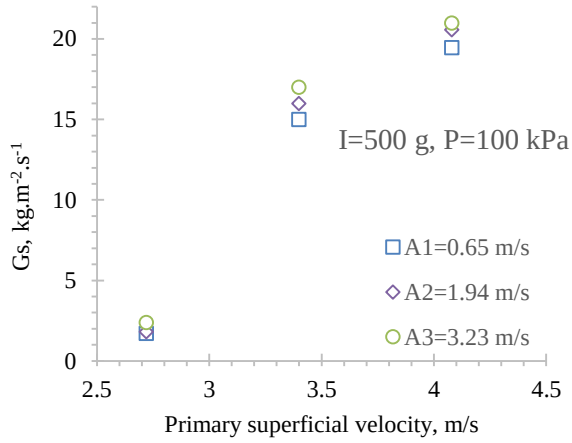

Figure 5.3 Variation of solid re-circulating rate with three aeration rates and three flow rates.

Additionally, it is observed that the solid re-circulating rate (SRR) increases from 2 $kg.m^{-2}.s^{-1}$ to 20 $kg.m^{-2}.s^{-1}$ with increased primary velocity from 2.72 up to 4.08 m/s. Meanwhile, the increment of aeration by almost 3 m/s increases the solid re-circulating rate by 2 $kg.m^{-2}.s^{-1}$. As a result, it could be inferred that, the aeration velocity has a limited effect over the solid re-circulation rate for this type of return leg. An extensive study is required for enhancing the solid re-circulation rate by aeration flow rates using different non-mechanical valves like loop-seal, L-valve, J-valve). Moreover, sand plugged the return-leg during experiments without using aeration. This observation shows the impact of aeration on flow dynamics in a CFB. And it is found that, the optimum aeration velocity is 0.63, which counts 4.4 times of the minimum fluidization velocity (U_{mf}=0.14). This findings are important for CFB oxy-combustion, since an enhanced SRR is an auxiliary technique for absorbing the increased heat of high oxygen concentration combustion. Seddighi et al. (2015b) increased the SRR up to 32 $kg.m^{-2}.s^{-1}$ for combustion of 70% oxygen concentration, to absorb the elevated heat release.

5.1.2 Effects of the operating pressure

Figure 5.4 illustrates the bed voidage at three different operating pressures of 150, 200, and 250 kPa; particle size of 427 μm; bed inventory of 500 g; and primary velocity of 3.4 m/s. The increased operating pressure increases the bed axial voidage. This increment is attributed to the higher density of the gaseous mixture under higher pressure, so the buoyancy force and holding up of the particles in the riser increases, and the bed inventory increases. This observation matches with the results of Cheng and Basu (1999). A sharp voidage decrement is located above the entrance from return-leg, because of the alignment of the aeration direction with the return-leg's axis.

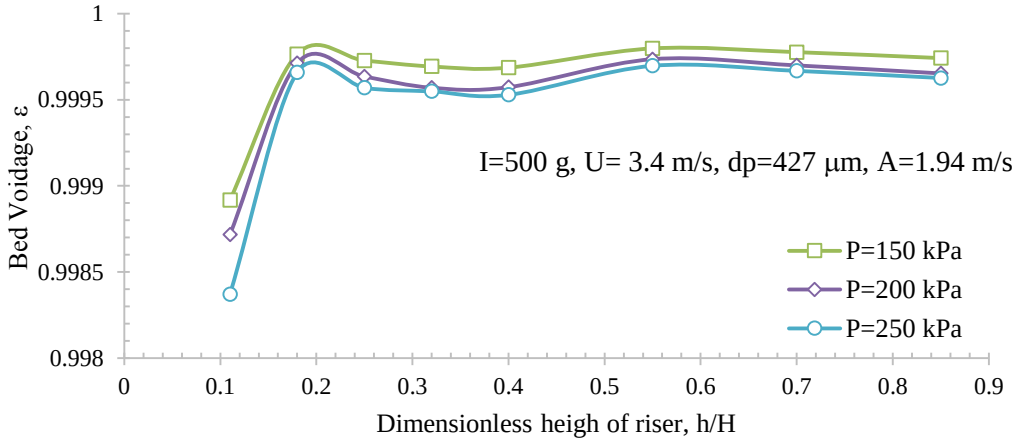

Figure 5.4 Variation of bed voidage along the riser height for different operating pressure levels.

Furthermore, the operating pressure affects the suspension density as seen from Figure 5.5. At the bottom, the highest suspension density (as much as 3.5 to 5 kg/m^3) is found directly above the return-leg entrance level. This suspension density profile is pertained to higher solid phase density, where the particles axial velocity accelerates form 0 m/s. The suspension density, then decreases down to almost 1 kg/m^3, as the particles diffuse along the riser. Kalita et al. (2013) reported the same behaviour, increasing of suspension density with increasing the operating pressure.

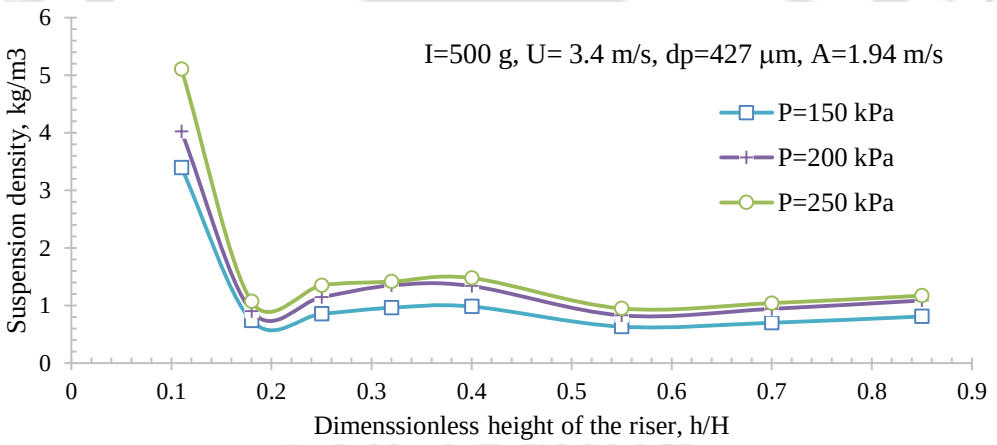

Figure 5.5 Variation of suspension density along the riser height with three operating pressure levels.

5.1.3 Effects of the aeration flow rate

The main task of aeration flow rate is to entrain smoothly the particles from return-leg to the riser, in other non-mechanical valves like loop-seal, aeration control the rate of SRR. Figure 5.6 illustrates the variation of bed voidage with three aeration velocities viz. 0.65, 1.94, and 3.23 m/s, at primary velocity of 2.72 m/s, operating pressure P=200 kPa, and inventory of I = 500 g. The same general pattern is detected, for instance a higher voidage at the bottom of the riser

compared to the upper part. The increased aeration velocity enhances the particle entraining into the riser, as a result, the voidage decreases. Chovichien et al. (2013) observed the same trend of bed voidage profile for L-valve also, where the axial bed voidage increased with an increased aeration velocity.

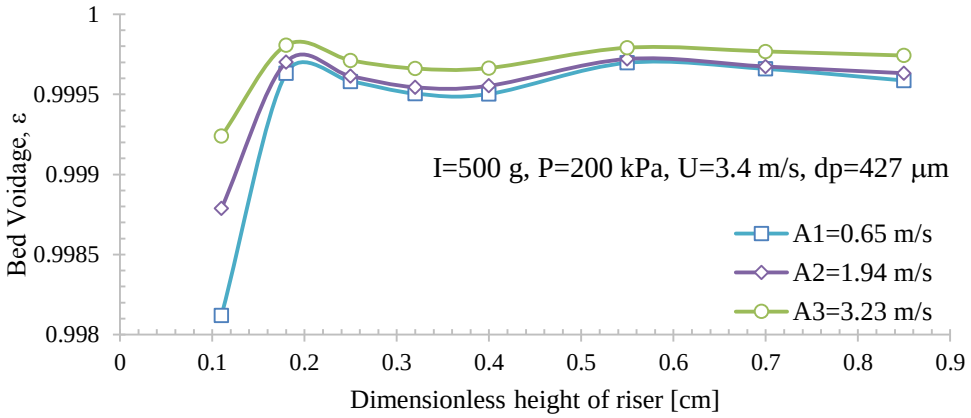

Figure 5.6 Variation of bed voidage along the riser height for different aeration flows.

The comparison of suspension density is shown in Figure 5.6 under the following operating conditions of a 200 kPa operating pressure; three aeration rates of 0.65, 1.94, and 3.23 m/s; primary velocity of 2.72 m/s and a sand bed inventory of 500 g. When the aeration rates increase, the suspension density decreases along the riser height. This is because the higher aeration will increase the voidage.

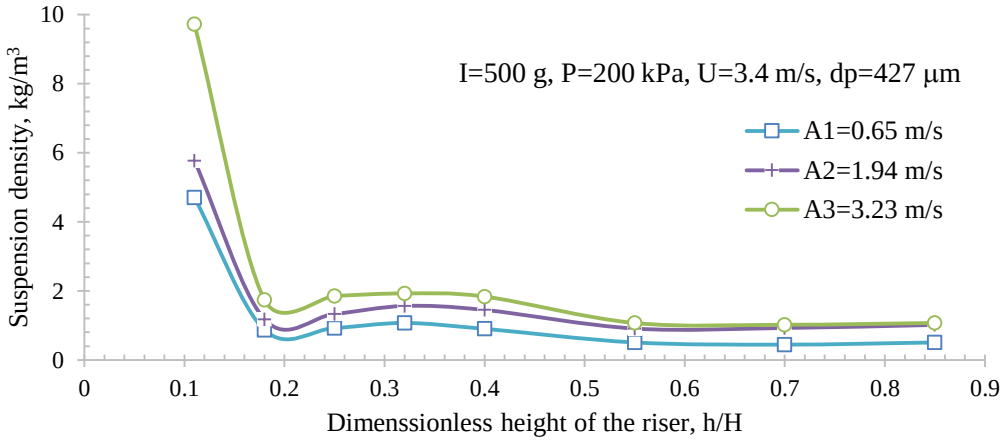

Figure 5.7 Variation of suspension density with three aeration rates.

As explained in section (5.1.1), the suspension density increase with the bed voidage decrement and vice versa. Gupta and Nag (2002) reported a similar behaviour. A dense suspension density zone is observed in the lower half of the riser; meanwhile, a diluted zone is found in the upper half of the riser, as a direct result of voidage profile and particles diffusion.

5.1.4 Effects of the particle size

The particle size affects the axial bed voidage because of different terminal velocities and drag coefficients. Subsequently, the heat transfer and operating conditions of the bed are affected (Basu, 2015). Figure 5.8 shows axial bed voidage at three particle sizes viz. 160, 302, and 427 μm; three superficial velocities 1.3, 2.5, and 3.3 m/s; bed inventory of 500 g; and 100kPa operating pressure.

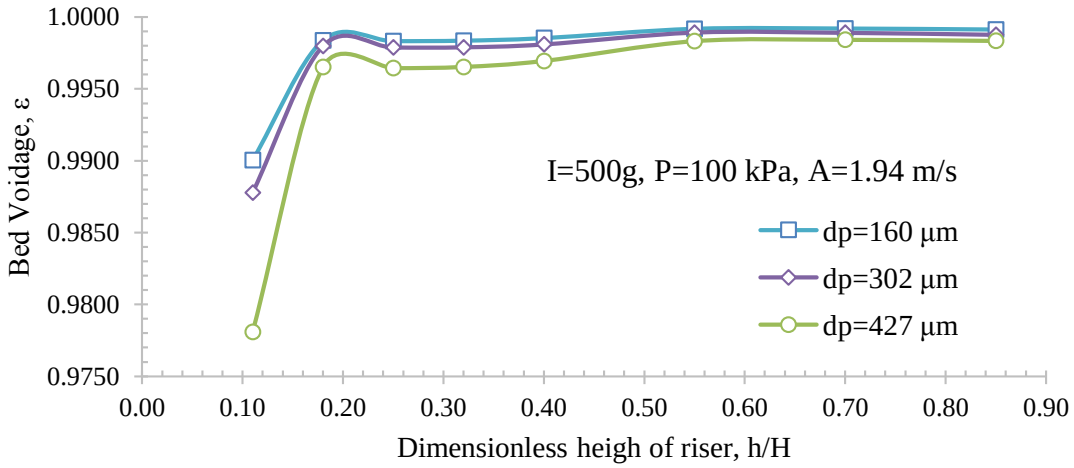

Figure 5.8 Variation of bed voidage along the riser with different particle sizes.

In the aim to compare the effects of different particle size groups with different terminal velocities, the percentage of maintained velocities to the terminal velocity of each particle size is fixed at the value of U/U_{tr}=2.2. At three cases, the same typical CFB voidage profile is observed with lower voidage value in the bottom and higher voidage in the upper part of the riser. The increased particle size from 160 μm, 302 μm to 427 μm leads to higher bed voidage.

The drag coefficient is calculated for sand particles of 2600 kg/m^3 density, and air as a medium gas at 30°C (Haider and Levenspiel, 1989). The drag coefficient decreases with increased Reynolds number. When the particle size increases, Reynolds number increases, and this leads to a lower drag coefficient (Figure 5.9). Moreover, the gravitational force increases with the particle size and lowers the overall entraining force over the particles, so, the bed voidage increases.

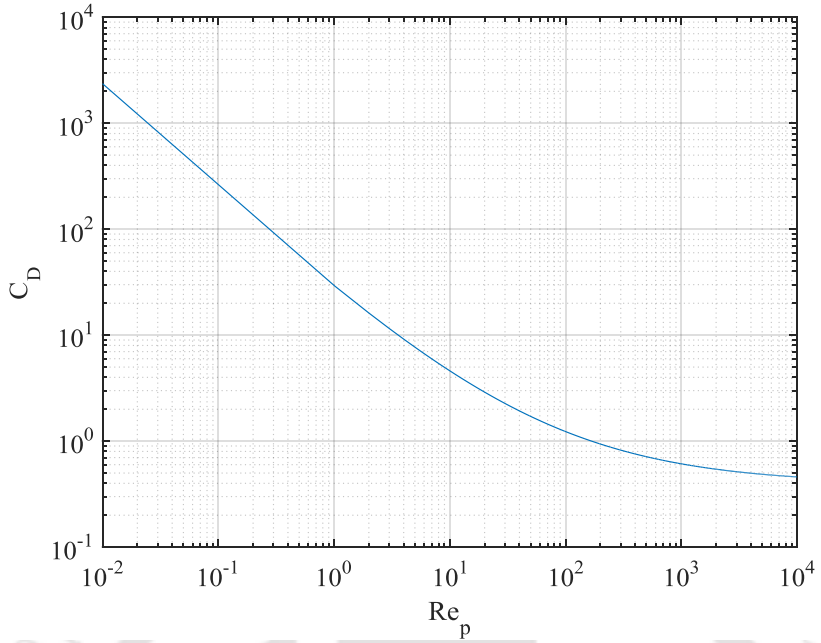

Figure 5.9 Drag coefficient variation with particle Reynolds number

Additionally, the suspension density increases with increased particle sizes (Figure 5.10), these findings helps to enhance the heat transfer in the bed (Basu, 2015).

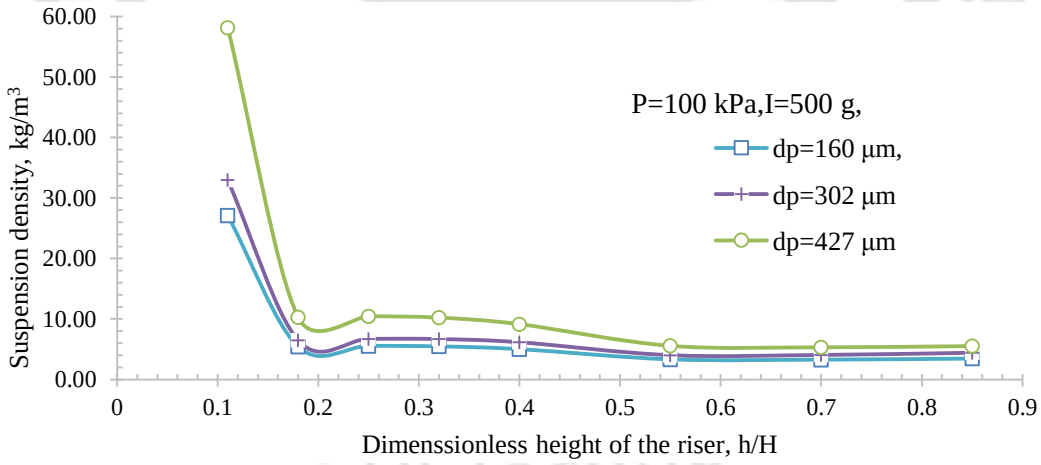

Figure 5.10 Variation of suspension density with three particle sizes.

5.1.5 Effects of the bed inventory

The bed inventory has an increasing importance in oxy-combustion of CFB, since the increased circulated inventory absorb the enhanced and elevated heat of high concentration oxy-combustion. Figure 5.11 shows the increased axial bed voidage with increased bed inventory. Using other types of non-mechanical valves with external heat exchanger may lead to higher

SRR, larger bed inventory and lower bed voidage, which is recommended for absorbing higher RoHR.

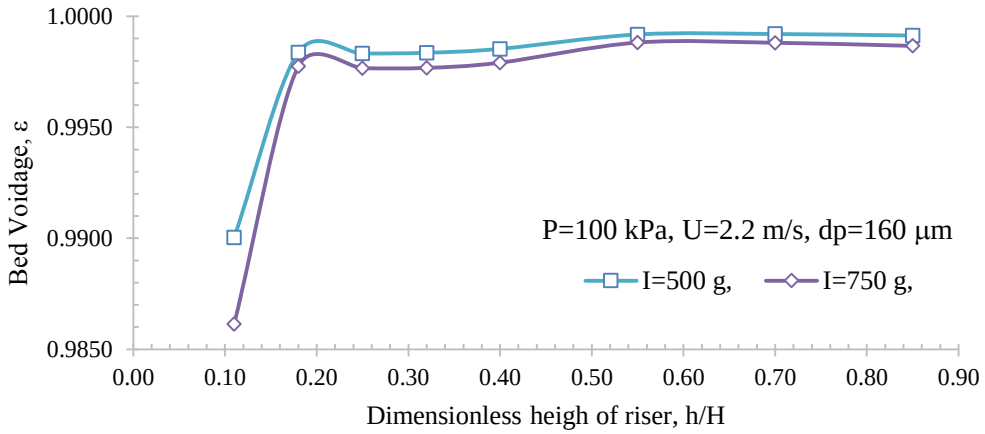

Figure 5.11 Variation of bed voidage along the riser with two different bed inventories.

On the other hand, the suspension density increases with increased bed inventory as illustrated in Figure 5.12, which leads to better heat transfer coefficient. The bed inventory in the riser could be enhanced using an external heat exchanger (Bolea et al., 2014).

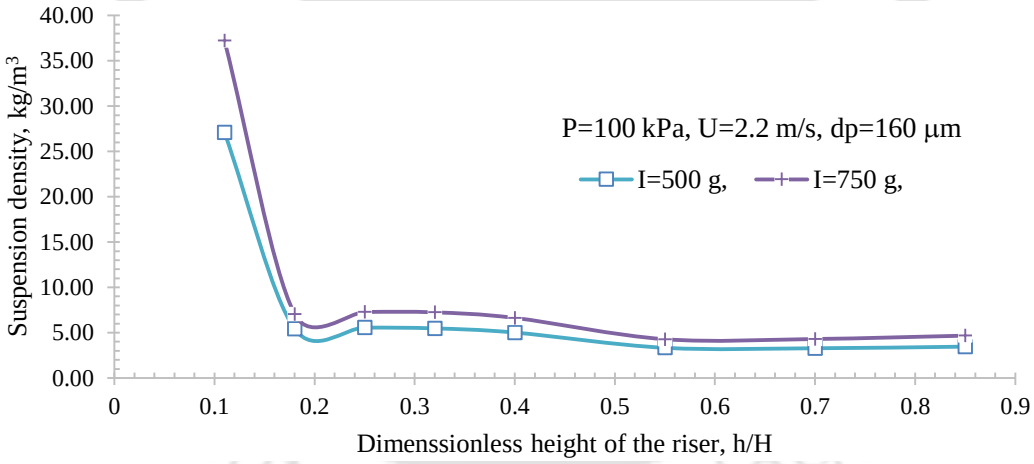

Figure 5.12 Variation of suspension density with bed inventory.

5.1.6 Effects of the O_2-CO_2 concentrations in oxy-CFB condition

The properties of fluidization gaseous medium viz. density, dynamic viscosity, specific heat capacity, oxygen diffusivity affects the hydrodynamic behaviour, reactions, and heat transfer. In this work, the effects of oxy-operating conditions are studied over bed voidage and suspension density, with an aim to, predicates the hydrodynamic behaviour of hot CFB unit. Figure 5.13 shows a higher bed voidage, where the pure CO_2 and O_2 are used for comparison. In both cases, the particle size d_p=427 μm, and a fixed velocity of 2.78 m/s are used.

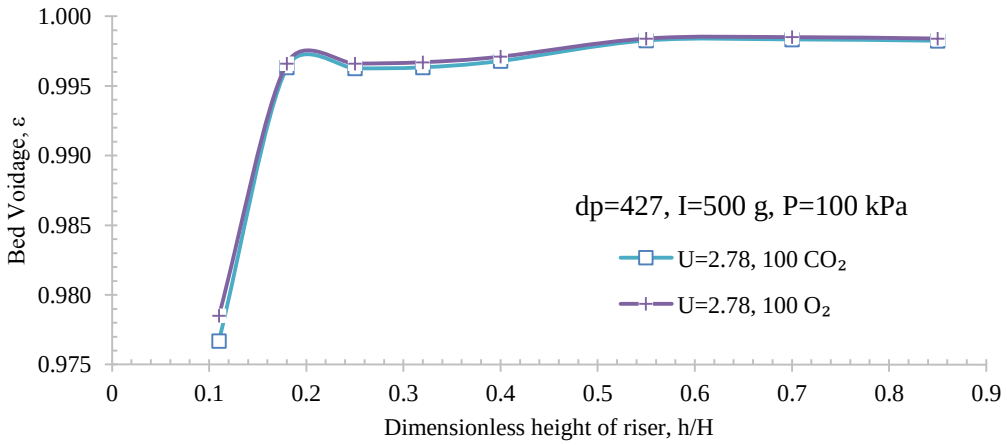

Figure 5.13 Variation of bed voidage along the riser with different gases, O_2 and CO_2.

This difference is pertained to the different terminal velocities of CO_2 and O_2. As it is shown by Eq. 2.11, the terminal velocity is a function of gas density, and dynamic viscosity. The terminal velocity changes due to different properties of operating gases i.e., the density of CO_2 is higher than densities of N_2, air, and O_2. Meanwhile, O_2 dynamic viscosity is greater than of dynamic viscosities, of N_2, air, and CO_2.

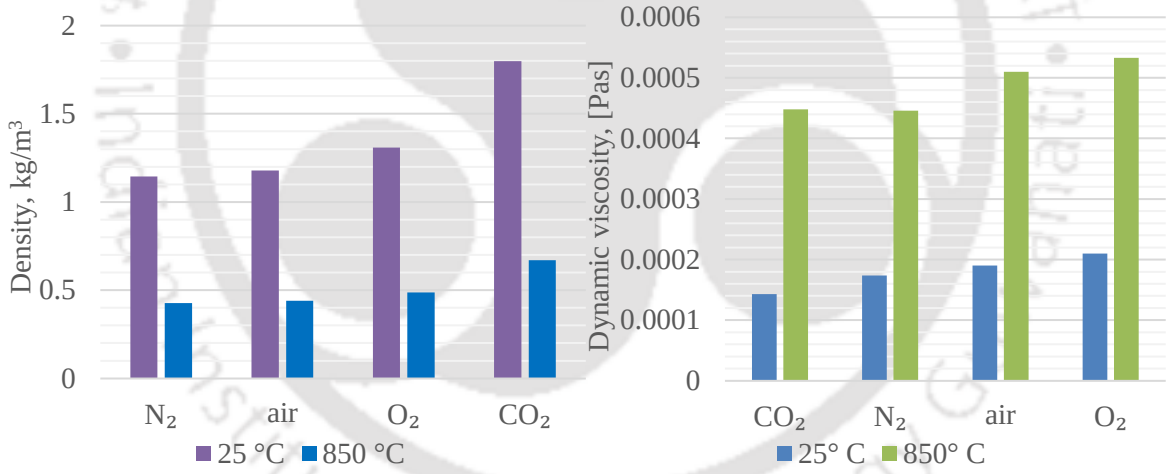

Figure 5.14 Variation of densities and viscosities of N_2, air, O_2, and CO_2, with temperatures from 25°C to 850°C

To explore the effect of these properties, the terminal velocity is calculated using Eq.(2.13) for these conditions; sand particles of 0.7 sphericity, particle size range from 0 to 500 µm, and four gases viz. N_2, air, O_2, and CO_2, at two different temperatures namely 25°C and 850°C (Haider and Levenspiel, 1989). The terminal velocities of O_2 are slightly lesser than that of CO_2 (Figure 5.15), this results a higher holding up force for O_2 comparing with this of CO_2 at the same velocity, and hence, the bed inventory is higher in CO_2 case. This explains the slight difference of bed voidage. Moreover, the maximum velocities difference is ΔU=0.157 m/s

between U_{CO_2}=0.759 m/s at 850°C and U_{N_2}=0.916 m/s at 25°C. Also, for the same temperature degree of 850°C, the maximum terminal velocity is ΔU=0.11 m/s between U_{CO_2}=0.759 m/s at 850°C and U_{N_2}=0.8682 m/s at 25°C.

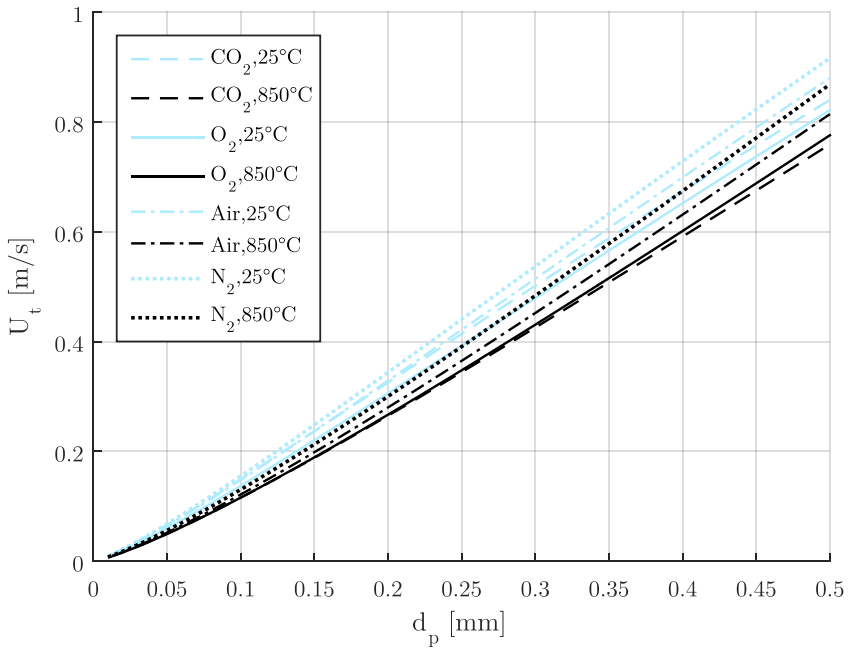

Figure 5.15 Variation of terminal velocity of sand particles with particle size for different gases

Figure 5.16 shows the lower suspension density with pure O_2 compering with 25%-75% O_2-CO_2 and 35%-65% O_2-CO_2, and as explained in subsection (5.1.1), the suspension density increases with bed voidage decrement, and vice versa.

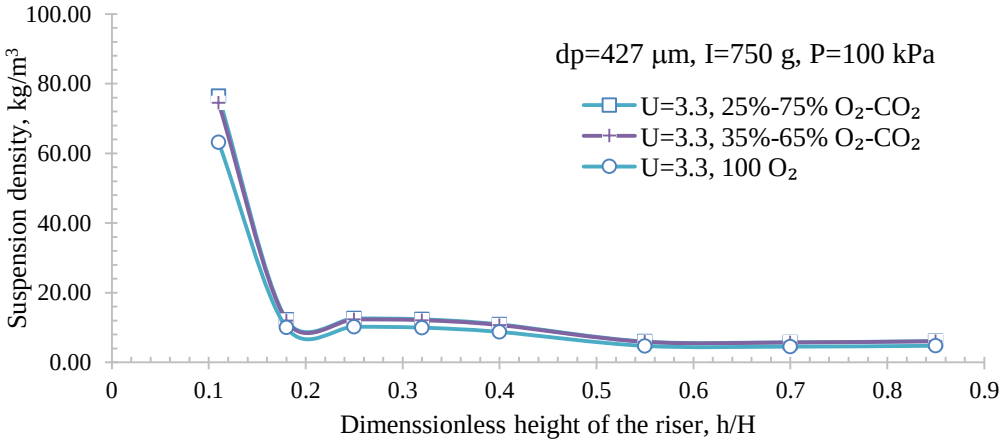

Figure 5.16 Variation of suspension density with bed three O_2 concentrations.

It can be inferred that, the effect of oxy-operating conditions over terminal velocity is not huge, and can be in range of ±10% comparing with air-operating conditions at 850°C. On the other hand, the change of density and dynamic viscosity due to higher temperature shall be taken in

account. All above mentioned experiments match with the fast and circulating system zones, as explained in details by Avidan and Yerushalmi (1982).

5.1.7 Experimental Uncertainties

The theory of sequential perturbation technique by Kline and McClintok (1953) and Moffat (1982) is used to calculate the uncertainties of the parameters. The procedure is shown in details in Appendix E. Table 5.1 and Table 5.2 show the overall uncertainty for bed voidage measurements and overall uncertainty for solid circulation rate

Table 5.1 Overall uncertainty for bed voidage measurements

L_m [m]	Δh [cm]	U [±%]
0.077	5	5.0
0.016	4.9	18.8
0.177	5.7	3.5
0.022	5.8	13.9
0.14	5.9	4.0
0.138	6.1	4.0
0.142	6.3	4.0
0.014	6	27.2
0.162	6.5	3.9
0.3	6.7	2.9
0.3	6.8	2.9
Overall Uncertainty average		8.2

Table 5.2 Overall uncertainty for solid circulation rate

L_m [m]	Δh [cm]	U [±%]
0.077	5	3.254234
0.016	4.9	23.48721
0.177	5.7	2.126118
0.022	5.8	15.44387
0.14	5.9	2.456272
0.138	6.1	2.516408
0.142	6.3	2.515981
0.014	6	36.536
0.162	6.5	2.376766
0.3	6.7	1.745422
0.3	6.8	1.758152
Overall Uncertainty average		8.56513

Appendix E contains a detailed procedure of Overall uncertainty calculation.

5.2 CFB Combustion under Pure O_2 Concentration

Figure 5.17 illustrates the variation of temperature along the riser starting with pure oxy-biomass combustion case; followed by pure oxy-coal combustion with three different

stoichiometric cases; and finally shutting down with air combustion. The thermocouples along the riser are numbered from 101 up to 108, the numbering starts with the bottom side and moving towards the upper portion.

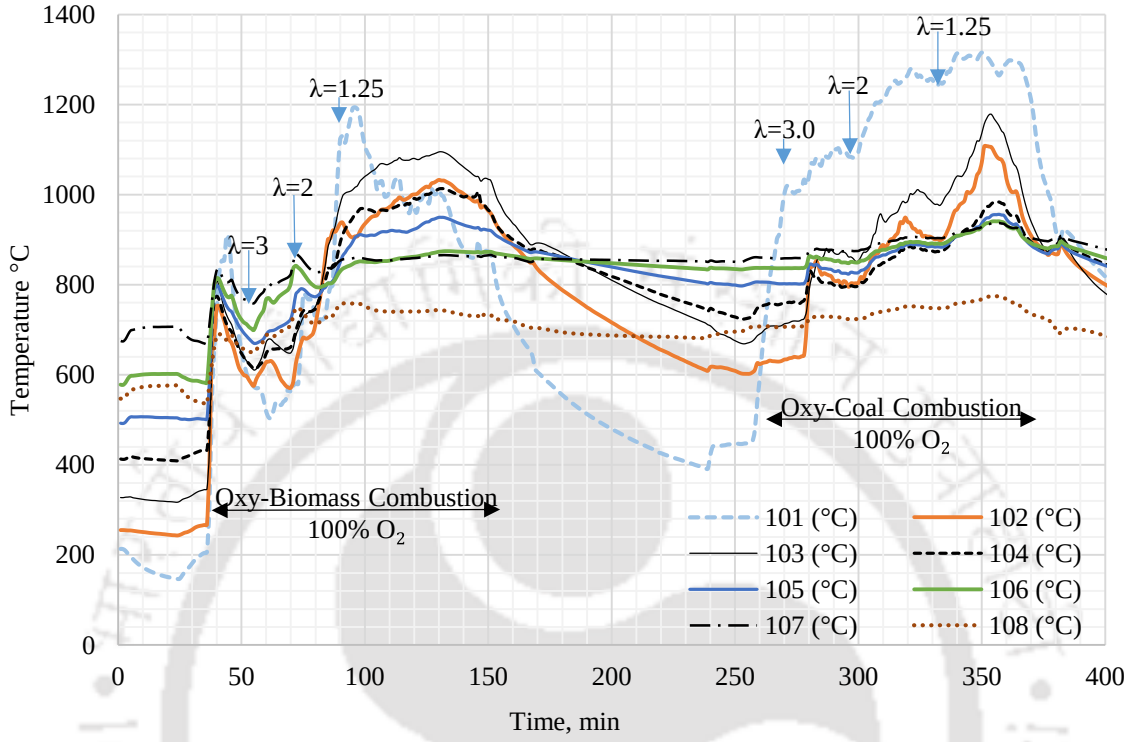

Figure 5.17 Variation of temperature along the riser for different fuel types and conditions through time

In the oxy-biomass CFB combustion, the variation of the temperature through the riser height (with different fuel mass flow rate) is pertained to distributed combustion along the riser. Interestingly, the lower stoichiometric λ=1.25 ratio leads to higher temperature at the bottom portion (1031°C) since the rate of heat release is higher due to higher fuel mass flow rate (higher RoHR) and the large fuel particles fall and react at the bottom due to their higher terminal velocity comparing with used superficial velocity. In contrast, the increased stoichiometric ratio leads to lower temperature along the riser. The average temperatures along the riser (oxy-biomass CFB combustion case) are 1031°C, 950°C, and 798°C for λ=1.25, 2.0, and 3.0, respectively.

In the oxy-coal CFB combustion case, the highest temperature level is located at the bottom of the riser, and the temperature increases with the increased coal mass flow rate and lower stoichiometric ratio. The average temperatures along the riser (oxy-bituminous CFB combustion case) are 1129 °C, 1051 °C, and 961 °C for λ=1.25, 2.0, and 3.0, respectively.

For both of coal and biomass, as predicted, the temperature is maximum under λ=1.25 condition, and it subsequently decreases under λ=2.0 and λ=3.0. Additionally, it is recognised that, the variation of temperature along the bottom portion of the riser is more than the variation at the upper portion, since the reaction takes part mainly at the lower portion In contrast, the temperature at the upper portion is lower as measured by thermocouples (no.: 105, 106, 107, and 108). The coal and biomass CFB combustion results are explained below.

5.2.1 Pure oxy-fuel CFB combustion

The pure oxy-biomass combustion under 100% O_2, stoichiometric ratio, λ=1.25 results the temperature profile as shown in Figure 5.18. The highest temperature is located directly at the level of feeding port with almost 1200°C, the lowest temperature is 900°C, and the average is 1150°C along the riser. Interestingly the concentration of CO_2 at the outlet is quite high as 76.8%, the excess O_2 is 20.7%, which is an excess O_2 to control the stoichiometric ratio, and N_2 is 2.5%.

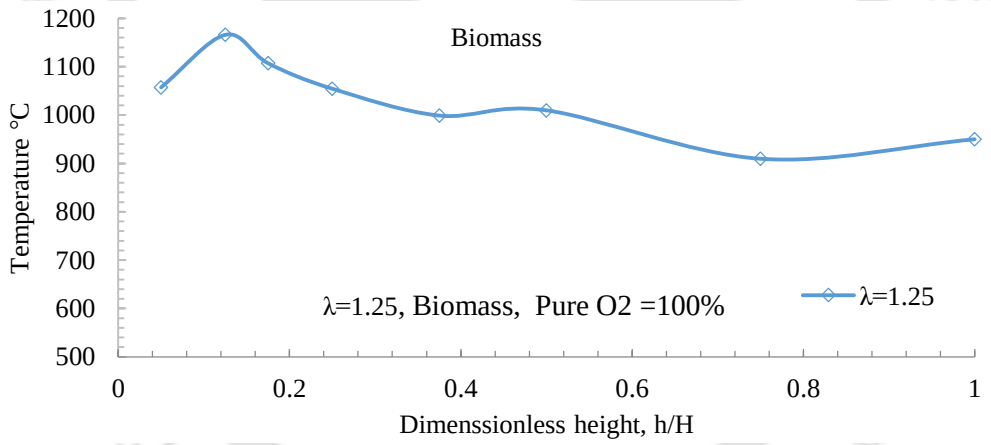

Figure 5.18 variation of temperature along the riser with pure oxy-biomass combustion λ=1.25

The same trend of temperature profile is found for the stoichiometric ratios of λ=2, and 3, and the average temperature of 950 °C and 800 °C. There is no CO detected by gas chromatography analysis Figure 5.19. This finding agrees with results of Tondl et al. (2011), where the concentration of CO from 1200 mg/MJ to below than 200 mg/MJ for increased O_2 from 3.9% up to 10%, and this explains the undedicated CO.

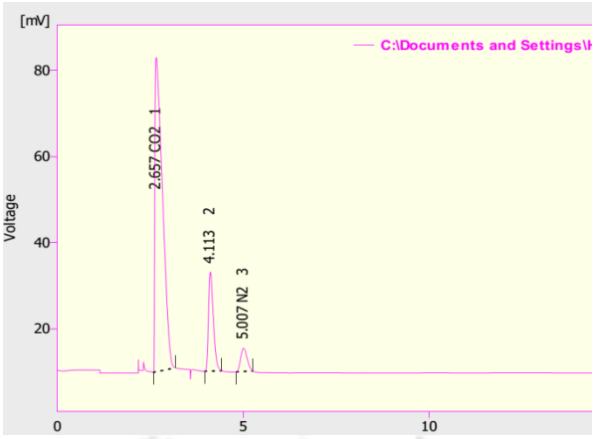

Figure 5.19 Sample of Gas Chromatography analysis

The effect of stoichiometric ratios viz. λ=3.0, 2.0, 1.25 on the bed temperature profile shows that the combustion using pure oxygen for coal combustion instead of air or mixture of CO_2-O_2 (Figure 5.20). In all cases, the temperature profile starts with a high peak temperature of more than 1100 °C, and gradually it decreases. A significant drop in temperature is found at the level of the aeration entrance. This pertained to the lower temperature of the aeration (~5°C) which flows directly from the cylinder of CO_2 without pre-heating. Additionally, the temperature profile is found almost uniform at the medium height of the riser, where, the temperature drop from 900°C to 700°C at the exit which is not insulated.

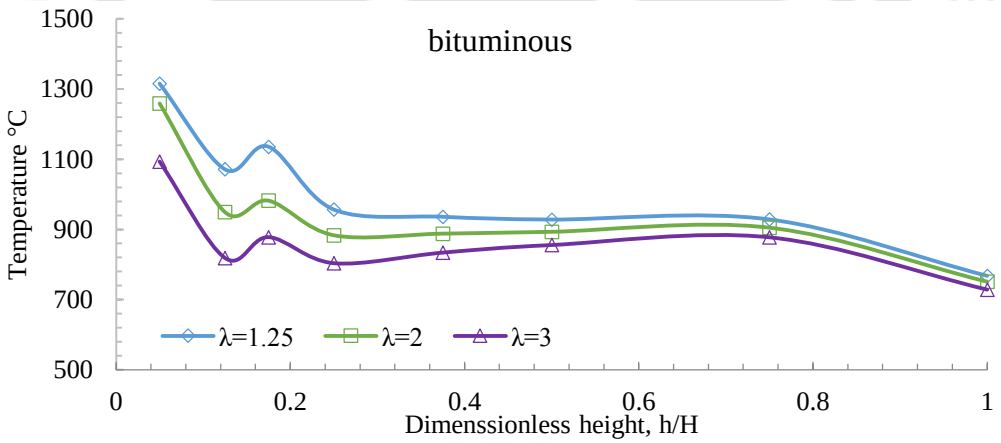

Figure 5.20 Variation of temperature profile with stoichiometric ratio along the riser height for coal fuel

From the temperature profile it is inferred that, the combustion takes place mainly at the bottom of the riser. This is pertained to the higher terminal velocity of the coal particle (of d_p=0.85~1.70mm) compared to the used superficial velocity U=2.0 m/s. As a result, the coal particles at the early stages of combustion (drying, devolatilization, ignition) remain slugging

at the bottom till losing sufficient weight by reaction and getting lower terminal velocity to rise up (the terminal velocity of 1.0 mm coal particle size is 2.0 m/s (Figure A.2).

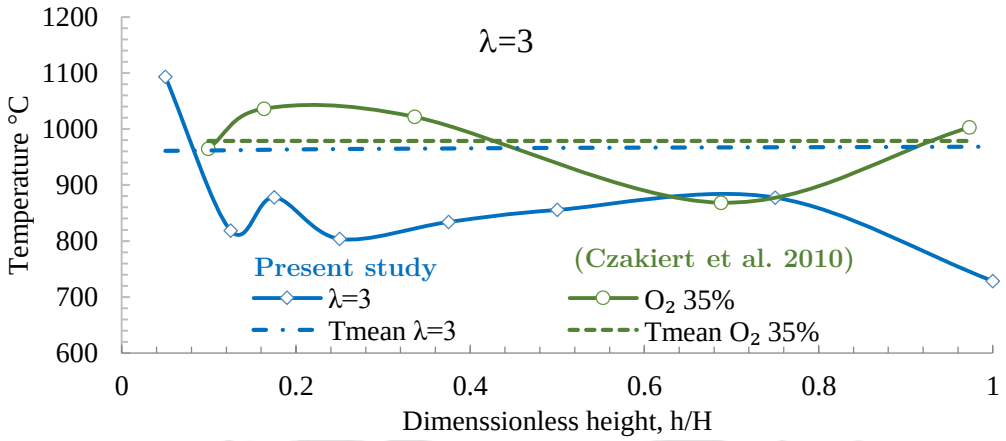

Figure 5.21 Comparing temperature profile with results of Ref. (Czakiert et al. 2010)

Czakiert et al. (2010) conducted enhanced oxy-fuel CFB combustion. They used coal particle size of 1 mm and superficial velocity of ~4.85 m/s, the temperature profile for O_2 concentration of 35% is compared with the result of present study for λ=3.0 in Figure 5.21. Where, the higher superficial leads to more uniform temperature profile along the rise, comparing with the present study where we used coal particle size of 0.85~1.70 mm and terminal velocity of U_{tr}= 1.8~2.8 m/s (Czakiert et al., 2010). In both studies the temperature profile has almost the average temperature, about ~970 °C.

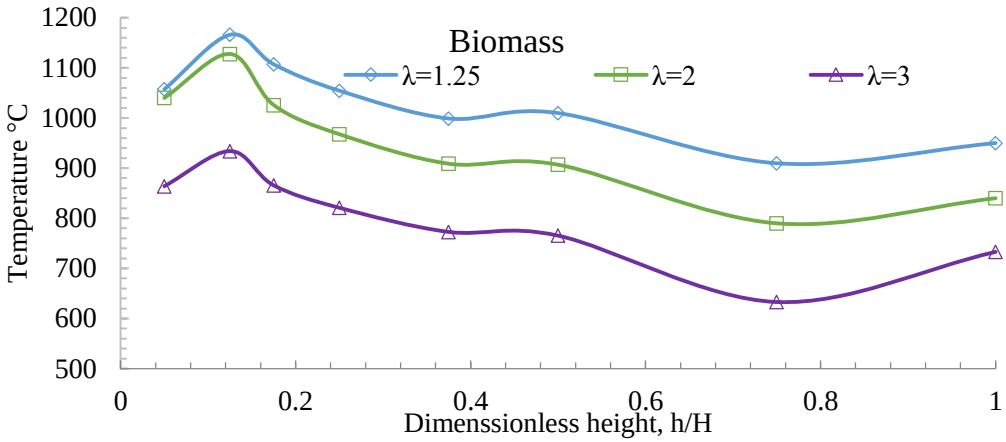

Figure 5.22 Variation of the temperature profile with λ= 1.25, 2, and 3 along the riser height for biomass fuel

In contrast with pure oxy-coal CFB combustion the temperature profile along the riser (Figure 5.22) for pure oxy-biomass CFB combustion shows peak at the aeration port level that is because of the instant firing of the biomass particles, which have lower ignition temperature compared to coal, and the lower terminal velocity of biomass.

These results optimize the stoichiometric ratio for the first stage of pure oxy-fuel CFB combustion. And the stoichiometric value λ =3.0 is considered as the best value to achieve the required temperature in range of 800 °C up to 700 °C. This ratio is suitable for three stages as illustrated in Figure 3.3 and Figure 3.4, and λ =2.0 could be used for two stages of pure oxy-fuel CFB combustion arrangements. The pure oxy-fuel CFB combustion could minimize the cost of power plant by compacting the setup and enhancing the overall efficiency (Seddighi et al., 2011a,b).

This technique could open the door widely for the 3rd generation of oxy-fuel CFB combustion with higher efficiency. So far, up to the best of the authors' knowledge, there is no pure oxy-fuel CFB combustion; the highest used percentage was 60% O_2 concentration that achieved by Bolea et al. (2014), where external fluidized heat exchanger was used with enhanced recirculation rate to absorb the released heat. Still, the cost of installing and operating cost of recirculation setup is required. Our proposed method eliminate the recirculation setup and cut down the cost of power plant and the operating cost, compact the CFB power plant and cut down the set up overall cost.

5.2.2 Effect of stoichiometric ratio over concentration of CO_2 and O_2

The measurement of the exhaust volumetric percentage is essential for the proposed method, since, the outlet of the first stage is the inlet of the later stage. And, consequently the fuel mass flow rate of the later stages could be calculated accordingly. Figure 5.23 shows the volumetric concentration of CO_2 and O_2, where the O_2 concentration increases with increased λ, in contrast, the CO_2 concentration decreased with increased λ. Based on this data, the preferred stoichiometric ratio for two stages arrangements is 2. In this case, the rate of heat release could be controlled, and two fuel feeding system are sufficient for single CFB arrangements, or two CFBs are sufficient for the second arrangement as explained in Figure 3.3 and Figure 3.4. This technique of controlling the temperature with high oxygen concentration in has a superiority over the EGR, where the moisture, SO_x, and NO_x concentration increase dramatically, and even the recirculated moisture reacts with the SO_2 and SO_3 producing acid (Duan et al., 2015).

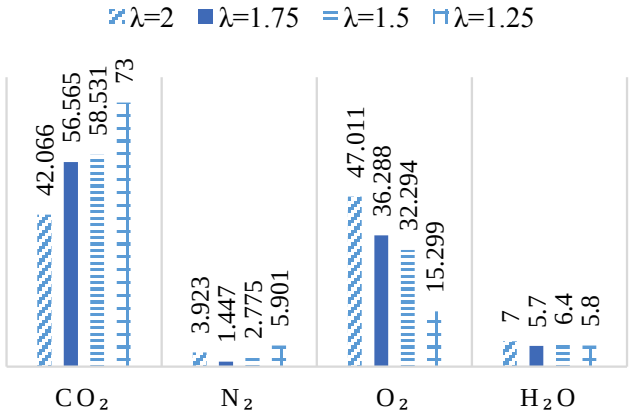

Figure 5.23 Variation of the CO_2 and O_2 with Stoichiometric Ratio

So far, the experimental results using mini-CFB are promising, and extra experiments using pilot scales are required to pass the technique to the industrial application.

5.3 Summary

The present chapter carries out the experimental results of cold and hot CFB units, which described as following:

- ✓ Increased primary flow rate increases the bed voidage and solid re-circulating rate; and decrease the suspension density along the riser.
- ✓ Increased operating pressure reduces both of bed voidage and suspension density.
- ✓ For this mini-CFB, increased aeration rises both of bed voidage and suspension density.
- ✓ Increased particle size leads to higher drag coefficient and suspension density; and less bed voidage.
- ✓ Enhanced bed inventory decreases the bed voidage and increase the suspension density.
- ✓ Interestingly, the mixture of CO_2-O_2 has insignificant effects over the hydrodynamic behaviour. And the terminal velocity for air and CO_2-O_2 has the same value ±10%.
- ✓ Pure oxy-fuel CFB combustion is conducted successfully for both of biomass (sawdust) and coal. Under different operating conditions, with different stoichiometric ratios. These results validate the proposed method of pure oxy-fuel CFB combustion.
- ✓ The bed temperature is controlled successfully with high stoichiometric ratio instead of recirculation flue gases. This lead to eliminating the recirculation setup. The average temperature along the riser is about 950 °C.
- ✓ The optimized stoichiometric ratio for two stages of mini-CFBs is λ=2.

6 Fuel and Reaction Exergy Analysis for Oxy-fuel CFBC

Overview

In general, first law of thermodynamics is used to evaluate the power plant performance, and only assesses the quantity of energy, meanwhile, exergy analysis is based on the second law of thermodynamics and justify the real useful energy, and exergy assesses both of quality and quantity of energy (Kaushik et al. 2011). And the thermodynamic analysis gives better understanding of the process and way which energy flows through. On the other hand, new tactics and technologies are proposed to maximize the efficiency of power plants such like (Enhanced oxygen combustion, oxy-fuel CFB combustion, Gas Turbine Companied Cycle (GTCC) etc.). Therefore, thermodynamic analysis is highly required for clarifying the changes over the thermal system performance, clarifying the effects of different parameters (pressures, temperatures, flow rates etc.), and maximizing the overall efficiency. Moreover, the fuel analysis is desirable to be extended to use second law of thermodynamics (exergy) side by side with the first law of thermodynamics, and quality of the fuel is presented as a ratio of exergy to energy (Ghamarian and Cambel, 1982). In general, solid fuel (biomass, coal) can be categorized based on O/C and H/C atomic ratio (Krevelen, 1961). In literature, several papers concerns the exergy analysis of coal combustion power plant and assessing the performance of the different parts of power plant as reported in reference (Yazdanfar et al., 2015); these studies analyse air combustion mode of the power plant only, therefor, an exergy study is required to assess the oxy-fuel CFB combustion. This is a fundamental study to compare air combustion case with several scenarios of oxy-fuel combustion.

Chapter outline:

The Objectives of this chapter

Since, the oxy-fuel CFB combustion technology is dawning, and in absence of assessment studies on oxy-fuel combustion sufficiency, a basic thermodynamic exergy analysis is required to clear up several points as following:

- How does the fuel exergy vary over wide range of H/C and O/C?
- How does air CFB combustion differ from oxy-fuel CFB combustion and pure oxy-fuel CFB combustion at the reaction exergy level?
- How the exhaust gases' temperature does affect the exergy efficiency?
- How the preheating does affect the exergy efficiency?
- What is the optimum oxygen concentration of oxy-fuel combustion?

These are the main objective of this fundamental study of chemical reaction exergy.

6.1 Exergy (Quality) of Solid Fuel

6.1.1 Heating value of the solid fuel

Solid fuel has a wide range of types, and Krevelen diagram maps both of coal and biomass fuel and clarify the distribution of fuel over the ranges of O/C and N/C ratios (Krevelen, 1961), this diagram is limited only for C, H, and O elements. We have extended this diagram to include nitrogen N and sulphur S . Figure 6.1 illustrates the carbon percentage C% as a function of fuels' ratios O/C, H/C, and N/C, this diagram considers the ranges of O/C, H/C, and N/C as following a= [0.0-1.0], b= [0.0-2.0], and c= [0.0-0.2] respectively for fixed value of S=d. Finally, we solved the set of Eq. (6.2) using MATLAB 2015, and the percentages of C, H, N, O, and S are found.

$$\left.\begin{aligned} a &= O/C \\ b &= H/C \\ c &= N/C \\ d &= S \\ C+H+N+S+O &= 100\% \end{aligned}\right\} \qquad (6.1)$$

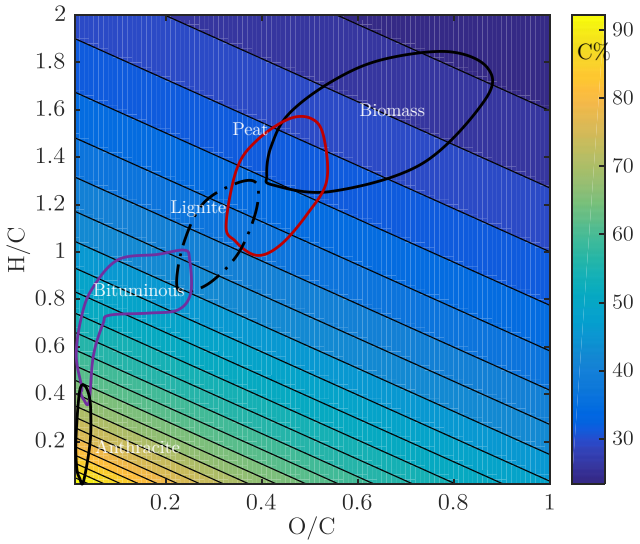

Figure 6.1 Variation of Carbon percentage with fuels' ratios O/C, H/C, and N/C

Figure 6.1 shows the change of fuel's carbon content which decrease along the direction from anthracite regime to biomass regime through bituminous, lignite, and peat regimes. The biomass carbon percentage C% falls in range of 20% to 40%. Meanwhile, anthracite has a carbon contents of 70% up to 100%. This figure (Figure 6.1) could include other carbohydrate solid fuel which uncategorised under coal or biofuel. This figure could be re-plotted for specific ratio to zoom in categories and plot the sub-categories, for instance, biomass regime can be re-plotted based on the used type of fuel. On the other hand, to increase the accuracy for specific fuel group the ratio of N/C could be varied accordingly (Figure 6.2).

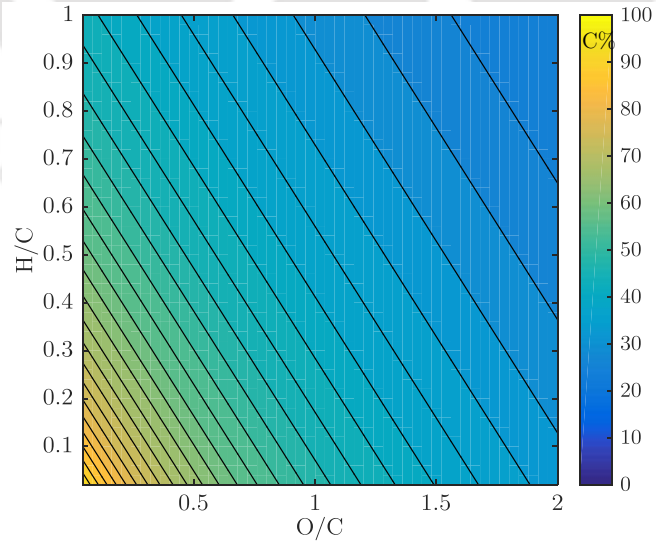

Figure 6.2 Variation of Carbon with fuels' ratios O/C, H/C, and N/C of biomass.

A survey by Khan et al. shows that for several biomass types viz. wood pellets, demolition wood pellets, pepper plant residue, greenhouse residue, wheat straw, sunflower pellets, olive cake pellets, and sewage sludge, the percentages of C, O, H, and N are [30%-60%], [30%-50%], [0%-10%], and [%0-10%] respectively (Khan et al., 2009). For zero S contents, we have proposed the ratios of O/C, H/C, and N/C of biomass, as following [0.6-2.1], [0.025-0.25], and [0.025-0.25] respectively (Figure 6.2).

6.1.2 Calculation

Furthermore, in aim to calculate the quality of fuel both of lower heating value (LHV) and fuel exergy are required to be calculated. Since, the LHV is not sufficient to give real rank and value of the fuel, where the solid fuel has several components based ultimate analysis viz. C, H, N, S, and O; and based on proximate analysis viz. fixed carbon, ash, moisture and volatile matter plays crucial role in specifying the quality of the solid fuel. Based on ultimate analysis, the LHV is calculated using Eq. (6.2) of a 0.70% average deviation and Eq. (6.3) of a 2.0% average deviation (Ghamarian and Cambel, 1982). The number of moles is calculated by Eq. (6.4).

$$L.H.V._{CHNS} = 427.03482n_C + 90.88110n_H - 207.46434n_O + 297.0116n_S [MJ/kg] \quad for\ n_O/n_C \le 0.5 \tag{6.2}$$

$$L.H.V._{CHNS} = 425.73849n_C + 91.51107n_H - 199.15224n_O + 297.0116n_S [MJ/kg] \quad for\ n_O/n_C \le 1.0 \tag{6.3}$$

$$n_i = \frac{w_i}{M_i} \tag{6.4}$$

Moisture and ash contents of the solid fuel are considered for higher reliability of the LHV calculation. Table 6.1 shows the proximate and ultimate analysis of four types of fuel viz. Assam coal, Tikak coal, Ledo coal, and biomass, these types are used for the comparison. Meanwhile, the Table 6.2 shows the proximate and ultimate analysis of several solid fuel types with ash.

Table 6.1 The proximate and ultimate analysis of several solid fuel types, for exergy and energy calculation

Species	Assam	Tikak	Ledo	Sawdust
Ash	47.52	16.9	10.35	0.7
Moisture	2.18	2.6	3.07	2.6
Volatile Matter	22.96	34.9	43.38	77
Fixed Carbon	27.34	45.6	43.2	19.9
C	38.944	71.2	72.6	44.87
H	3.608	7.2	5.33	5.323
N	0.994	1	0.92	0.57
S	1.71	2.91	3.57	0.0
O	54.744	17.69	17.58	49.237

Table 6.2 Ultimate analysis of several solid fuel types with respect of ash

	Assam	Tikak	Ledo	Sawdust
C	26.39	60.91	65.79	44.56
H	2.44	6.16	4.83	5.29
N	0.67	0.86	0.83	0.57
S	1.15	2.49	3.24	0
O	37.11	15.13	15.93	48.89
Ash	32.21	14.46	9.48	0.70
Σ	100	100	100	100

The next step to calculate the LHV is finding out the Percentage weight for component of each the fuel (Table 6.3).

Table 6.3 Percentage weight of fuel components

	Assam	Tikak	Ledo	Sawdust
C	26.39	60.91	65.79	44.56
H	2.20	5.870221	4.489	5.0
N	0.67	0.86	0.83	0.57
S	1.15	2.49	3.24	0
O	36.38	14.27	14.91	48.03
Ash	32.21	14.46	9.48	0.70
Moisture	2.18	2.6	3.07	2.6
Σ	100	100	100	100

Finally, calculating the Element content of moles (moles/100 kg) (Table 6.4).

Table 6.4 Element content of moles (moles/100 kg)

	Assam	Tikak	Ledo	Sawdust
$n_C=w_i/w_C$	2.20	5.07	5.48	3.71
$n_H= w_i/w_H$	2.19	5.82	4.45	4.96
$n_N= w_i/w_N$	0.048	0.061	0.06	0.04
$n_S= w_i/w_S$	0.036	0.08	0.10	0
$n_O= w_i/w_O$	2.20	0.80	0.83	2.91
Moisture	0.12	0.14	0.17	0.14

In aim to compare LHV based on ultimate analysis and ultimate-proximate analysis, we have applied Eq. (6.2) and Eq. (6.3), and used values in Table 6.1 and Table 6.4. The lower heat values are presented by Figure 6.3, the predicted values of LHV based on the ultimate analyse are higher comparing with LHV based on ultimate-proximate analysis which takes in account the ash and moisture contents (Figure 6.3).

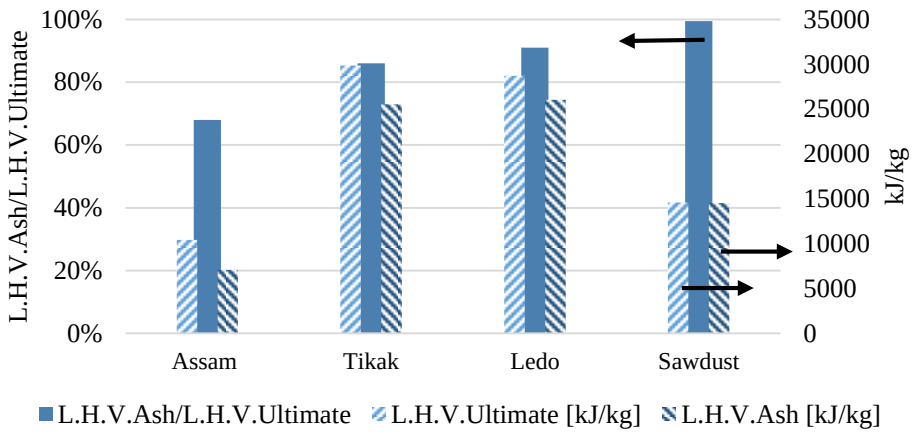

Figure 6.3 Variation of LHV based on ultimate and ultimate-proximate analysis for different fuel types

Assam coal (high ash contents) has the lowest LHV (based on ultimate and ultimate-proximate analysis) of 10423 kJ/kg and 7087 kJ/kg respectively, the experimental value –we have obtained– is 13280 kJ/kg. As a result the accuracy percentage is 78.5%. Meanwhile, the sawdust has the lowest LHV (based on ultimate and ultimate-proximate analysis) of 14608 kJ/kg and 14531 kJ/kg respectively, and the experimental value –we have obtained– is 17641 kJ/kg. As a result the accuracy percentage is 82.8%, where the HHV and LHV are calculated based on Standard Test Method (ASTM, 2007). Interestingly, Figure 6.3 shows an increasing matching between LHV based on ultimate and ultimate-proximate analysis, with decreased ash contents. And the LHV increases with increased ratio of H/C, in contrast increased ratio of O/C decreases the LHV of solid fuel, and the highest LHV is counted for Bituminous. Figure 6.4 illustrates the direction of LHV which increase with decreasing of O/C ratio and increment of H/C ratio. Furthermore, different fuel types and ranks of coal could have the same heating value, this plot can help in choosing the alternative fuels to keep the thermal load of the power plant, and enhance the flexibility of the power plant by categorising the suitable similar fuel types. Alongside, blending different types of fuel could be done in light of the desired heating value and the heating value of the mixed fuels.

The experimental LHV values matches 80% with the calculated LHV values, and the calculated LHV counts almost 99% of HHV of the studied ranges. Figure 6.5 shows the HHV with fuels' ratios O/C, H/C, and N/C, where, the HHV is plotted in respect of Krevelen diagram limits. Moreover, the different types of fuel could have the same LHV and HHV even for different ratios of O/C, H/C, and N/C.

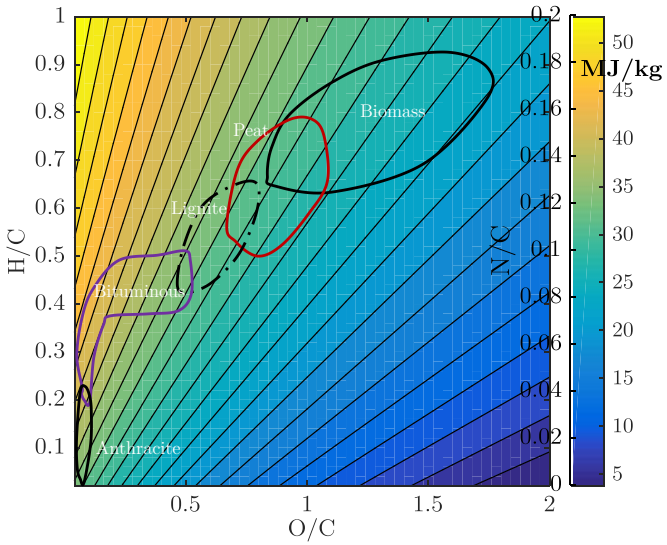

Figure 6.4 Variation of LHV with fuels' ratios of O/C, H/C, and N/C, based on Krevelen diagram.

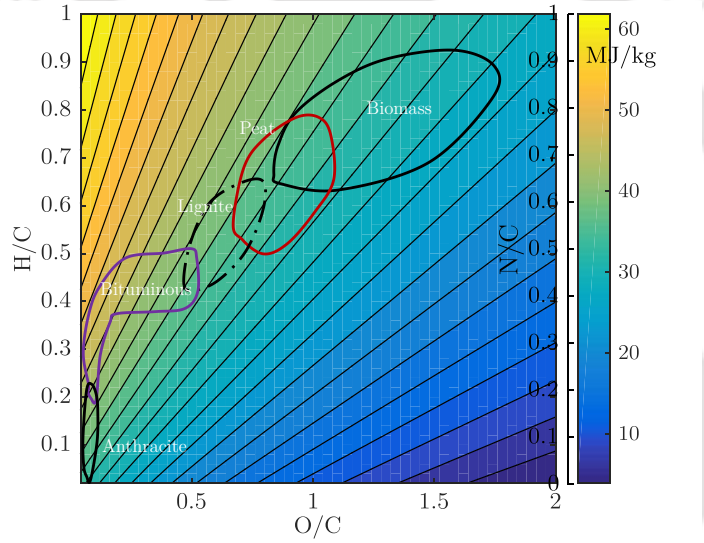

Figure 6.5 Variation of HHV with fuels' ratios of O/C, H/C, and N/C, based on Krevelen diagram.

6.1.3 Exergy of different types of fuel

Exergy represents the maximum available useful energy (work or ability of work producing), when the system reaches dead state, which can be obtained depending on the system and surrounding status. Exergy can measure both of quantity and quality of energy, and qualify the exhaust heat waste (Dincer and Rosen, 2007). For chemical reaction, exergy is corresponded to the maximum work gained from reactant when the products reach the equilibrium state (dead state) at temperature of 298.16K° and pressure of 0.1 MPa. The standard exergy *Ex.* per mole can be calculated by Eq. (6.5) (Szargut and Styrylska, 1964). Where T_0, P_{O2}, $P_{P,0}$ represent ambient temperature, oxygen partials pressure, and partial pressure of the combustion products, respectively.

$$Ex = H.V. + T_0 S^{\circ} + RT_0 \left(n_{O_2} \ln \frac{P_{O_2}}{P_0} - \sum_P n_P \ln \frac{P_{P,0}}{P_0} \right) \tag{6.5}$$

Exergy can calculated using empirical Eqs. (6.6) and (6.7) (Ghamarian and Cambel, 1982).

$$\begin{aligned} Ex_{CHNS} &= 443.35208 n_C + 105.30292 n_H - 184.17053 n_O \\ &\quad + 32.65797 n_N + 513.159 n_S [MJ/kg] \; for \quad n_O / n_C \le 0.5 \end{aligned} \tag{6.6}$$

$$\begin{aligned} Ex_{CHNS} &= 441.41299 n_C + 106.98818 n_H - 171.14510 n_O \\ &\quad + 20.59097 n_N + 20.59097 n_S [MJ/kg] \; for \quad n_O / n_C \le 1.0 \end{aligned} \tag{6.7}$$

Figure 6.6 shows the fuel exergy variation as a function of O/C and H/C ratios.

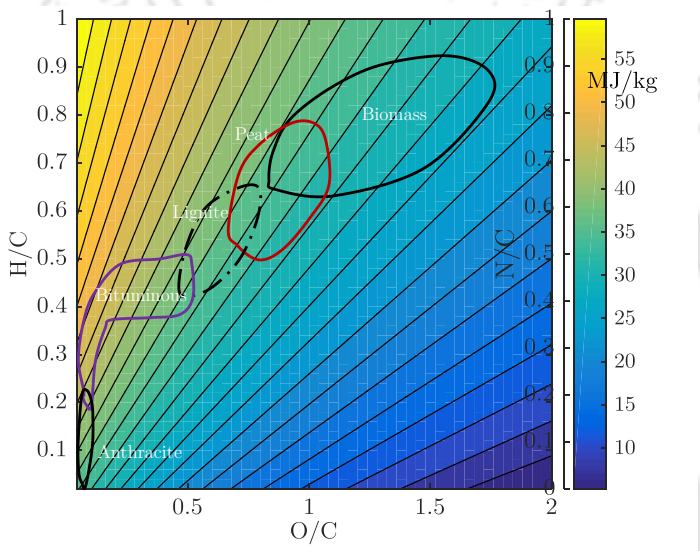

Figure 6.6 Variation of exergy with fuels' ratios of O/C, H/C, and N/C, based on Krevelen diagram

The exergy of fuel could be higher than the heating value, when there is a heat supply from the environment, and the entropy of the final state is higher than the initial one (Ghamarian and Cambel, 1982). These are an elementary fuel energy analysis (LHV, HHV), and exergy fuel analysis, which mainly calculated based on the components of fuel, several factors could affect the energy and exergy based on the system and surrounding environment conditions and the process conditions. In the following section detailed study of the reaction exergy under different fuel combustion conditions.

6.2 Chemical Reaction Exergy and Energy Analysis

In a combined system and specific environment conditions, the system attains the dead state (temperature of 298.16K and pressure of 0.1 MPa) when the system and environment are in the thermal and mechanical equilibrium. And the total exergy is contributed by

thermomechanical exergy and chemical exergy (Figure 6.7), (Mahanta, 2012).

Total exergy = Thermomechanical exergy + Chemical exergy

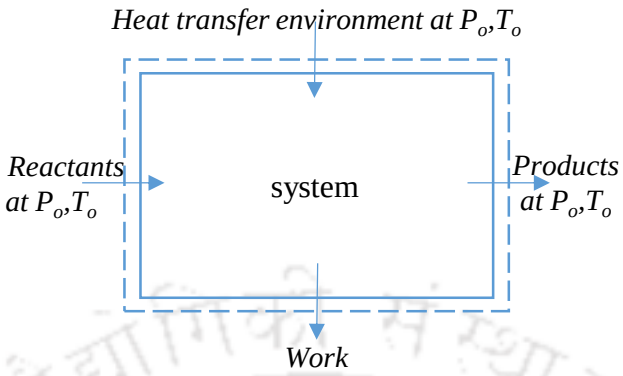

Figure 6.7 Exergy concept of fuel

As illustrated by Figure 6.7, the exergy of the system is affected by the pressure and temperature of the reactants and products, and transferred heat to the system. The overall exergy includes $Ex_{ch.}$ Chemical, $Ex_{ph.}$ Physical, $Ex_{kn.}$ Kinetic, and $Ex_{pt.}$ Potential exergy components. The Kinetic, and Potential are to the velocity and elevation and both exergy terms are not accounted in for reaction exergy calculation (Orhan et al., 2009; Wu et al., 2014; Dai et al., 2016).

$$Ex = Ex_{ch.} + Ex_{ph.} + Ex_{kn.} + Ex_{pt.} \tag{6.8}$$

The chemical exergy of reaction Eq. (6.9), can be calculated by Eq. (6.10) where the first and second terms represent the physical exergy, meanwhile the last term represent the chemical exergy.

$$\nu_1.A_1 + \nu_2.A_2 \rightarrow \nu_3.A_3 + \nu_4.A_4 \tag{6.9}$$

$$Ex = \left[\sum_{x=1}^{n} \nu_x.h_{x_i,r} - \sum_{y=1}^{m} \nu_y.h_{y_i,p}\right] - T_0\left[\sum_{x=1}^{n} \nu_{x_i}.S_{x_i,r} - \sum_{y=1}^{m} \nu_{y_i}.S_{y_i,p}\right] - \frac{T_0.S_{gen}}{n} \tag{6.10}$$

For maximum work and in terms of Gibbs function, the Eq. (6.10) can be rewritten for respective substances as Eq. (6.11)

$$Ex = \left[\sum_{i=1}^{n} \nu_i.g_{i,r} - \sum_{j=1}^{m} \nu_j.g_{j,p}\right]_{(at T_0, P_0)} + RT_0 \ln\left(\prod_{i=1}^{n} x_{i,r}^{\nu_i}\right) - RT_0 \ln\left(\prod_{j=1}^{m} x_{j,p}^{\nu_j}\right) \tag{6.11}$$

In the following analysis, 1 kmol of oxygen is involved in the reaction, the reactants and products have unit of kmol. And the following assumption are taken in account:

- The environmental temperature and temperature are T_0=298.15 K and P_0=1 atm.
- The process is an adiabatic one.
- The process has a steady state.
- The mass is conserved in the process, $\Sigma m_{in} = \Sigma m_{out}$.
- It is an adiabatic process.

Energy

In parallel, the input and output energies of the reactants and products of the Eq. (6.9) could be written as following Eq. (6.12).

$$E = \sum_{i=1}^{n} m_i . Cp_i . \left(T_i - T_{amb.} \right) \tag{6.12}$$

And for combustion reaction the heating value of the fuel can be added to the E_{in}. $T_{amb.}$, Cp_i, *and m* represent the ambient temperature, specific heat, and mass flow rate respectively.

6.2.1 Exergy and energy chemical reaction of air-fuel combustion

Effects of exhaust (products) temperature over exergy and energy

The air-fuel combustion is a conventional case Eq. (6.13), it can be considered as reference case to compare with it.

$$C + \lambda O_2 + \lambda 3.76 N_2 \rightarrow CO_2 + \lambda 3.76 N_2 + (\lambda - 1) O_2 \tag{6.13}$$

We calculate the exergy (availability) of reaction by applying Eq. (6.11). The effect of ambient (exhaust) temperature is studied for a stoichiometric value of λ=1, fixing the pressure at 101.325 kPa for the products and reactants, fixing the temperature of the reactants at 298.15 K. It is found that, the chemical reaction exergy decreases with increased exhaust temperature as a result of lost exergy with the exhaust. And, for increased temperature from 298 K up to 598 K, the overall exergy decreases from 411.741 kJ up to 330.890 kJ.

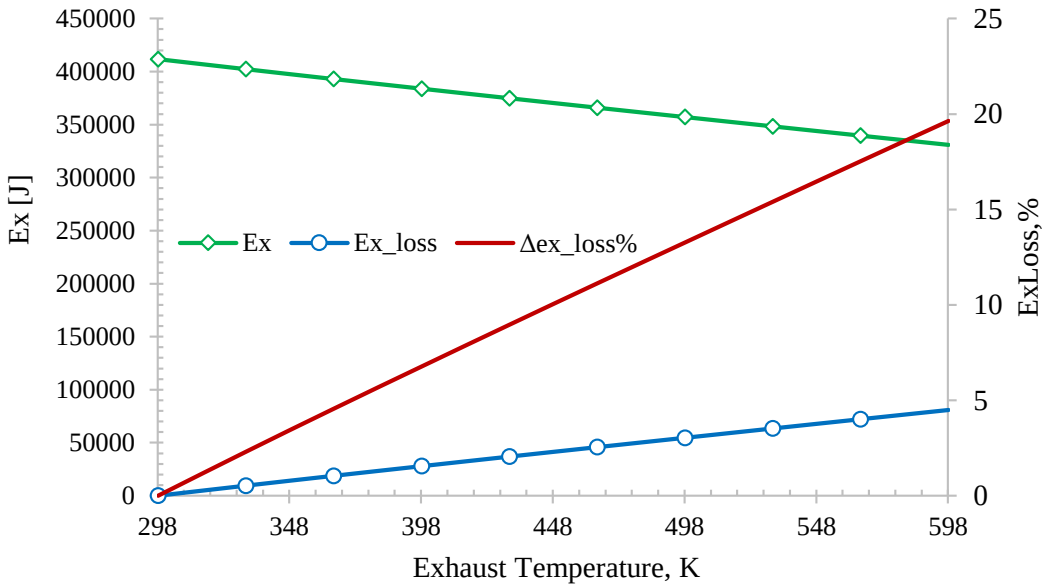

Figure 6.8 Exergy variation with exhaust temperature (products temperature at the outlet)

In terms of exergy loss percentages, this decrement matches 0% up to 25% exergy loss of the exergy at the exhaust temperature of 298.15 K. As a result, as decreased as possible to minimize the exergy loss, this matches (at the level of operating power plant) with findings by Ameri and Ahmadi (2007). Where the exhaust increment of 1 K degree can decrease the power output by 0.7%. Additionally, the loos of exergy is an exponential function of exhaust temperature as shown in the Figure 6.8. This analysis predicts the effect of ambient temperature over the exergy depending on the temperature differences due to surrounding weather.

Energy

On the other hand, of thermodynamic analysis, Figure 6.9 shows the loss of energy with flue gases (exhaust gases), the same general trend of exergy loss is found. Where the energy loss increases with increased product (exhaust) temperature. Interestingly, the percentage of energy loss at 598 K is only 12% comparing with 20% of exergy loss percentages, this is pertained to the irreversibility of the process, and due to energy distraction.

Subsequently, the lower exhaust gas temperature minimize the energy loss. Approximately, the lost energy is almost 5% for each 100 K of flue gases temperature above 298 K. to achieve lower flue gases temperature in the CFB power plants, the concentration of SO_x and NO_x shall be minimized to avoid formation of acids.

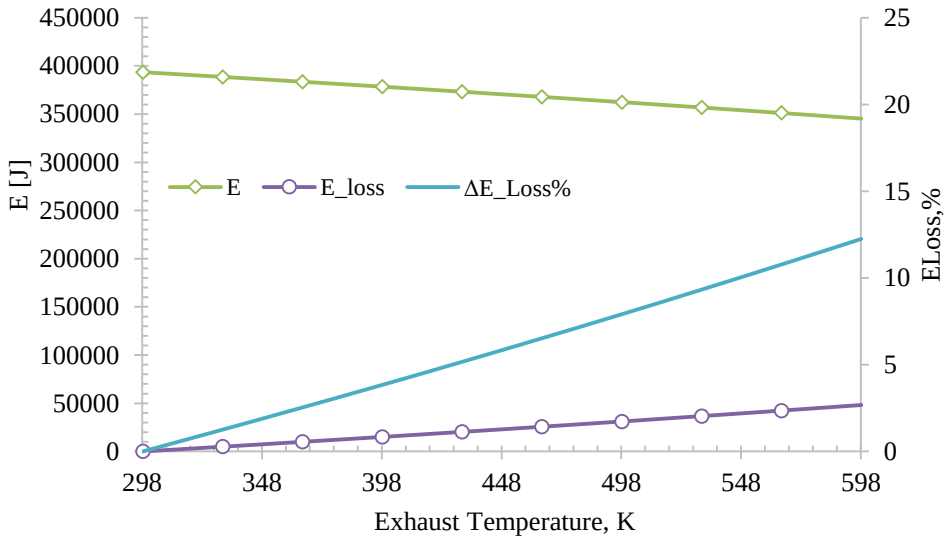

Figure 6.9 Energy variation with exhaust temperature (products temperature at the outlet)

Effects of (Pre-Heating) Reactants Temperature over Exergy and Energy

Exergy

The pre-heating technique is used in the operating power plant level to improve the overall efficiency and enhance the parameters of the oxidant, and at the level of chemical reaction exergy, it has been found that pre-heating reactants from 298.15 K up to 598.15 K improves the exergy by 20.5% (Figure 6.10).

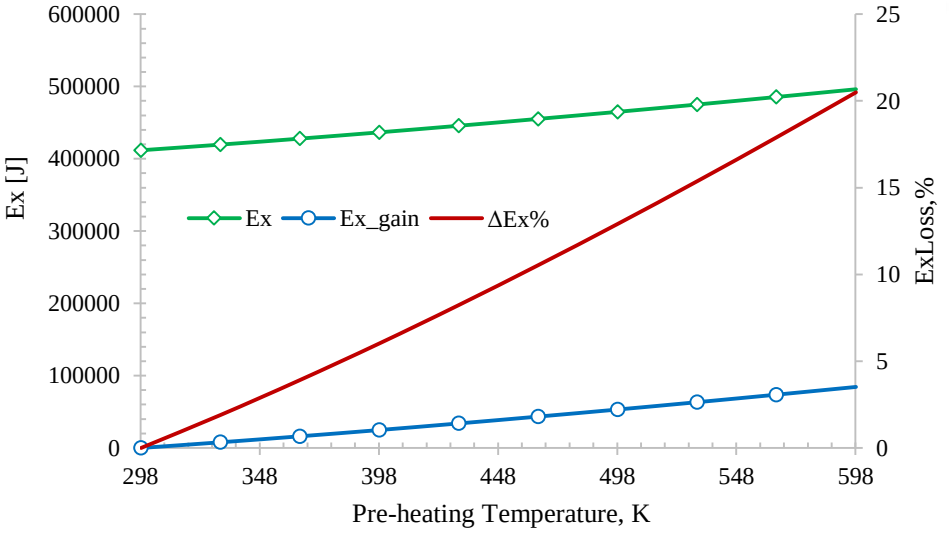

Figure 6.10 Variation of Exergy with reactants temperature (pre-heating)

Interestingly, the same level of temperature pre-heating (from 298.15 K up to 598.15 K) does not recover the exergy loss with exhaust (products) for the same temperature. For instance, at

598.15 K pre-heating temperature the gain in exergy is 84.389 kJ comparing with exergy loss of 80.851 kJ with products for the same temperature level 598.15 K. as a result (at the level of chemical reaction), the pre-heating is slightly more effective in terms of recovering exergy comparing with minimizing the temperature of the exhaust (products).

Energy

The effect of preheating (reactants temperature) is higher for the gained energy comparing with exergy, for the same temperature pre-heating level from 298 K to 598 K the energy gain percentage is 22% comparing with 20% for exergy.

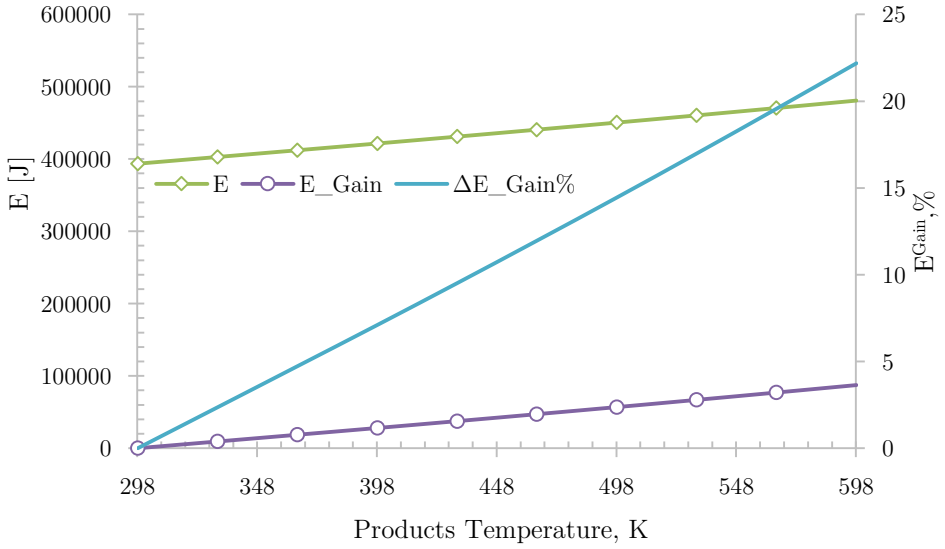

Figure 6.11 Variation of energy with reactants temperature (pre-heating)

In all cases, the available energy (exergy) is less than the energy due to irreversibility, the gained exergy is less than the gained energy due to pre-heating, and the loss of exergy is higher than loss of energy due to gases flue loss.

Effects of excess air over exergy

In aim find out the effects of stoichiometric ratio with different temperature levels of the exhaust over the exergy; we calculated the exergy loss percentage for rage of λ from 1.0 up to 2.0, over exhaust temperature range of 298.2 K up to 598.2 K. At the zero state conditions - 101.325 kPa and 298.15 K- there is no effect of stoichiometric ratio over the exergy loss, this is pertained to the same exergy value of the excess air species as a reactants and products, with increased exhaust temperature the loss of exergy (rejected exergy to the environment)

increases, and the magnitude of stoichiometric ratio effect rises up with temperature (Figure 6.12). The increased ambient temperature rises the absolute Gibbs function values (second term of Eq. (6.11)) which increases the exergy lost with products (exhaust), moreover, the higher stoichiometric (λ) value magnifies the stoichiometric coefficients (ν) and the exergy losses increase.

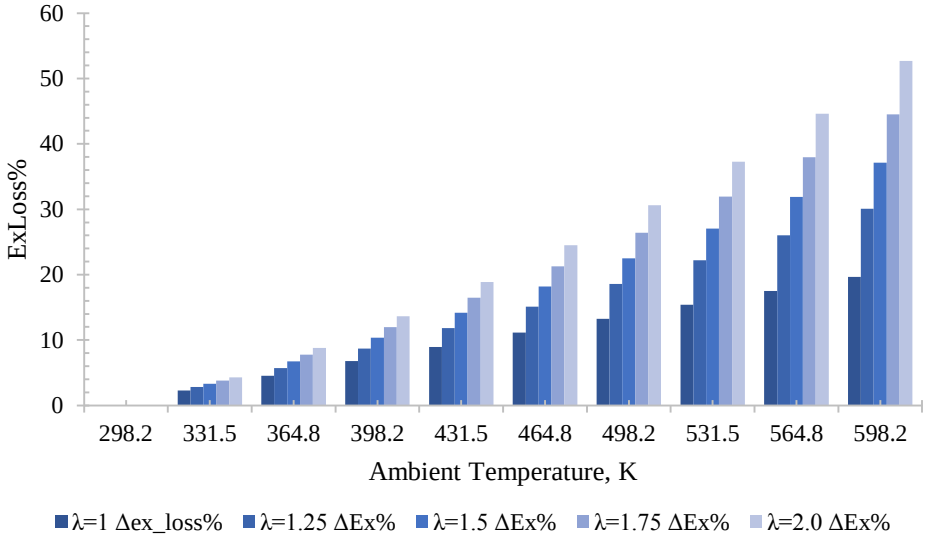

Figure 6.12 Variation of exergy loss percentage with different stoichiometric ratios and ambient temperatures

The lost exergy with exhaust is unavoidable in the operating power plants, since the minimum temperature is governed by dew point of some products such like sulphuric acid (Huijbregts and Leferink, 2004), as a result, minimizing the excess oxidant helps in reducing the exergy loss with exhaust.

Energy

The same general trend of energy loss due to increased stoichiometric ration (λ) only in the reference case (zero state) the loss is zero whatever the value of stoichiometric ratio varies, meanwhile, the loss of energy increase with stoichiometric ratio along with ambient temperature. Interestingly, a small variation of temperature leads to higher loss of exergy comparing with loss of energy. This is pertained to the second term of Eq. (6.10), where the irreversibility increases with temperature.

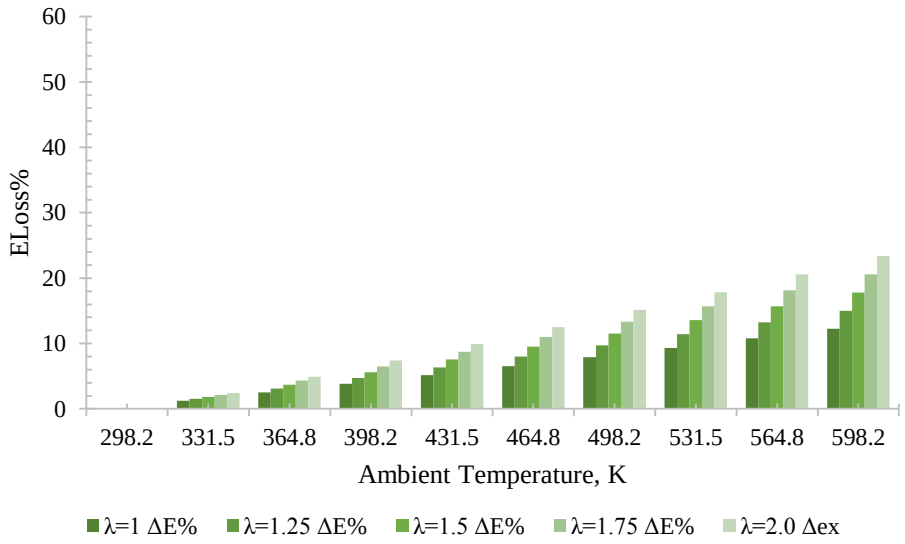

Figure 6.13 Variation of energy loss percentage with different stoichiometric ratios and ambient temperatures

6.2.2 Chemical reaction exergy and energy of oxy-fuel combustion

The oxy-fuel combustion is a presented by Eq. (6.14), where the oxidant is a mixture of O_2 and CO_2, and (a) presents the percentage of the O_2 in the oxidant mixture, and the outlet is CO_2, which combination of supplied CO_2 and reaction's produced CO_2. This oxy-fuel reaction is a simplified one, where the fuel is considered only to be carbon, with complete reaction and absence of CO.

$$C + O_2 + \left(\frac{100-a}{a}\right)CO_2 \rightarrow \left(1 + \frac{100-a}{a}\right)CO_2 \qquad (6.14)$$

We calculate the exergy (availability) of reaction by applying Eq. (6.11). Firstly, the reactant temperature (pre-heating) is varied from 298.15 K up to 498.15 K over wide range of O_2 percentages from 21% up to 100%. In all cases, the exergy is calculated and presented as a percentage of the base case exergy (air combustion at 298.15 K and 101.325 kPa for reactants and products (6.13)). And the exergy increases along with increased pre-heating levels, with different rates of increasing (Figure 6.14). With increased O_2 concentration, the improvement rate of exergy decreases, and interestingly, the r case is matching with oxy-fuel combustion of O_2 90% case. This is related to the enthalpy of the species CO_2, O_2, N_2 at different temperature levels, and the enthalpy of CO_2 has highest magnitude, as a result the pre-heating of CO_2 would increase the overall exergy more comparing with the increment due to effects of O_2 or N_2. On the other hand, in the absence of pre-heating, there is no effects of CO_2, O_2 percentages over the exergy enhancement.

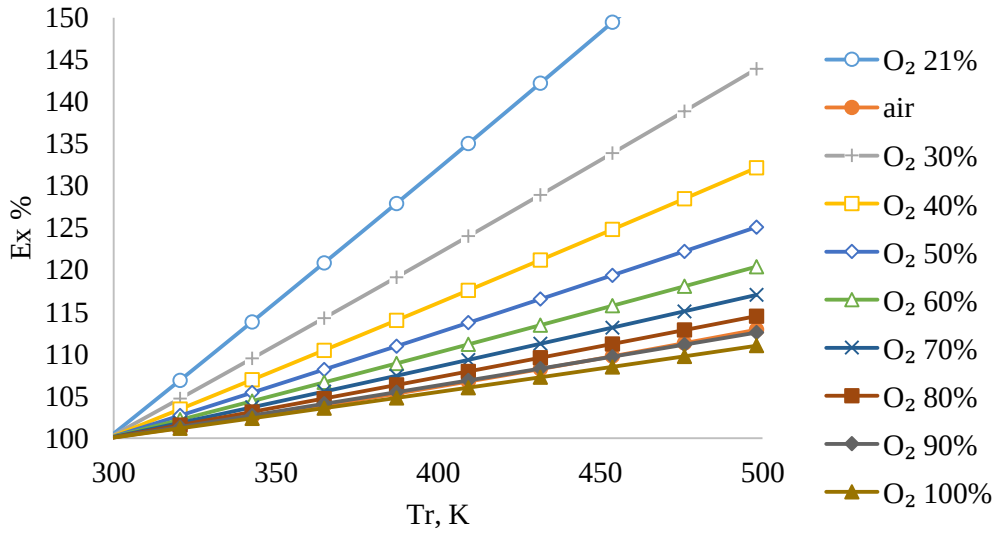

Figure 6.14 Variation of exergy with O_2 concentration and reactants temperature

In contrast, the product (exhaust) temperature varied to find its effect with different CO_2, O_2 percentages. The exergy loss rate with exhaust increases with increased CO_2 percentage, the highest exergy loos is for O_2 21%, and lowest one for air case which matches with O_2 100% case (Figure 6.15).

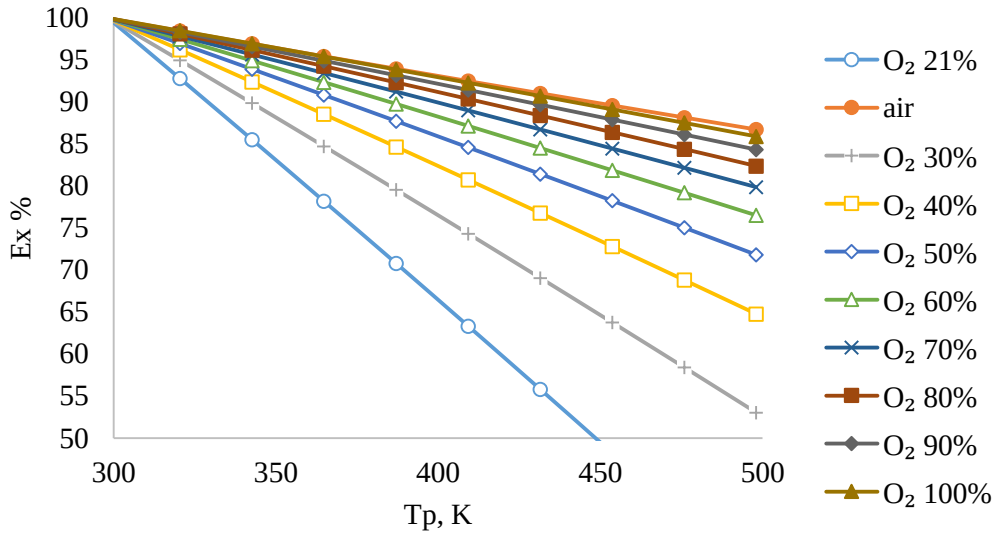

Figure 6.15 Variation of exergy with O_2 concentration and products temperature

This calculated exergy of these cases are compared with air combustion at 298.15 K and 101.325 kPa for reactants and products as a reference case (Eq. (6.13)), to get exergy percentage. Since the energy of pre-heating is gained from the fuel energy itself, and not from any other external sources, we may (even after clarifying the effects of pre-heating) we may

consider the reactants' condition at the inlet 298.15 K and 101.325 kPa. In this case, and the studied effects of products temperature can be limited to temperature of dew point of sulphuric acid, about 130~150 °C. In this range of exhaust (products) temperature, the highest exergy goes for O_2 100% and air case, where the loss of exergy is around 5% only. Moreover, the in situ sulphur capturing advantage of CFB leads to lower concentration of SO_x emissions. That results lower dew point of the sulphuric acid, finally, the energy of exhaust gases could be recovered more efficiently and its temperature could be getting down without condensed .Never the less, applying the proposed technique chapter 3 can achieve higher exergy efficiency side-by-side cutting the cost of installation and operating by eliminating the recirculation setups.

Energy

Figure 6.16 shows the gained energy by pre-heating of reactants for different O_2 concentration from 21% up to 100%. The energy is presented as a percentage to the reference case at zero state condition (298.15 K and 101.325 kPa) for both of reactants and products. The general trend shows increased energy along with increased pre-heating temperature degree. The highest energy gain goes for O_2 21% with 11% improvement in energy at 498 K. the decreased O_2 concentration leads to higher energy efficiency, since the heat capacity of O_2 is lower than CO_2 one.

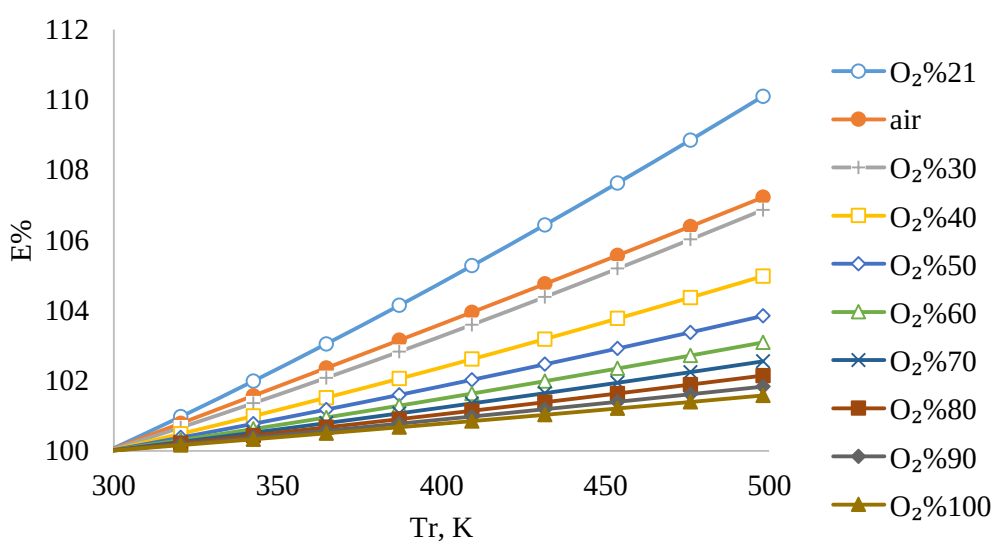

Figure 6.16 Variation of energy with O_2 concentration and reactants temperature

Figure 6.17 shows the energy efficiency as a function of temperature of the flue gases for different O_2 percentages, the trend of energy change is similar to exergy change but with lower decreasing slop (Figure 6.15, Figure 6.17). Remarkably, the pure oxy-fuel combustion has the lowest energy loss with flue gases.

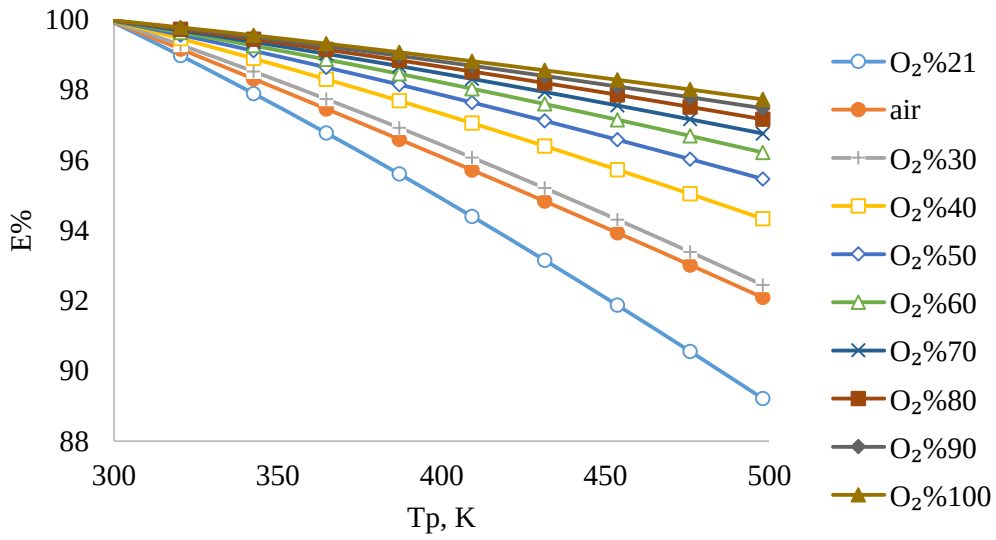

Figure 6.17 Variation of energy with O_2 concentration and products temperature

In general, the dew point temperature (DPT) of SO_x must be exceeded to avoid formation of sulphuric acid (H_2SO_4) and sulphurous acid (H_2SO_3), and the DPT is a function of SO_x concentration (Blanco and Pena, 2008). The proposed pure oxy-fuel CFB combustion method may reduce the NO_x and SO_x emissions; where the exhaust gases are not recirculated. As a result, the sulphur and nitrogen will have less probability to oxidize.

6.3 Summary

This exergy and energy study is considered as a fundamental one, it gives an elementary result of the effects of reactants temperature, products temperature, O_2 concentration in the oxidant, and stoichiometric ratio over the exergy and energy of the combustion reaction. Furthermore, in the conventional oxy-fuel CFB combustion, the increased O_2 concentration leads to lower flue gases loss, on the other hand, applying pure oxy-fuel combustion could lead to the lowest loss of both energy and exergy with flue gases. Moreover, at this level the pure oxy-fuel combustion is promising, side by side, at the level of power plant level, where the re-circulation setup of flue gases could be eliminated, and subsequently the cost of installation and operating will be minimized to compensate the efficiency penalty of oxy-fuel combustion.

7 Conclusions and Future Scopes

Overview

The demand of energy will keep growing in the future, due to increased population and modern life style, at least for the next few decades, the conventional fossil fuel will be one of the main energy source, even the proposed renewable energies won't be sufficient to cover the energy demand or to become a dominant source. As a result, the research for alternating the fossil fuel to economical free CO_2 source of energy is highly necessitated. The carbon capture and sequestration (CCS) came into practice commercially by 2015 with first power plant in Canada, which runs under post-combustion technology for capturing CO_2. The oxy-fuel CFB combustion is a very promised technology of CCS and to many research groups and researchers are paying effort (Hotta, 2009; Kiriishi et al., 2009; IEA, 2011b; Czakiert et al. 2012; Obras-Loscertales et al. 2013; Lupion et al. 2013), but the main barrier of this technology is high cost of running the air separation unit (ASU) and the auxiliary setups vis. recirculation of flue gases. Subsequently, the insisting question to be answered is "In terms of economic, is oxy-fuel combustion visible under the present conditions and operating costs with 15~25% efficiency penalty?", and "what could be done to bring this dawning technology to practice?" In the present work, we proposed pure oxy-fuel CFB combustion method, subjected to experiments, and a thermodynamic analysis (exergy and energy) is done at the level of chemical reaction. Side by side, a hydrodynamic behaviour is studied under the new circumstance to find out the effects of oxy-fuel operating condition.

Chapter outline:

7.1 Conclusion of the Present Work

The cold CFB unit is designed, fabricated and run under air and oxy conditions. The results show similar behaviour of both cases namely air and oxy. The operating conditions of the hot CFB unit are experimented and obtained from cold CFB unit vis. terminal velocity, bed voidage, pressure drop, sold recirculation rate. A novel method of pure oxy fuel combustion is proposed and it is subjected to several experiments. It is found that controlling stoichiometric ratio λ is an effective way to control AFT. This method could be used not only for oxy-fuel CFB combustor. It could be used for pulverized coal, solid waste management etc. The thermodynamic analysis shows increased oxygen concentration in oxidant leads to lower energy losses.

7.2 Contribution of the Present Work

The hydrodynamics behaviour, reaction characteristics, and thermal behaviour of the CFB are all coupled together, therefor, any applied technique to improve any parameter shall take in account the rest of operating parameters. And the core of the present work propose a pure oxy-fuel CFB combustion technique, in this case a pure oxygen is used as an oxidant, and two arrangements are proposed to divide and feed the fuel at different levels of the CFB riser; or using series of connected mini-CFBs with pure oxygen primary inlet of the first CFB with portion of the overall fuel fed to the first CFB with stoichiometric ratio λ>1.0, the out let of the first CFB is the inlet of the next and so on, the last CFB has reaction under stoichiometric ratio of λ~1.0. On the other hand, the hydrodynamic behaviour under oxy-fuel CFB combustion condition is studied. In the following, we conclude the present work subsequently.

7.2.1 CFB hydrodynamic investigation (cold CFB unit study)

The main objective of the cold unit study is carrying out a comparative study of different operating gases vis. Air, CO_2-O_2, and compare the effects of several parameters over the hydrodynamic behaviour viz. operating pressure, particle size, bed inventory weight, aeration flow rate, and superficial velocity are studied. Three groups of particle size are used namely 160, 302, 427 μm. The experiments are conducted under three aeration rates of 0.25×10^{-3}, 0.75×10^{-3}, and 1.25×10^{-3} m^3/s (match with three superficial velocities, U_{sup}= 0.65, 1.94, and 3.23 m/s respectively), and three velocities of primary flows viz. 0.65, 1.94, and 3.23 $m.s^{-1}$.In

each experiment, the air is supplied at three pressure levels of 100, 200, and 250 kPa. The main finding of this work are discussed below

- The primary flow rate investigation shows that increased flow rate from 2.7 up to 4.08 m/s leads to higher bed voidage, side by side, lower suspension density, and increases the solid recirculation rate from 2 up to 20 kg/m2.s, which is advised for absorbing elevated heat release in the oxy-fuel CFB combustion.
- The increased operating pressure from 150 kPa up to 250 kPa decreases the bed voidage due to higher gas density and buoyancy force, and the suspension density increases along the riser height, this leads to higher desired heat transfer coefficient.
- In all cases, the bed voidage has an S-shape profile, with dense zone at the bottom and lean bed voidage profile at the higher zone of the riser, the same shape is recognized for suspension density.
- The change of aeration velocity from 0.65 up to 3.23 m/s increases the solid recirculation rate slightly almost ~2 kg/m2.s. Moreover, in all cases the maximum maintained solid recirculation rate (SRR) is 20 kg/m2.s, for higher SRR, it is recommended to use external heat exchanger to meet the requirements of oxy-fuel CFB combustion in terms of absorbing the released heat.
- The study of particle size effects shows that higher particle size leads to lower bed voidage, due to increased particle terminal velocity. On the other hand, the higher bed inventory decreases the bed voidage.
- Interestingly, the terminal velocities of air, CO_2-O_2 mixture, O_2, and N_2 have values of ±10 % difference from each other, over temperature range of 25°C to 850°C. As a result, there is not significant effects over the hydrodynamic behaviour in this mini-CFB. Moreover, the maximum velocities difference is ΔU=0.157 m/s between UCO_2=0.759 m/s at 850°C and UN_2=0.916 m/s at 25°C. And for the same temperature degree of 850°C, the maximum terminal velocity is ΔU=0.11 m/s between UCO_2=0.759 m/s at 850°C and UN_2=0.8682 m/s at 25°C; this is pertained to contradictory behaviour of density and dynamic viscosity under increased temperature where the density decreases and this leads to higher terminal velocity meanwhile dynamic viscosity increases with temperature and leads to lower terminal velocity, finally, the effects of density and dynamic viscosity partially eliminate each other. And, the effects of the oxy-fuel combustion conditions over the mini-CFB

hydrodynamic is small enough to be neglected, and an extended investigation is required for industrial scales.

7.2.2 Oxy-fuel CFB combustion investigation (hot CFB unit study)

The core of this work is attempted to revolutionize the oxy-fuel CFB combustion by increasing the O_2 concentration to reach pure oxy-fuel CFB combustion, and minimizing the waste energy with flue gases and finally eliminating the flue gases recirculating, in this case the temperature controlling is achieved by one of these following arrangements:

- Using series of mini-CFB, where the overall fuel divided and is being fed into the mini-CFBs subsequently (3.4). In parallel, the primary stream of pure oxygen flows through the first CFB and combustion occurs under high stoichiometric value $\lambda>1.0$ to mitigate the temperature, the exhaust of the first mini-CFB flows through the sequenced one. In the conducted experiments, we have used one mini-CFB rig and varied the oxidant flow rate and the solid fuel rate to control the stoichiometric ratio λ. The average temperatures along the riser (oxy-biomass CFB combustion case) are 1129°C, 1051°C, and 961°C for λ=1.25, 2.0, and 3.0, respectively; meanwhile, The average temperatures along the riser (oxy-bituminous CFB combustion case) are 1129°C, 1051°C, and 961°C for λ=1.25, 2.0, and 3.0, respectively.
- The temperature profile along the riser is more uniformed for oxy-biomass CFB combustion comparing with oxy-coal CFB combustion. This is pertained to the higher terminal velocity of the coal particles (dp= 0.85~1.70 mm of terminal velocity of Utr= 1.8~2.8 m/s) than the used superficial velocity U=2.0 m/s, as a result, the coal particles at the early stages of combustion (drying, devolatilization, ignition) remain slugging at the bottom till losing sufficient weight by reaction and getting lower terminal velocity to rise up (the terminal velocity of 1.0 mm coal particle size is 2.0 m/s Figure . In contrast, the superficial velocity of the used biomass (sawdust) particles is less than 1 m/sec.
- Using pure oxy-fuel combustion 100% O_2, the flue gases is reduced 5 times, as a result the energy and exergy loss due to flue gases loss is almost 5 times less under the same conditions of operating pressure, temperature, and fuel flow rate.
- Biomass namely sawdust is used as a fuel, and gives a better uniformed temperature profile along the riser comparing with coal firing case, this is due to lower density and

matching of the sawdust terminal velocity of particle size dp=1.0 mm is Utr=0.6 m/sec with the superficial velocity U=1.0 m/sec. the setup run smoothly using sawdust without a significant operating problems.

7.2.3 Thermodynamics analysis (exergy and energy analysis)

- On an average the heating value of the solid fuel (coal and biomass) falls in range of 20000 kJ/kg up to 45000 kJ/kg, where, the bituminous has the highest heating value of 30000 up to 45000 kJ/kg. The energy analysis shows that different types of fuel with varied percentages of O/C, H/C, and N/C could have the same heating value, this fact gives a flexibility of determining and using an alternative fuel to run the power plant.
- The fuel exergy analysis shows similar Lower Heating Value (LHV) to the exergy value of the fuel, and both of LHV and exergy increase with increased H/C ratio, and decrease with increase O/C ratio. Moreover, biomass solid fuel demine has wide range of exergy and lower heating values match with coal values, this gives a possibility to replace coal with biomass for the same mass flow rate and considering the thermal load.
- The chemical reaction exergy analysis shows a decreased exergy by 20% from 400kJ to 340kJ with increased product temperature (exhaust gases) from 298 up to 598 K, for air combustion case of C. meanwhile, for the same case, energy decreased 12% only, since the energy analysis neglect the energy destruction. The exergy analysis reveals more accurate analysis, since it takes in account the irreversibly.
- The chemical reaction exergy analysis shows an increased exergy by 20% from 410 kJ up to 500 kJ for a combustion of one mole of C, when the oxidant (air) is pre-heated from 298 K up to 598 K. The effect of preheating (reactants temperature) is higher over the increased energy comparing with increased exergy, for the same temperature pre-heating level from 298 K to 598 K the energy gain percentage is 22% comparing with 20% for exergy.
- The excess air has no effect over the exergy and energy in case the reactants and products are under the zero state conditions (298.15K and 101.325 kPa). On the other hand, the loss of exergy increase with increased ambient temperature (product temperature) from 298.15 K to 598.15 K and the magnitude of the loss increases up to

55% with increased excess air up to λ=2.0 under 598.15 K; under the same condition the energy loss is almost 20% only comparing with 55% of exergy loss.

- The increased exergy of oxy-fuel combustion case due to pre-heating increase with decreased percentage of O_2 in the oxidant mixture CO_2-O_2. Excitingly, the gained exergy of air combustion case is similar to oxy-fuel combustion case of 10%-90% concentration of CO_2-O_2, This is related to the enthalpy of the species CO_2, O_2, N_2 at different temperature levels, and the enthalpy of CO_2 has highest magnitude, as a result the pre-heating of CO_2 would increase the overall exergy more comparing with the increment due to effects of O_2 or N_2. On the other hand, in the absence of pre-heating, there is no effects of CO_2, O_2 percentages over the exergy enhancement.
- The gained energy by pre-heating of reactants for different O_2 concentration from 21% up to 100%. The energy is presented as a percentage to the reference case at zero state condition (298.15 K and 101.325 kPa) for both of reactants and products. The general trend shows increased energy along with increased pre-heating temperature degree. The highest energy gain goes for O_2 21% with 11% improvement in energy at 498 K. the decreased O_2 concentration leads to higher energy efficiency, since the heat capacity of O_2 is lower than CO_2 one.
- Applying pure oxy-fuel combustion technique minimize the loss of energy and exergy, side by side, minimizing the operating cost by eliminating the recirculating flue gases and the cost of installations.

7.3 Application Probabilities

The proposed method is not only promising theoretically, but also, it has been proofed practically at lab experimental level. The gained results open the door widely to the 3rd Generation of Oxy-fuel CFB combustion technology, which has been decelerated due to high efficiency penalty. Still, extra experiments are required along with scaling up toward adapting the technology industrially.

7.4 Limitation of the study

- In the present study, two mini-CFB rigs are used to conduct the experiments, one cold unit for hydrodynamic investigation and one hot unit for combustion, the height of each mini-CFB is 2.0 m, and it is considered as a pilot scale.
- A simple stand-pipe with return leg is used, without any non-mechanical valve.

- There is no external heat exchanger, which is recommended to be used in aim to enhance solid recirculation rate and subsequently the heat transfer.
- The second proposed arrangement of pure oxy-fuel CFB combustion requires a bigger CFB with multi feeding ports. The small scale is not adequate for applying such an arrangement due to technical difficulties.

7.5 Recommendations and Future Scopes

In this present work, an attempt has been made to revolutionise the oxy-fuel CFB combustion technology through proposing and experiencing a novel method of oxy-fuel CFB combustion. The findings of the present study have been already discussed in section (7.1); however, further improvements can be done to mature the technique and applied industrially. In this connection some scope and suggestion for future scholars are presented here.

7.5.1 Cold CFB unit Future Scopes

- External heat exchanger in required for enhancing the rate of solid recirculation to service heat transfer. Where the stand-pipe with return leg is an experimental lab scale and a simplification of the industrial scales, moreover, the External heat exchanger is more demanded under oxy-fuel CFB combustion condition to absorb the elevated heat release. Finally, further investigation is required for hydrodynamic behavior using external heat exchanger and high solid recirculation rate.
- The effects of oxy-fuel CFB conditions are studied using mini-CFB, further investigation could be done using bigger CFB scale side by side with numerical simulation could be done, in aim to find the scaling effects over hydrodynamic behaviour under oxy-fuel CFB conditions.
- The effect of operating pressure is studied in range of 100~250 kPa. Hence the higher operating pressure may lead to liquefying the CO_2 of flue gases and eliminate one stage of the oxy-fuel CFB process, this minimize the cost of applying carbon capturing and storage (CCS). As a result, it highly recommended to investigate the hydrodynamic behaviour under both high operating pressure and oxy-fuel CFB condition, and both of the numerical simulation and experimental approaches are recommended for this study.

- It is suggested to find out the effects of replacing air with CO_2-O_2 mixture for big CFB scales running under oxy-fuel CFB conditions, this investigation is required to generalize the hydrodynamic study results of the mini-CFB under oxy-fuel conditions.

7.5.2 Oxy-fuel CFB combustion Future Scopes

- Mini-CFB is used for conducting the experiments of pure oxy-fuel CFB combustion, two arrangements could be applied for future work viz. using series of mini-CFBs which are connected to each other with one inlet of the oxidant of the first mini-CFB with one outlet of the last mini-CFB, or applying multi-feeding arrangements along a riser of big CFB scale. In both cases, the temperature is going to be controlled based on stoichiometric ratio. This future work can be done firstly numerically, secondly by experiments.
- It is highly recommended to use air case for starting up and switching down the CFB, assuring there is no remained O_2 at the starting up of the next run, and using CO_2 only in case of entraining the fuel by gas, to avoid oxidant leakage into the full hopper.
- In this present study, the investigation are done by conducting short term testes. However, long term tests should be done to examine the problems like corrosion the CFB, due to SO_x, NO_x and their formed acids. As a result, the long term tests are required to promote the oxy-fuel CFB combustion and the proposed technique commercially.
- A comprehensive economic analysis of the pure oxy-fuel CFB combustion needs to be carried out for promotion of this technology. Therefore, a cost analysis of the can be executed by considering various economic terms, and finding the setup costs and operating costs under new conditions. The performance and emission study along with the economic assessment can provide a competitive characteristic of the pure oxy-fuel CFB combustion as the alternative costly oxy-fuel CFB combustion.
- In the first suggested arrangement of pure oxy-fuel CFB combustion (series of connected mini-CFBs), the number of mini-CFB shall be optimized, it could be only two or three connected mini-CFBs.

7.5.3 Thermodynamics analysis (exergy and energy) Future Scopes

- Thermodynamic modelling of oxy-fuel CFB combustion is lacking in the literature, and the overall process of power plant is a complex phenomena, where to many factors affect the efficiency of the power plant. And higher thermodynamic analysis is recommended at the level of power plant not only the chemical reaction level, this future work could be done in aim to clarify the economic cost and efficiency of the power plant under oxy-fuel combustion conditions. Software like Aspen plus (Kannan et al., 2012) could be used, which could also allow optimizing the rigorous experimentation, as well as, saving the cost of time and money.

Finally, the main aims of the work are achieved, where the pure oxy-CFB combustion is proposed, experimentally experienced, and leads to zero recirculation of flue gases, higher efficiency due to minimized loss of exergy comparing with conventional oxy-fuel CFB combustion, additionally, biomass (sawdust) is used and shows a smooth operating process, and the biomass oxy-fuel CFB combustion is a promising technology toward less than zero CO_2 emissions.

References

Abdulally I., (2012). Oxygen-Fired CFB Development Oxy-CFB 350 MW Reference Concept. 2nd International Workshop on Oxyfuel FBC Technology. Stuttgart.

Abraham B. M., Asbury J. G., Lynch E. P., and Teotia A. P. S., (1982). Coal-oxygen process provides CO2 for enhanced recovery. Oil & Gas Journal, 80(11), pp.68–70.

Adfinez J., Gayfin P. and Diego L.F., (1994). Axial voidage profiles in fast fiuidized beds. Powder Technology, 81, pp.259–268.

Agbor E., Zhang X. and Kumar A., 2014. A review of biomass co-firing in North America. Renewable and Sustainable Energy Reviews, 40, pp.930–943.

Ahn J., Okerlund R., Fry A., and Eddings E. G., (2011). Sulfur trioxide formation during oxy-coal combustion. International Journal of Greenhouse Gas Control, 5, pp.S127–S135.

Alstom, (2013). Alstom Introduces the ultra-supercritical circulated fluidised bed (CFB) boiler, Report.

Altmeyer, S. et al., (2004). Comparison of different models of cyclone prediction performance for various operating conditions using a general software. , 43, pp.511–522.

Ameri M. and Ahmadi P., (2007). The Study of Ambient Temperature Effects on Exergy Losses of a Heat Recovery Steam Generator. Chapter, Challenges of Power Engineering and Environment. pp. 55–60.

Anthony E. J., (2013). Current State of Development in Oxy- CFB Technology for Coal-Fired Power Plants. In 3rd Oxyfuel Combustion Conference.

Anthony E. J., (2014). The Future of Oxy- Fuel Fluidized Bed Combustion Technology. In 4th International Workshop on Oxy-fuel FBC technology. Nanjing.

Arena U., Bartoli C. and Cammarota A., (1998). L-valve behaviour with solids of different size and density. Powder Technology, 98(98), pp.231–240.

ASTM, (2007). Standard Test Method for Chemical Analysis of Wood Charcoal. , 84, pp.1–2.

Avidan A. A. and Yerushalmi J., (1982). Bed expension in high velocity fluidization. Powder Technology, 32(2), pp.223–232.

Backhurst J. R. and Richardson J.F., (2002). Coulson & Richardson's Chemical Engineering: Solutions to the Problems in Chemical Engineering, Volume 2 (5th Edition) and Volume 3 (3rd Edition), Butterworth-Heinemann.

Basu P., (2015). Circulating Fluidized Bed Boilers - Design, Operation and Maintenance, Springer.

Basu P., (2006). Combustion and Gasification in Fluidized Beds, CRC Press.

Basu P. and Butler J., (2009). Studies on the operation of loop-seal in circulating fluidized bed boilers. Applied Energy, 86(9), pp.1723–1731.

Baukal C.E., (1998). OXYGEN-ENHANCED COMBUSTION First, CRC Press.

Bejarano P. A. and Levendis Y. A., (2008). Single-coal-particle combustion in O2/N2 and O2/CO2 environments. Combustion and Flame, 153, pp.270–287.

Blanco J.M. and Pena F., (2008). Increase in the boiler's performance in terms of the acid dew point temperature: Environmental advantages of replacing fuels. Applied Thermal Engineering, 28(7), pp.777–784.

Bolea I., Romeo L.M. and Pallarès D., (2014). Heat transfer in the external heat exchanger of oxy-fuel fluidized bed boilers. Applied Thermal Engineering, 66(1-2), pp.75–83.

Brix J., Jensen P.A. and Jensen A.D., (2011). Modeling char conversion under suspension fired conditions in O2/N2 and O2/CO2 atmospheres. Fuel, 90(6), pp.2224–2239.

Broek V., (2000). Sustainability of biomass electricity systems, Utrecht: Department of Science, Technology and Society, The Netherlands Utrecht University.

Buragohain B., Mahanta P. and Moholkar V.S., (2009). First Principles Design of a Circulating Fluidized Bed (CFB) Biomass Gasifier. In J. P. Shukla, ed. New Technologies for Rural Development Having Potential of Commercialisation. New Delhi: Allied Publishers Pvt Ltd., pp. 210–233.

Cahyadi S.A. and Nugroho Y.S., (2013). Predicting behavior of coal ignition in oxy-fuel combustion. Energy Procedia, 37, pp.1423–1434.

Casleton D.K., Shadle L.J. and Ross A.A., (2010). Measuring the voidage of a CFB through image analysis. Powder Technology, 203(1), pp.12–22.

Cheng L. and Basu P., (1999). Effect of pressure on loop seal operation for a pressurized circulating fluidized bed. Powder Technology, pp.203–2011.

Chitester. D.C., Kornosky R.M., Fan L. and Danko J.P., 1984. Characteristics of fluidization at high pressure. Chemical Engineering Science, 39(2), pp.253–261.

Chovichien N., Pipatmanomai S. and Chungpaibulpatana S., (2013). Estimate of solids circulation rate through an L-valve in a CFB operating at elevated temperature. Powder Technology, 235, pp.886–900.

Coal India Limited, (2015). North-Eastern Coal fields.

Cole W. A. and Wakeham W. A., (1985). The Viscosity of Nitrogen, Oxygen, and Their Binary Mixtures in the Limit of Zero Density. Journal of Physical and Chemical Reference Data, 14(1), pp.209–226.

Cremers M.F., (2009). Technical status of biomass co-firing. IEA, Bioenergy Task 32: KEMA Nederland B.V., IEA Bioenergy Task 32, pp.1–43.

Cung K., Moiz A., Johnson J., Lee S., Kweon C. and Montanaro A., (2015). Spray–combustion interaction mechanism of multiple-injection under diesel engine conditions. Proceedings of the Combustion Institute, 35(3), pp.3061–3068.

Czakiert T., Muskala W., Jankowska S., Krawczyk G., Borecki P., Jesionowski L. and Nowak W., (2012). Combustible matter conversion in an oxy-fuel circulating fluidized-bed (CFB) environment. Energy and Fuels, 26(9), pp.5437–5445.

Czakiert T., Sztekler K., Karski S., Markiewicz D. and Nowak W., (2010). Oxy-fuel circulating fluidized bed combustion in a small pilot-scale test rig. Fuel Processing Technology, 91(11), pp.1617–1623.

Dai B., Zhang L., Cui J., Hoadley A. and Zhang L. L., (2016). Integration of pyrolysis and entrained-bed gasification for the production of chemicals from Victorian brown coal — Process simulation and exergy analysis. Fuel Processing Technology.

Das M., Bandyopadhyay A., Meikap B. C. and Saha R. K., (2008). Axial voidage profiles and identification of flow regimes in the riser of a circulating fluidized bed. Chemical Engineering Journal, 145, pp.249–258.

Davison J., (2007). Performance and costs of power plants with capture and storage of CO2. Energy, 32(7), pp.1163–1176.

Dincer I. and Rosen M.A., (2007). Exergy, Energy, Environment and Susatinable Development, Elsevier.

Duan L., Zhao C., Zhou W., Qu C., and Chen, X., (2011). Effects of operation parameters on NO emission in an oxy-fired CFB combustor. Fuel Processing Technology, 92(3), pp.379–384.

Duan L., Duan Y., Sarbassov Y., Li Y., and Anthony E. J., 2015. SO3 formation under oxy-CFB combustion conditions. International Journal of Greenhouse Gas Control, 43, pp.172–178.

Duan L. and Zhao C., (2014). Development on Oxy-CFB Combustion at Southeast University. 4th International Workshop on Oxyfuel FBC Technology.

Eddings E.G. and Okerlund R., (2009). Pilot Scale Evaluation of Oxycoal Firing in Circulating- Fluidized Bed and Pulverized Coal-Fired Test Facilities. 1st IEA GHG International Conference on Oxy-fuel Combustion. Cottbus, Germany.

Elsayed K., (2011). Analysis and Optimization of Cyclone Separators Geometry Using RANS and LES Methodologies. Vrije Universiteit Brussel.

Ergun S. and Orning A.A., 1949. Fluid Flow through Randomly Packed Columns and Fluidized Beds. Industrial and Engineering Chemistry, 41(6), pp.1179–1184.

Ersoy L. E., Golriz M. R., Koksal M. and Hamdullahpur F., (2004). Circulating fluidized bed hydrodynamics with air staging : an experimental study. Powder Technology, 145, pp.25–33.

Faulkner W. B., Buser M. D., Whitelock D. P. and Shaw B. W., (2008). Effects of cyclone diameter on performance of 1D3D cyclones: cutpoint and slope. American Society of Agricultural and Biological Engineers, 51(1), pp.287–292.

Finesso R. and Spessa E., (2014). Ignition delay prediction of multiple injections in diesel engines. Fuel, 119, pp.170–190.

Geldart D., (1973). Types of gas fluidization. Powder Technology, 7(5), pp.285–292.

Ghamarian A. and Cambel A.B., 1982. Exergy analysis of Illinois No. 6 coal. Energy, 7(6), pp.483–488.

Gibbins J. and Chalmers, H., (2008). Carbon capture and storage. Energy Policy, Vol. 36(12), pp.4317–4322.

Gibilaro, L.G., (2001). Fluidization Dynamics. Elsevier, p.36. ISBN-9780750650038

Gómez M., Fernández A., Llavona I. and Kuivalainen R., (2014). Experiences in sulphur capture in a 30 MWth Circulating Fluidized Bed boiler under oxy-combustion conditions. Applied Thermal Engineering, 65(1-2), pp.617–622.

Grace, J.R., (1986). Contacting modes and behaviour classification of gas-solid and other two-phase suspensions. The Canadian Journal of Chemical Engineering, 64(3), pp.353–363.

Guedea I., Díez L. I., Pallarés, Javier R. and Luis M., (2011). Influence of O2/CO2 mixtures on the fluid-dynamics of an oxy-fired fluidized bed reactor. Chemical Engineering Journal, 178, pp.129–137.

Gupta A.V.S.S.K.S. and Nag P.K., (2002). Bed-to-wall heat transfer behavior in a pressurized circulating fluidized bed. Heat and Mass Transfer, 45, pp.3429–3436.

Gupta S.K. and Berruti F., (2000). Evaluation of the gas-solid suspension density in CFB risers with exit effects. Powder Technology, 108(1), pp.21–31.

Horst H., Monica L., Arto H. and Alvarez J., (2012). Initial Operation of the CIUDEN Oxy-CFB Boiler Demonstration Project. 11th Annual Carbon Capture, Utilization & Sequestration Conference, p.15.

Hack H., Lupion M., Otero P. Alvarez I., Muñoz F., Hotta A., Lantto J., Kuivalainen R. and Alvarez J., (2012). Testing in the CIUDEN Oxy-CFB Boiler Demonstration Project. The 37th International Technical Conference in Clean Coal & Fuel Systems, Clearwater, Florida.

Haider A. and Levenspiel O., (1989). Drag coefficient and terminal velocity of spherical and nonspherical particles. Powder Technology, 58(1), pp.63–70.

Hiwase S. D., Moorthy S., Prasad H., Dumpa M. and Metkar R. M., 2013. Multidimensional Modeling of Direct Injection Diesel Engine with Split Multiple Stage Fuel Injections. Procedia Engineering, 51, pp.670–675.

Hofbauer G., Beisheim T., Dieter H. and Scheffknecht G, (2014). Experiences from oxy-fuel combustion of bituminous coal in a 150 kW th circulating fluidized bed pilot facility. Energy Procedia, 51, pp.24–30.

Hotta A., (2009). Foster wheeler's solutions for large scale CFB boiler technology: features and operational performance of Łagisza 460 MWe CFB boiler. In 20th Int. Conf. on Fluidized Bed Combustion. pp. 59–70.

Hu N., Zhang H., Yang H., Yang S., Yue G., Lu J. and Liu Q., (2009). Effects of riser height and total solids inventory on the gas – solids in an ultra-tall CFB riser. Powder Technology, 196(1), pp.8–13.

Hu Y., (2011). CO2 capture from oxy-fuel combustion power plants, Ph.D. thesis, KTH Royal Institute of Technology, School of Chemical Science and Engineering, Department of Chemical Engineering and Technology, Energy Processes Stockholm, Sweden.

Huijbregts W.M.M. and Leferink R.G.I., (2004). Latest advances in the understanding of acid dewpoint corrosion: corrosion and stress corrosion cracking in combustion gas condensates. Anti-Corrosion Methods and Materials, 51(3), pp.173–188.

Hultgren M., Ikonen, E. and Kovács J., (2014). Oxidant control and air-oxy switching concepts for CFB furnace operation. Computers and Chemical Engineering, 61, pp.203–219.

Hussain A., Ahmed I., Sait H. H., Bassyouni M. I., Hegab A. M., Waheed S. and Ani F. N., (2013). Experimental and Simulation Study of Fluidization Behavior of Palm Biomass in a Circulating Fluidized Bed Riser.

Industrial & Engineering Chemistry Process Design and Development.

IEA, (2011a). World Energy Outlook 2011.

IEA, (2011b). Developments in fluidized bed conversion during 2005 - 2010 A summary from the member countries of the IEA-FBC Implementing Agreement, Göteborg.

IEA, 2010. Energy Technology Perspectives 2010,

IEA, (2013a). Global Action to Advance Carbon Capture and Storage, Available at: https://www.iea.org/publications/freepublications/publication/CCS_Annex.pdf

IEA, (2013b). Tracking Clean Energy Progress. Technology, pp.1–82. Available at: http://www.iea.org/media/etp/Tracking_Clean_Energy_Progress.pdf

IEA, (2014). Coal Information 2014, Available at: www.iea.org/Textbase/nptoc/coal2014TOC.pdf.

IEA, (2014b). The Impact of Global Coal Supply on Worldwide Electricity Prices, Paris, France.

IEA-CIAB, (2013). 21st Century Coal, Advanced Technology and Global Energy Solution,

INC. ALSTOM, (2003). Bench-scale Fluidized Bed Combustion Testing, Report, Greenhouse Gas Emissions Control by Oxygen Volume Ii: Bench-Scale FBC Testing Firing In Circulating Fluidized Bed Boilers, Phase 1 – A Preliminary Systems Evaluation, ALSTOM Power Inc., VOLUME II: BENCH-SCALE FBC TERSTING, Windsor.

Jia L., Tan Y. and Anthony E.J., 2010. Emissions of SO2 and NOx during Oxy-Fuel CFB combustion tests in a mini-circulating fluidized bed combustion reactor. Energy and Fuels, 24(2), pp.910–915.

Jones J.M., Saddawi A., Dooley B., Mitchell E.J.S., Werner J., Waldron D.J., Weatherstone S. and Williams A., (2015). Low temperature ignition of biomass. Fuel Processing Technology, 134, pp.372–377.

Kalita P., Mahanta P. and Saha U.K., (2013). Some studies on wall-to-bed heat transfer in a pressurized circulating fluidized bed unit. Procedia Engineering, 56, pp.163–172.

Kalita P., SahaU.K. and Mahanta P., (2013). International Journal of Heat and Mass Transfer Effect of biomass blending on hydrodynamics and heat transfer behavior in a pressurized circulating fluidized bed unit. International Journal of Heat and Mass Transfer, 60, pp.531–541.

Kannan P., Shoaibi A. A. and Srinivasakannan C., 2012. Optimization of Waste Plastics Gasification Process Using Aspen-Plus. INTECH, http://dx.doi.org/10.5772/48754

Kaushik S.C., Reddy V.S. and Tyagi S.K., (2011). Energy and exergy analyses of thermal power plants : A review. Renewable and Sustainable Energy Reviews, 15(4), pp.1857–1872. Available at: http://dx.doi.org/10.1016/j.rser.2010.12.007

Khan A. A., De Jong W., Jansens P. J. and Spliethoff H., 2009. Biomass combustion in fluidized bed boilers: Potential problems and remedies. Fuel Processing Technology, 90(1), pp.21–50.

Khatami R., Stivers C. and Levendis Y. a., (2012). Ignition characteristics of single coal particles from three different ranks in O2/N2 and O2/CO2 atmospheres. Combustion and Flame, 159(12), pp.3554–3568.

Kiriishi K., Fujimine T. and Hayakawa A., (2009). High Efficiency Furnace with Oxy-Fuel Combustion and Zero-Emission by CO2 Recovery. In 24th World Gas Conference, Buenos Aires, Argentina.

Kline S.J. and McClintock F.A., (1953). Describing UNCERTIANTIES in SINGLE-SAMPLE EXPERIMENTS. Mechanical Engineering, pp.3–8.

Kobayashi H. and Bool L.E., (2011). Direct oxy-coal combustion with minimum or no flue gas recycle. Chapter. Oxy-fuel combustion for power generation and carbon dioxide (CO2) capture. Cambridge: Woodhead Publishing Limited, p. 374.

Krevelen D.W., (1961). Coal 3rd , Amsterdam: Elsevier Science.

Kunii D. and Levenspiel O., (1991). Fluidization Engineering 2nd. Howard Brenner, ed., Butterworth Heinemann.

Kwauk M., Ningde W., Youchu L., Bingyu C. and Zhiyuan S., (1985). Fast fluidization at ICM. Proceedings of the First International Circulating Fluidized Bed Technology. Halifax, Canada.

Obras-Loscertales M., Rufas A., De Diego L. F., García-Labiano F., Gayán P., Abad A. and Adánez J., (2013). Effects of temperature and flue gas recycle on the SO2 and NOx emissions in an oxy-fuel fluidized bed combustor. Energy Procedia, 37, pp.1275–1282.

Leahy M., Barden J.L., Murphy B.T., Slater-thompson N. and Peterson D., (2013). International Energy Outlook 2013.

Leva M., (1959). Fluidization, McGraw-Hill.

Li C., Li H. and Zhu Q., (2014). A hydrodynamic model of loop-seal for a circulating fl uidized bed. Powder Technology, 252, pp.14–19.

Li H., Li S., Ren Q., Li W., Xu M., Liu J. Z., and Lu Q., 2014. Experimental Results for Oxy-fuel Combustion with High Oxygen Concentration in a 1MWth Pilot-scale Circulating Fluidized Bed. Energy Procedia, 63, pp.362–371.

Liljedahl G., Turek D., Ya N., Mohn Nc, and Fout T., (2006). Alstom's oxygen-fired CFB technology development status for CO2 mitigation. 31st Int. Tech. Conf. on Coal Utilization & Fuel Systems.

Lin H., Zhou M., Ly J., Vu J., Wijmans J., Merkel T., Jin J., Haldeman A., Wagener E.,

and Rue D., (2013). Membrane-Based Oxygen-Enriched Combustion. Industrial & Engineering Chemistry Research, 52, pp.10820–10834.

Liu Y., Wall T., and Khare S., (2011). Oxy-fuel combustion for power generation and carbon dioxide (CO2) capture , Chapter, Woodhead Publishing Limited.

Lupion M., Alvarez I., Otero P., Kuivalainen R., Lantto J., Hotta A. and Hack H., (2013). 30 MWth CIUDEN Oxy-CFB boiler - First experiences. Energy Procedia, 37, pp.6179–6188.

Maffei T., Khatami R., Pierucci S., Faravelli T., Ranzi E. and Levendis Y. A., (2013). Experimental and modeling study of single coal particle combustion in O2/N2 and Oxy-fuel (O2/CO2) atmospheres. Combustion and Flame, 160(11), pp.2559–2572.

Maffei T. and Milano P.D.I., (2013). Kinetic Model of Coal Combustion. Thesis, Dipartimento Di Chimica, Materiali Eingegneria Chimica, Politecnico di Milano.

Mahanta P., (2012). Advance Engineering Thermodynamic. NPTEL.

Mahmoudi S., Baeyens J. and Seville J., (2011). The solids flow in the CFB-riser quantified by single radioactive particle tracking. Powder Technology, 211(1), pp.135–143.

Metz B., Davidson O.R., Bosch P.R., Dave R. and Meyer L.A., (2007). Contribution of Working Group III to the Fourth Assessment Report of the Intergovernmental Panel on Climate Change. Cambridge University Press.

Metz B., Davidson O., Bosch P., Dave R., and Meyer L., (2007). Climate Change 2007 Mitigation of Climate Change, Contribution of Working Group III to the Fourth Assessment Report of the Intergovernmental Panel on Climate Change, Published for the Intergovernmental Panel on Climate Change, Cambridge University Press.

Moffat R.J., (1988). Describing the uncertainties in experimental results. Experimental Thermal and Fluid Science, 1(1), pp.3–17.

Molina A. and Shaddix C.R., (2007). Ignition and devolatilization of pulverized bituminous coal particles during oxygen/carbon dioxide coal combustion. Proceedings of the Combustion Institute, 31(2), pp.1905–1912.

Moroń W. and Rybak W., (2015). Ignition behaviour and flame stability of different ranks coals in oxy fuel atmosphere. Fuel, 161, pp.174–181.

Nag P.K., (2008). Power Plant Engineering, 3rd Edition, Tata McGraw Hill, New Delhi.

Nakamura M., Hamada Y., Toyama S., Fouda A. E. and Capes C. E., (1985). An experimental investigation of minimum fluidization velocity at elevated temperatures and pressures. The Canadian Journal of Chemical Engineering, 63(1), pp.8–13.

Nsakala N., Liljedahl G., Marion J., Levasseur A., Turek D., Chamberland R. and MacWhinnie R., (2004). Oxygen-fired circulating fluidized bed boilers for greenhouse gas emissions control and other applications. In 3rd annual conference on carbon capture & sequestration, conference proceedings. pp. 1–21.

Nussbaumer T., (2003). Combustion and Co-combustion of Biomass: Fundamentals, Technologies, and Primary Measures for Emission Reduction. Energy and Fuels, 17(6), pp.1510–1521.

Ochs T., Oryshchyn D., Woodside R., Summers C., Patrick B., Gross D., Schoenfield M., Weber T. and Brien D., (2009). Results of initial operation of the Jupiter Oxygen Corporation oxy- fuel 15 MWth burner test facility. Energy Procedia, 1(1), pp.511–518.

Oka S. and Dekker M., (2004). Fluidized Bed Combustion,

Orhan M.F., Dincer I. and Rosen M.A., (2009). Energy and exergy analyses of the fluidized bed of a copper-chlorine cycle for nuclear-based hydrogen production via thermochemical water decomposition. Chemical Engineering Research and Design, 87(5), pp.684–694.

Patil R.S., Pandey M. and Mahanta P., 2011. Parametric studies and effect of scale-up on wall-to-bed heat transfer characteristics of circulating fluidized bed risers. Experimental Thermal and Fluid Science, 35(3), pp.485–494.

Petit, R.J., Raynaud D., Basile I., Chappellaz J., Ritz C., Delmotte M., Legrand M., Lorius C., and Pe L. (1999). Climate and atmospheric history of the past 420,000 years from the Vostok ice core, Antarctica. Nature, 399, pp.429–413.

Pikkarainen, T., Saastamoinen J., Saastamoinen H., Leino T., and Tourunen A., (2014). Development of 2nd Generation Oxyfuel CFB Technology – Small Scale Combustion Experiments and Model Development Under High Oxygen Concentrations. Energy Procedia, 63, pp.372–385.

Ponzio A., Senthoorselvan S., Yang W., Blasiak W. and Eriksson O., 2008. Ignition of single coal particles in high-temperature oxidizers with various oxygen concentrations. Fuel, 87(6), pp.974–987.

Qiao Y., Zhang L., Binner E., Xu M. and Li C., 2010. An investigation of the causes of the difference in coal particle ignition temperature between combustion in air and in O2/CO2. Fuel, 89(11), pp.3381–3387.

Quadrelli R. and Peterson S., (2007). The energy-climate challenge: Recent trends in CO2 emissions from fuel combustion. Energy Policy, Vol. 35(11), pp.5938–5952.

Rathnam R. K., Elliott L. K., Wall T. F., Liu Y. and Moghtaderi B., (2009). Differences in reactivity of pulverised coal in air (O2/N2) and oxy-fuel (O2/CO2) conditions. Fuel Processing Technology, 90(6), pp.797–802.

Rhodes M., (2008). Introduction to Particle Technology, Second edition, John Wiley & Sons.

Riaza J., Álvarez L., Gil M.V. V., Pevida C., Pis J.J. and Rubiera F., (2011). Effect of oxy-fuel combustion with steam addition on coal ignition and burnout in an entrained flow reactor. Energy, 36(8), pp.5314–5319.

Scala F., (2013). Fluidized bed technologies for near-zero emission combustion and gasificatio, Woodhead Publishing Limited.

Scarlat N., Dallemand J., Skjelhaugen O. J., Asplund D. and Nesheim L., (2011). An overview of the biomass resource potential of Norway for bioenergy use. Renewable and Sustainable Energy Reviews, 15(7), pp.3388–3398.

Schoenfield M., 2009. Jupiter Oxygen. In IEA GHG 1st Oxyfuel Combustion Conference. pp. 1–45.

Seddighi S., Pallarès D., Normann F. and Johnsson F., 2013. Progress of Combustion in an Oxy-fuel Circulating Fluidized-Bed Furnace: Measurements and Modeling in a 4 MWth Boiler. Energy & Fuels, 27(10), pp.6222–6230.

Seddighi S., Pallares D., Normann F., Johnsson F., and Yla-Outinen V., (2015). Heat transfer in a 4-MWth circulating fluidized bed furnace operated under oxy-fired and air-fired conditions: Modeling and measurements. International Journal of Greenhouse Gas Control, 37, pp.264–273.

Seddighi S., Pallarès D., Normann F., and Johnsson F., 2015. Heat extraction from a utility-scale oxy-fuel-fired CFB boiler. Chemical Engineering Science, 130, pp.144–150.

Seddighi, S., Pallarès, D. and Johnsson, F., (2011). Assessment of Oxyfuel Circulating Fluidized Bed Boilers – Modeling and Experiments in a 5 MW Pilot Plant. In 2nd Oxyfuel Combustion Conference. pp. 5–7.

Shaddix, C.R. and Molina, A., 2009. Particle imaging of ignition and devolatilization of pulverized coal during oxy-fuel combustion. Proceedings of the Combustion Institute, 32(2), pp.2091–2098.

Shiyuan L. I., Qiangqiang R., Wei L. I., Li T. and Enguang S., (2013). Study of oxy-fuel CFB combustion at high oxygen concentrations at IET-CAS. In The 3rd International Workshop on Oxyfuel-FBC Technology.

Souza-Santos M.L., (2004). Solid Fuels Combustion and Gasification. CRC press, ISBN-13: 978-1420047493, pp.1– 431.

Spliethoff, H. and Hein, K.R.., (1998). Effect of co-combustion of biomass on emissions in pulverized fuel furnaces. Fuel Processing Technology, 54(1-3), pp.189–205.

Stangeland A., (2007). Why CO2 Capture and Storage (CCS) is an Important Strategy to Reduce Global CO2 Emissions. Bellona, (1), pp.1–8

Stéphenne K., (2014). Start-up of World's First Commercial Post-combustion Coal Fired CCS Project: Contribution of Shell Cansolv to SaskPower Boundary Dam ICCS Project. Energy Procedia, 63, pp.6106–6110.

Stewart M.C., (2009). Sulfation Phenomena Under Oxy-Fuel Circulating Fluidized Bed Conditions. Thesis, Chemical Engineering, University of Ottawa.

Szargut J. and Styrylska T., (1964). Brennstoff-wärme-kraft. , 16, p.589.

Tan Li, Li S., Li W., Shou E. and Lu Q., 2014. Effects of Oxygen Staging and Excess Oxygen on O2/CO2 Combustion with a High Oxygen Concentration in a Circulating Fluidized Bed. Energy & Fuels, 28(3), pp.2069–2075.

Tan, Y., Jia L., Wu Y., and Anthony E. J., (2012). Experiences and results on a 0.8MWth oxy-fuel operation pilot-scale circulating fluidized bed. Applied Energy, 92, pp.343–347.

Tondl G., Penthor St., Wöß D., Pröll T., Höltl W. and Rohovec J., 2011. From Oxygen enrichment to Oxyfuel combustion. In 63rd IEA FBC Meeting, Ponferrada, Spain, Spain, pp. 63–63.

Tourunen A., Lehto J., Hämäläinen J. and Pikkarainen T., 2014. Development of oxyfuel CFB technology at VTT. In The 4th Korea CCS International conference.

Trengove R.D. and Wakeham W., (1987). The Viscosity of Carbon Dioxide, Methane, and Sulfur Hexafluoride in the Limit of Zero Density. Journal of Physical and Chemical Reference Data, 16(2), pp.175–187.

U.S. Department of Energy, 2007. Improving Process Heating System Performance : A Source book for Industry Second., Berkeley, California, USA.

U.S. DOE, 2005. Energy Tips 3– Process Heating, ISBN: 1020072482

UKCCSRD, (2015). 200 KW Circulating Fluidised Bed Combustion CFBC.

UN, (2013). Population Division of the Department of Economic and Social Affairs of the United Nations Secretariat, NewYork.

Utikar R., Darmawan N., Tade M., Li Q, Evans G., Glenny M. and Pareek V., (2010). Hydrodynamic Simulation of Cyclone Separators. Computational Fluid Dynamics. InTech.

Wang C.S., Berry G.F., Chang K.C. and Wolsky A.M., (1988). Combustion of pulverized coal using waste carbon dioxide and oxygen. Combustion and Flame, 72(3), pp.301–310.

Wang L., (2004). Theoretical study of cyclone design. Texas A&M University.

Wen C.Y. and Yu Y.H., (1966). A generalized method for predicting the minimum fluidization velocity. AIChE Journal, 12(3), pp.610–612.

Wen, C.Y. and Yu, Y.H., (1977). Measurement of Incipient Fluidisation Velocities in a Bed of Coarse Dolomite at Temperature and Pressure. Trans Inst. Chem. Eng., 55(3), pp.184–189.

Arto Hotta, (2009). Development and demonstration of oxy CFB for power plants with CO2 contents of presentation, 1st International Oxyfuel Combustion Conference, Cottbus, Germany.

Winaya N.S., Basu P. and Reddy B. V, (2003). Experimental investigations on heat transfer from suspension to impact separators in the riser column of a circulating fluidized bed combustor, International Journal of Heat and Mass Transfer, 46, pp.71–75.

Wu, Y., Yang, W. and Blasiak, W., (2014). Energy and exergy analysis of high temperature agent gasification of biomass. Energies, 7(4), pp.2107–2122.

Wu D., Huang X., Norman F., Verplaetsen F., Berghmans J., and Van den Bulck E., (2015). Experimental investigation on the self-ignition behaviour of coal dust accumulations in oxy-fuel combustion system. Fuel, 160, pp.245–254.

Yang W., (1998). Fluidization Solids Handling And Processing Andustrial Applications, Pittsburgh, Pennsylvania: Noyes Publication.

Yang H., Lu J., Zhang H., Yue G. and Guo Y., (2005). Coal ignition characteristics in CFB boiler. Fuel, 84, pp.1849–1853.

Yang W.C., (2007). Modification and re-interpretation of Geldart's classification of powders. Powder Technology, 171, pp.69–74.

Yazdanfar J., Mehrpooya, M., Yousefi H. and Palizdar A., (2015). Energy and exergy analysis and optimal design of the hybrid molten carbonate fuel cell power plant and carbon dioxide capturing process. Energy Conversion and Management, 98, pp.15–27.

Yuzbasi, N.S. and Selçuk, N., 2011. Air and oxy-fuel combustion characteristics of biomass / lignite blends in TGA-FTIR. Fuel Processing Technology, 92(5), pp.1101–1108.

Zanganeh K. E., Salvador C., Mitrovic M., and Shafeen A., (2008). 3rd Generation Oxy-Fuel Combustion Systems CO2 Strategy Options for Power Sector. 3rd IEA GHG International Oxy-Combustion Workshop. Yokohama, pp. 1–23.

Zheng L., (2011). Oxy-fuel combustion for power generation and carbon dioxide (CO2) capture, Woodhead Publishing Limited.

Zhang H. L., Degrè J., Baeyens J., and Dewil R., (2015). The voidage in a CFB riser as function of solids flux and gas velocity. Procedia Engineering, 102(40), p.260.

Appendices

Appendix A: Design of Distributor Plate

In this section, several fluidization velocity equations, and CFB design procedure are presented following the procedures outlined by Buragohain et al. (2009) who used biomass as as solid fuel. In the present investigation, the coal is used as fuel, and thus, the distributor plate is designed accordingly. The materials of CFB construction is SS314, some materials are changed during operating the hot CFB. Buragohain et al. (2009) proposed dual particle usage (sand and biomass), where sand was used to enhance the heat transfer of the unit and distributing the fuel particle through the riser. Some power plant uses only fuel without inert materials (sand) viz. Alstom (2013). The following chart explains the steps of calculating of the riser section.

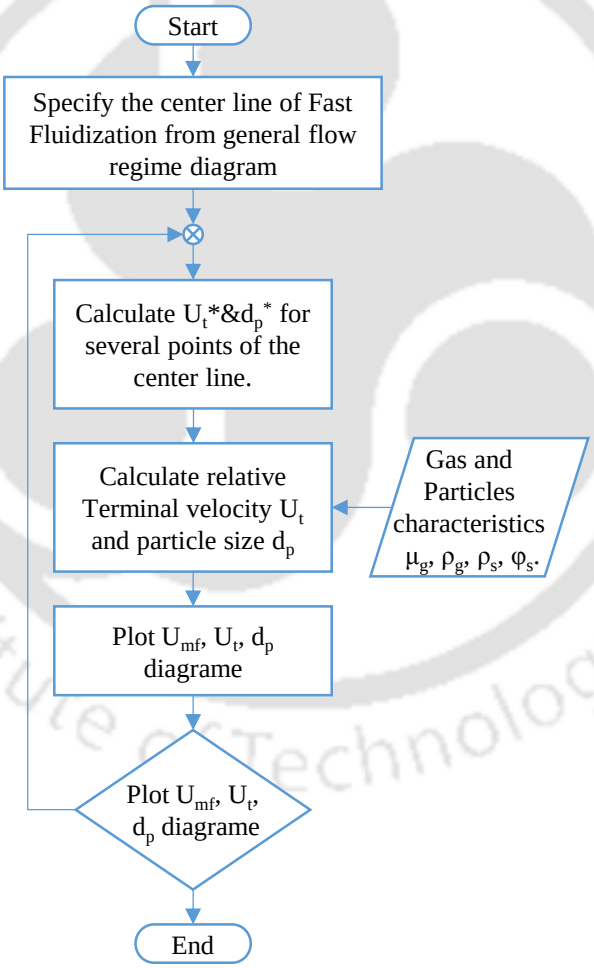

A.1 Flow chart of calculating and matching flow regime.

For estimating d_p^*, u^*, we used Eq.2.16, and Eq. 2.17 for estimating terminal velocity u_{tr}, we used Eq. 2.12, and Eq.2.14. For estimating minimum fluidization velocity u_{mf}, we used Eq. 2.9 with Wen and Yu correlation (1977). These calculation were used for wide range of particle size, coal and sand particles, sphericity of ϕ=0.65, operating used gasO_2, N_2, CO_2, and air at 25-850 °C, Table A.1, (Trengove and Wakeham 1987; Cole and Wakeham 1985).

Table 0A.0.1 Comparison of density and viscosity of O_2, N_2, CO_2, and air at 25°-850° C

Temp.	ρ_{O_2}	ρ_{N_2}	ρ_{CO_2}	ρ_{air}	μ_{O_2}	μ_{N_2}	μ_{CO_2}	μ_{air}
25° C	1.309	1.145	1.799	1.179	0.00021	0.000174	0.000143	0.00019
850° C	0.487	0.427	0.670	0.439	0.000533	0.000446	0.000448	0.00051
Ration 25/850	2.69	2.68	2.69	2.69	0.39	0.32	0.32	0.37

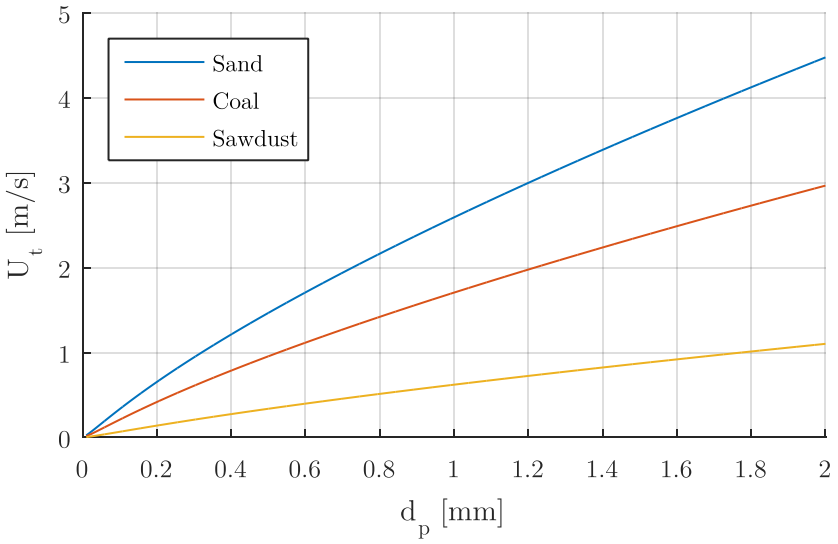

Figure A.2 Air case: Terminal velocity of sand, coal, and sawdust

Almost the terminal velocity (U_{tr}) of sand is 50% higher than U_{tr} of coal, meanwhile, the terminal velocity of the sawdust around 30% of the U_{tr} of the coal, due to, the lower density of the sawdust.

Appendix B: Aero cyclone Separator's Design

Since the first application of aero cyclones in 1886, theories for the estimation of both particle collection efficiency and pressure drop of cyclone have been developed by many contributors using different methods. For instance Barth model, The Muschelknautz method of modelling (MM), Stairmand model, Shepherd and Lapple model, Casal and Martinez-Bent model, Ramachandran model, Iozia and Leith model, and Rietema model (Altmeyer et al. 2004; Wang 2004; Elsayed 2011; Utikar, R., Darmawan, N., Tade, M., Li, Q, Evans, G., Glenny, M. and Pareek 2010). The cyclone geometry is an important parameter that affects the cyclone efficiency. Figure B.1 illustrates the dimensions of cyclone separator. The parameters of cyclone are presented in the Table 0.2

Table 0.2 Cyclone separator's design geometry

Nomenclature	Description
a	the inlet height
b	the inlet width
D_x	the vortex finder diameter (gas outlet D)
S	the vortex finder length
h	the cylindrical part height
H_t	the cyclone total height
B_c	the cone-tip diameter
D	the barrel diameter

Maximum gas flow rate, Q_m:

$$Q_m = U_m \times A_{riser} = 4 \times \frac{\pi}{4} \times 0.05^2 = 0.00784 \quad m^3/s$$
$$or, \quad Q_m = 28.27 \quad m^3/h \qquad \text{(B.1)}$$

Calculation of cyclone barrel diameter, D:

This design process allows to design the cyclone using a cyclone inlet velocity specific to the type of desired cyclone (Wang 2004). Knowing the design inlet velocities, a cyclone's dimensions could easily be determined by:

$$D = \sqrt{\frac{8 \times Q_m}{V_m}} = \sqrt{\frac{8 \times 0.00784}{12}} = 0.0723m \qquad 0\text{(B.2)}$$

Where U_m is the velocity in the riser. V_m is the velocity at the inlet of cyclone, and is taken three times of U_m. V_m=4×3=12 m/s, as a result the inlet section area 2 cm^2.

Cyclone design ratios: Using Elsayed (2011) optimized design data. The various ratios of cyclone separator are used as following.

Table 0.3 Design parameters of the cyclone

Proportion	Parameter
a/D=0.618	a=4.5cm
b/D=0.236	b=1.7cm
D_x/D=0.622	D_x=4.5cm
H_t/D=4.236	H_t=30.6 cm
h/D=1.618	h=11.7cm
S/D=0.620	S=4.5 cm
B_c/D=0.382	B_c=2.86cm

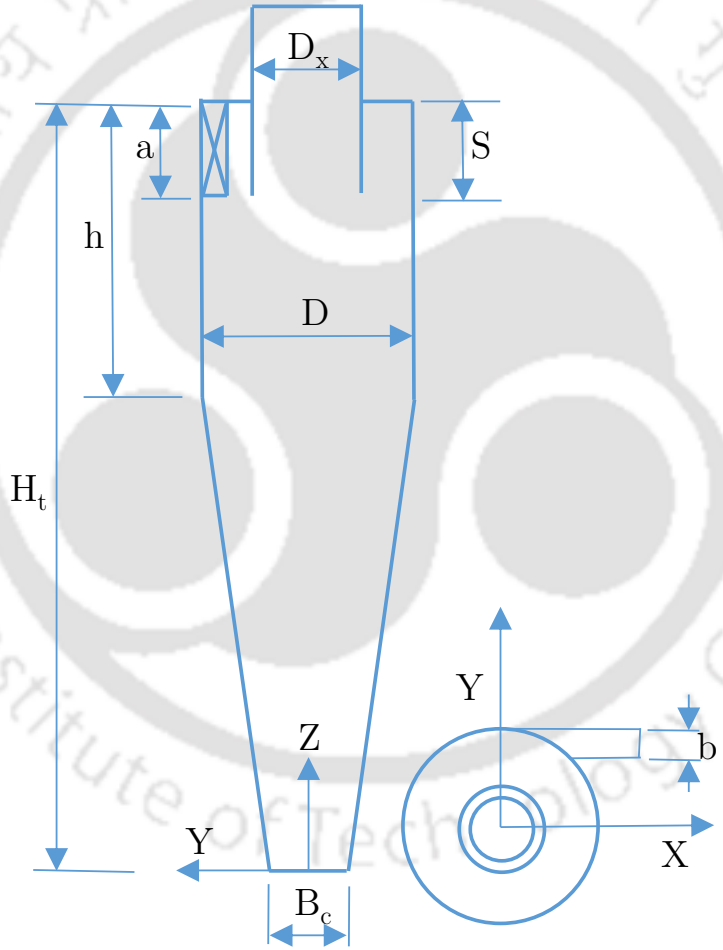

B.1 The cyclone separator dimensions

Appendix C: Sand Particle Size Distribution and Mean Particle Size

This distributor was calculated based on the Kunii and Levenspiel (1991) design procedure. The procedure of determining the particle size distribution of the sand and mean particle size sample is done, by sieving the sand using mesh of different sizes and segregating the sample into groups based on the particle size. For example, the first particle size group n_1 of 858 μm size is sieved by using mesh of 18 and 22 (BSS) British Standard Sieve, which has weight of W_1 grams. The second particle size group n_2 of 726 μm size is sieved by using mesh of size 22 and 25 (BSS), which has weight of W_2 grams, and so on, to sieve the entire sample. Then, the mean particle size is calculated by Eq.(C.3).

$$\bar{d}_p = \sum \frac{1}{\frac{X_i}{d_i}} \tag{C.3}$$

Where:

d_i represents the mean particle size of each sieved particle group.

W represents the weight of the overall sample.

W_i represents the weight of each sieved particle group.

$X_i = W_i/W$ represents the weight fraction of each sieved particle group.

Table C.1. The measurement of particle size

Mesh (BSS)	Mean particle size (di), µm	Weight in grams, Wi	Weight fraction (Xi= Wi/W)	Xi/ di
18 - 22	858.33	27	0.022113	2.58E-05
22 – 25	726.25	77	0.063063	8.68E-05
25 - 30	610.18	256	0.209664	0.000344
30 – 36	473.73	450	0.36855	0.000778
36 – 44	370.07	190	0.15561	0.00042
44 – 52	303.53	115	0.094185	0.00031
52 – 60	254.08	56	0.045864	0.000181
60 – 72	214.69	35	0.028665	0.000134
72 - Pan	195.80	15	0.012285	6.27E-05

The particle size distribution is explained in the Table C.1. by X_i/d_i fraction. Same procedure has been followed for each sample.

Appendix D: Design Calculation of CFB

This distributor was fabricated based on the Basu (2006); Kunii and Levenspiel (1991) design procedure. Initial parameters are given in table:

Table B.1 Basic parameters of calculating Distributor Plate

Description	Symbol	Value	Unit
Particle diameter	d_p	0.47	mm
Bed inventory	I	1	Kg
Operating velocity	u	2.5	m/s
Voidage at min. fluidization	ε_{mf}	0.5	---
Cross section area of the bed	A_b	2.29×10^{-3}	m^2
Density of the solid particles	ρ_s	2600	Kg/m^3
Density of the air	ρ_{air}	1.165	Kg/m^3
Gravity	g	9.81	m/s^2

Height of the bed at min. fluidization:

$$H_{mf}=\frac{\Delta P}{(1-\varepsilon_{mf})\times\rho_s\times g}=\frac{I\times g/A_b}{(1-\varepsilon_{mf})\times\rho_s\times g}=0.336m \quad (D.1)$$

Bed pressure drop, (ΔP_b)

$$\Delta P_b=(1-\varepsilon_{mf})\times\rho_s\times g\times H_{mf}=4285N/m^2 \quad (D.2)$$

Orifice diameter, (d_{or})

$$d_{or}=3\times d_p=1.23\times10^{-3}m \quad (D.3)$$

Minimum distributor pressure drop for uniform distribution (ΔP_D)

$$\Delta P_D=\Delta P_b\times\left(0.01+0.2\left(1.-\exp\left(-D/2/H_{mf}\right)\right)\right)=109N/m^2 \quad (D.4)$$

Rearrangement resistance between 3" and 2" tubes (ΔP_R)

$$\Delta P_R=\rho_a\times\left(\frac{u\times(A_b/A_t)^2}{2g}\right)=0.293N/m^2 \quad 0(D.5)$$

Thickness of the distributor plate (t): t=5mm=0.005m.

Orifice discharge coefficient (C_D)

$$C_D = 0.82 \times \left(t / d_{or}\right)^{0.13} = 0.984 \quad \text{(D.6)}$$

Gas velocity through the Orifice (U_{or})

$$u_{or} = C_D \times \left(2 \times \Delta P_b / \rho_g\right)^{1/2} = 13.46 m/s \quad \text{(D.7)}$$

Number of orifice per square meter of distributor (N_{or})

$$N_{or} = (u / u_{or}) \times (1 / A_{or}) = 39078 \text{Orfice/m}^2 \quad \text{(D.8)}$$

Total number on perforated distributor: $N_{or} \times A_b = 89.5$

Pitch of the orifice in the distributor: $1 / N_{or}^{1/2} = 0.0051 m = 5.1 mm$

Open area in the distributor: $N_{or} \times A_{or} = 4.2776 \times 10^{-4} \text{m}^2$

Percentage opening: $4.2776 \times 10^{-4} / A_{or} \times 100 = 46.7\%$

Appendix E: Experimental Uncertainties

The theory of sequential perturbation technique by Kline and McClintok (1953) and Moffat (1982) is used to calculate the uncertainties of the parameters. The method is described as follows. For dependent measured parameter U, which is function of variables x_1, x_2, x_3… x_n (Eq. E.1).

$$U = f(x_1, x_2, x_3, \ldots, x_n) \tag{E.1}$$

The uncertainty ΔU due to the individual uncertainties of the independent parameters termed as ΔU_1, ΔU_2, ΔU_3, ΔU_4… ΔU_n can be written as following (Eq. E.2),

$$U = \left[\left(\frac{\partial U}{\partial x_1} \Delta U_1 \right)^2 + \left(\frac{\partial U}{\partial x_2} \Delta U_2 \right)^2 + \ldots\ldots + \left(\frac{\partial U}{\partial x_n} \Delta U_n \right)^2 \right]^{\frac{1}{2}} \tag{E.2}$$

E. 1. Uncertainty in calculating voidage ε

Individual uncertainties are:

$$\rho_s = 2600 \pm 5 kg/m^3$$
$$\Delta(\Delta h) = \pm 0.2 cm$$
$$\Delta L_m = \pm 0.002 m$$

The voidage was calculated by using Eq. E.3,

$$\varepsilon = 1 - \frac{10 \times \Delta h}{\rho_s \times L_m} \tag{E.3}$$

Differentiating the above equation with respect to $\Delta h, L_m, and \rho_s$, we had,

$$\frac{\partial \varepsilon}{\partial(\Delta h)} = -\frac{10}{\rho_s \times L_m} \tag{E.4}$$

$$\frac{\partial \varepsilon}{\partial L_m} = -\frac{10 \times \Delta h}{\rho_s \times L_m^2} \tag{E.5}$$

$$\frac{\partial \varepsilon}{\partial \rho_s} = -\frac{10 \times \Delta h}{\rho_s^2 \times L_m} \tag{E.6}$$

Overall Uncertainty may be calculated as:

$$U = \sqrt{\left(\frac{\partial \varepsilon}{\partial(\Delta h)}\right)^2 \times (\Delta(\Delta h))^2 + \left(\frac{\partial \varepsilon}{\partial L_m}\right)^2 \times (\Delta L_m)^2 + \left(\frac{\partial \varepsilon}{\partial \rho_s}\right)^2 \times (\Delta \rho_s)^2} \quad \text{(E.7)}$$

For parameters of three experiment cases as following, we had overall uncertainty.

Table E.1 Overall uncertainty for bed voidage measurements

L_m [m]	Δh [cm]	U [±%]
0.077	5	5.0
0.016	4.9	18.8
0.177	5.7	3.5
0.022	5.8	13.9
0.14	5.9	4.0
0.138	6.1	4.0
0.142	6.3	4.0
0.014	6	27.2
0.162	6.5	3.9
0.3	6.7	2.9
0.3	6.8	2.9
Overall Uncertainty average		8.2

Uncertainty in calculating solid circulation rate G_s in kg.m^{-2}s^{-1}:

Individual uncertainties are:

$$\rho_s = 2600 \pm 5 kg/m^3$$
$$\Delta L_a = \pm 0.002 m$$
$$\Delta d_D = \pm 0.002 m$$
$$\Delta d_B = \pm 0.002 m$$
$$\Delta t = \pm 0.1 s$$

The voidage was calculated by using Eqs. E.8 and E.9,

$$G_s = \frac{\rho_s \times L_a \times A_D \times (1-\varepsilon_{mf})}{A_B t} \quad \text{(E.8)}$$

$$G_s = \frac{\rho_s \times L_a \times d_D^2 \times (1-\varepsilon_{mf})}{d_B^2 t} \quad \text{(E.9)}$$

Differentiating the above equation with respect to $\rho_s, L_a, d_D, d_B, and t$, we had,

$$\frac{\partial G_s}{\partial \rho_s} = \frac{L_a \times d_D^2 \times (1-\varepsilon_{mf})}{d_B^2 \times t} \quad \text{(E.10)}$$

$$\frac{\partial G_s}{\partial L_a} = \frac{\rho_s \times d_D^2 \times (1-\varepsilon_{mf})}{d_B^2 \times t} \quad \text{(E.11)}$$

$$\frac{\partial G_s}{\partial d_D} = \frac{\rho_s \times L_a \times d_D \times (1-\varepsilon_{mf})}{d_B^2 \times t} \quad \text{(E.12)}$$

$$\frac{\partial G_s}{\partial d_B} = \frac{\rho_s \times L_a \times d_D^2 \times (1-\varepsilon_{mf})}{d_B \times t} \quad \text{(E.13)}$$

$$\frac{\partial G_s}{\partial t} = \frac{\rho_s \times L_a \times d_D^2 \times (1-\varepsilon_{mf})}{d_B^2 \times t^2} \quad \text{(E.14)}$$

Overall Uncertainty may be calculated as:

$$U = \sqrt{\left(\frac{\partial G_s}{\partial \rho_s}\right)^2 \times (\Delta\rho_s)^2 + \left(\frac{\partial G_s}{\partial L_a}\right)^2 \times (\Delta L_a)^2 + \left(\frac{\partial G_s}{\partial d_D}\right)^2 \times (\Delta d_D)^2 + \left(\frac{\partial G_s}{\partial d_B}\right)^2 \times (\Delta d_B)^2 + \left(\frac{\partial G_s}{\partial t}\right)^2 \times (\Delta)^2} \quad \text{(E.15)}$$

For parameters of three experiment cases as following, we had overall uncertainty.

Table E.2 Overall uncertainty for solid circulation rate

L_m [m]	Δh [cm]	U [±%]
0.077	5	3.254234
0.016	4.9	23.48721
0.177	5.7	2.126118
0.022	5.8	15.44387
0.14	5.9	2.456272
0.138	6.1	2.516408
0.142	6.3	2.515981
0.014	6	36.536
0.162	6.5	2.376766
0.3	6.7	1.745422
0.3	6.8	1.758152
Overall Uncertainty average		8.56513

Appendix F: Feeder Calibration

A screw feeder is used to feed the sand inventory initially, and solid fuel (biomass and coal) during the experiments running. The screw is driven by electric motor as explained in chapter 4. The direct current regulated power supply is used to control the supplied current to the electric motor, as a result the R.P.M is controlled, and subsequently the feeding rate is controlled. For each fuel species, a correlation between the voltage and feeding rate is derived as shown in the Figure F.1.

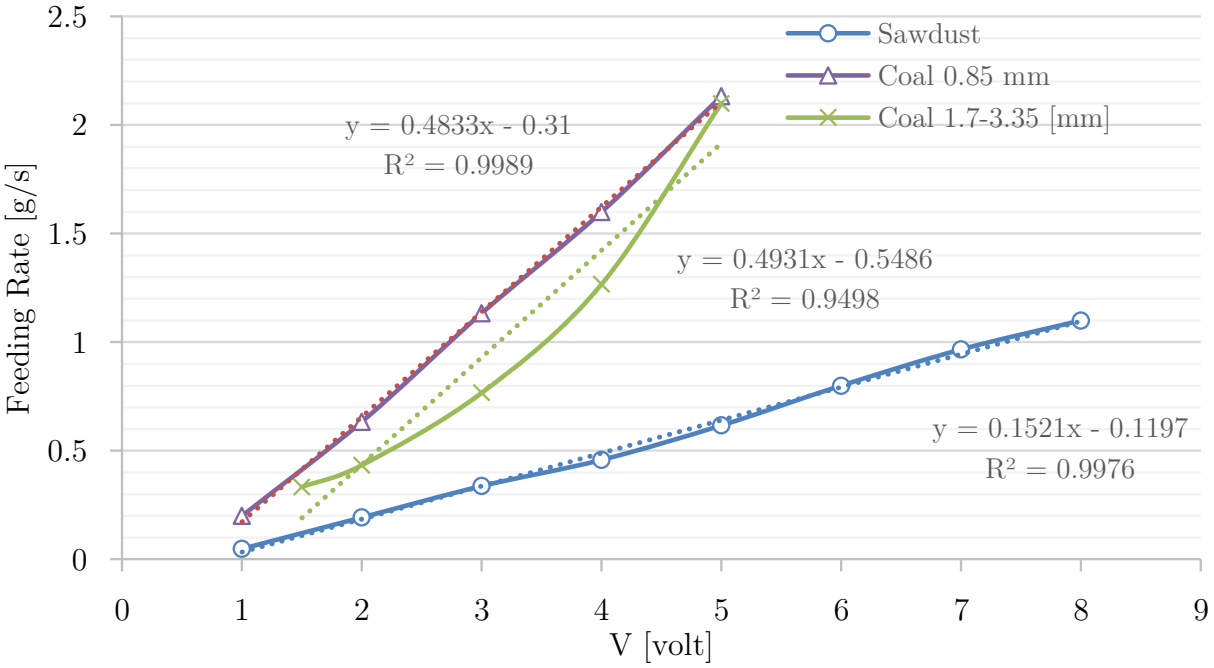

Figure F.1 Calibration curve of feeder for coal and biomass (sawdust)

Procedure of calibration:

After filling up the feeder with required fuel, the current of the DC motor is increased from 0 up to V= 1 volt, then the weight of the accumulated fuel w[grams] is measured along with time t [sec]. Finally, the feeding rate is calculated (FD) = w/t [grams/sec] which meets 1 volt. The whole process is repeated for increased voltage, and the FD is calculated at every and each time. For each type of fuel and particle size the process is conducted.

List of Publications

Journals

1. Yerbol Sarbassov, **Azd Zayoud**, Pinakeswar Mahanta, Sai Gu, Panneerselvam Ranganathan and Ujjwal K. Saha, (2016), Hydrodynamic experiments on a small-scale circulating fluidized bed reactor at elevated operating pressure, and under an O_2/CO_2 environment. Thermal Science 2016 On Line-First Issue 00, Pages: 68-68 doi:10.2298/TSCI150921068S

Book Chapter

1. Azd Zayoud, Yerbol Sarbassov, P. Mahanta, U. K. Saha , Sai Gu. 21 September 2016, Influence of Aeration on the Hydrodynamic Behavior of a Pressurized Circulating Fluidized Bed. Fluid Mechanics and Fluid Power – Contemporary Research Part of the series Lecture Notes in Mechanical Engineering pp 105-114, Springer.

Conferences

1. **Azd Zayoud**, Yerbol Sarbassov, P. Mahanta, U. K. Saha, Sai Gu, Influence of Aeration on the Hydrodynamic Behavior of a Pressurized Circulating Fluidized Bed, *Fluid Mechanics and Fluid Power (*FMFP*)*, December 12^{th}-14^{th} 2014, Indian Institute of Technology Kanpur, India.

2. **Azd Zayoud**, U. K. Saha, P. Mahanta, Novel Concept of Fuel Feeding Toward Pure Oxy-Combustion in a Circulating Fluidized Bed, *5^{th} International Conference on Advances in Energy Research*, December 15^{th} 2015, at Indian Institute of Technology Bombay, India.

3. Yerbol Sarbassov, **Azd Zayoud**, Sai Gu, Paneerselvam Ranganathan, Pinakeswar Mahanta, and Ujjwal K. Saha, Circulating Fluidized Bed Hydrodynamics Study at Elevated Pressure and Atmospheric O_2/CO_2 Environment, *22nd International Conference on Fluidized Bed Conversion*, June 14-17, 2015, Turku, Finland.